Reliability in Constrained Gauss-Markov Models: An Analytical and Differential Approach with Applications in Photogrammetry

by

Jackson Cothren

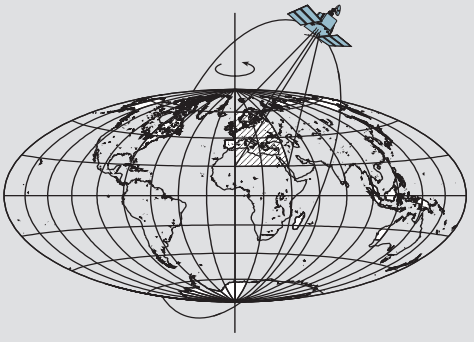

Report No. 473

Geodetic and GeoInformation Science
Department of Civil and Environmental Engineering and Geodetic Science
The Ohio State University
Columbus, Ohio 43210-1275

February 2005

Reliability in Constrained Gauss-Markov Models: An Analytical and Differential Approach with Applications in Photogrammetry

By

Jackson Cothren

Report No. 473

Department of Civil and Environmental Engineering and Geodetic Science
The Ohio State University
Columbus, Ohio 43210

February 2005

Abstract

Reliability analysis explains the contribution of each observation in an estimation model to the overall redundancy of the model, taking into account the geometry of the network as well as the precision of the observations themselves. It is principally used to design networks resistant to outliers in the observations by making the outliers more detectible using standard statistical tests.It has been studied extensively, and principally, in Gauss-Markov models. We show how the same analysis may be extended to various constrained Gauss-Markov models and present preliminary work for its use in unconstrained Gauss-Helmert models. In particular, we analyze the prominent reliability matrix of the constrained model to separate the contribution of the constraints to the redundancy of the observations from the observations themselves. In addition, we make extensive use of matrix differential calculus to find the Jacobian of the reliability matrix with respect to the parameters that define the network through both the original design and constraint matrices. The resulting Jacobian matrix reveals the sensitivity of reliability matrix elements highlighting weak areas in the network where changes in observations may result in unreliable observations. We apply the analytical framework to photogrammetric networks in which exterior orientation parameters are directly observed by GPS/INS systems. Tie-point observations provide some redundancy and even a few collinear tie-point and tie-point distance constraints improve the reliability of these direct observations by as much as 33%. Using the same theory we compare networks in which tie-points are observed on multiple images (n-fold points) and tie-points are observed in photo pairs only (two-fold points). Apparently, the use of two-fold tie-points does not significantly degrade the reliability of the direct exterior observation observations. Coplanarity constraints added to the common two-fold points do not add significantly to the reliability of the direct exterior orientation observations. The differential calculus results may also be used to provide a new measure of redundancy number stability in networks. We show that a typical photogrammetric network with n-fold tie-points was less stable with respect to at least some tie-point movement than an equivalent network with n-fold tie-points decomposed into many two-fold tie-points.

Preface

This report was prepared by Jackson Cothren, a graduate research associate in the Department of Civil and Environmental Engineering and Geodetic Science at the Ohio State University, under the supervision of Professor Burkhard Schaffrin.

This report was also submitted to the Graduate School of the Ohio State University as a dissertation in partial fulfillment of the requirements for the Ph.D. degree.

TABLE OF CONTENTS

CHAPTER 1

INTRODUCTION

Modern photogrammetric adjustment models no longer involve only tie and ground control point observations on stereo or convergent photography. Additional information from geometric constraints on ground points, observations of linear features, observations of camera orientation, and observations of ground point locations from other sources are routinely available. The theory behind integrating this additional information in the form of stochastic constraints is well understood and has been applied to GPS/INS observations of camera position and attitude, shape and position constraints on surfaces, and control point observations (Tamim and Schaffrin, 1995, Kraus, 1999, Schenk, 1999, Flood, 1999). In fact, extending the traditional photogrammetric observation equation model with constraints can be shown to reduce the variance of estimated parameters, reduce correlations between various parameters (especially in self-calibrating bundle adjustments), and increase the redundancy of the extended model (Koch, 1999, Kraus, 1999, Triggs, et al. 2000). Additional supplemental observations are becoming available as well. Most recently, laser profilers (terrestrial laser scanners) and airborne laser ranging (ALR) systems have seen use in both research and commercial mapping applications (Flood, 1999, and Schenk, et al. 2002). These systems provide extremely dense, and in some cases very precise, point observations of three-dimensional surfaces such as building facades, urban landscapes, and terrain. They suffer, however, from at least two important drawbacks (Baltsavias, 1999). First, individual points from the resulting point clouds cannot easily be traced to a corresponding feature on the surface. Second, because these systems measure azimuth, elevation, and range (or equivalently direction cosine and range) between points on a surface, they offer no redundancy in the estimation of the three-dimensional coordinates of these points. As a result, measurement accuracy is only as good as the calibration of the system (i.e. systematic errors are undetectible) and gross observational errors are statistically and practically undetectible. Indeed, these systems provide less redundancy (zero, in fact) than a directly oriented photogrammetric system (i.e. relative and absolute orientation achieved by tie points observed in overlapping images and GPS/INS observations of exposure centers without the use of ground control points) (Schenk, 2002). The advantages and limitations of laser scanners thus complement photogrammetric systems which provide interpretable and redundant, but relatively sparse, discrete point information about a surface. Integration of these two types of observations in an adjustment model has been studied by Jaw (1999), for example, who proposed augmenting aerial triangulation with planar constraints, estimated from a laser surface, on tie points. Other current research involves techniques to match the two surfaces (generally, but not necessarily, represented by a triangulated irregular network, or TIN) estimated from a photogrammetric system and a laser scanner (Schenk and Csathó, 2002, and Schenk, 2002). The relative dominance of a-posteriori matching can be attributed primarily to the general lack of correspondence between points in the two estimated surfaces. This approach does, however, provide some degree of systematic and gross error detection in the laser generated surface (Schenk, 2002).

The extended photogrammetric model (i.e. traditional photogrammetric observation equations augmented with stochastic constraints of various forms), in particular with those cases enumerated above, is a flexible and powerful tool for including incongruous information into a stochastically rigorous adjustment model. Another powerful tool, resulting from concepts first developed by the Dutch geodesist Baarda in 1968 and applied to photogrammetric networks by Förstner as early as 1985 (there exists some German language literature from the seventies as well), is the computation of inner and outer reliability of a geodetic and/or photogrammetric network. Reliability is a measure of a model's ability to help detect and/or locate gross errors (inner reliability) and of the estimated parameter's sensitivity to un-modeled gross errors (outer reliability). Both concepts make extensive use of a so-called "reliability" matrix which maps the observation vector to the residual vector. Both Baarda and Förstner initially applied the concept to the Gauss-Markov model and assumed uncorrelated observations. Furthermore, this early work assumed a gross error in a single observation. Since these initial studies, several researchers have expanded the scope of the concept. Wang and Chen (1994) studied the effects on correlated observations, and Schaffrin (1997) offered a similar approach that allowed better interpretation with a normalized reliability number.

Förstner expanded the concept by developing statistical tests for groups of observations - important for examining photogrammetric tie point measurements (Förstner, 1994). Most recently Schaffrin (2000) developed reliability measures for predictions obtained by Kriging. To date, there is no evidence beyond Schaffrin (2000) of any attempts to extend the concept of reliability beyond the Gauss-Markov model, and in particular to the constrained Gauss-Markov model. Because of the growing need for integrating incongruous observations – just four of potentially many examples are described above – it would be helpful to have a tool that allows a network designer to see the effects of additional observations or constraints not only on the estimated variance of the parameters but also on the reliability of the model. It is certainly possible to see the effects in a synthesized result by computing reliability with, and then without, the stochastic constraints. However, this method may well obscure the causes of the change in reliability. A truly analytical approach would separate the contribution of the observation equations from the effects of the stochastic constraints on model reliability. This method is currently used to evaluate the effects of stochastic constraints on the parameter vector and its covariance matrix (Koch, 1999) but apparently has not yet been extended to the computation of reliability.

Another approach would have us consider the reliability matrix as a non-linear matrix function of matrix variables and use the theory of differential calculus, extended to matrix functions, to examine how the reliability matrix behaves with respect to changes in the network or the addition of constraints (Magnus and Neudecker, 1999). With the "Jacobian" of the reliability matrix with respect to the design matrix or constraint matrix, we would have a tool to see how changes in the design matrix, resulting from changes in the initial parameter seed values, effect changes in observation reliability. We will therefore examine two approaches – first analytically examine the change in reliability (and consequently inner and outer reliability) induced by the constraints in the Gauss-Markov model and second, use the analytical results to develop differential relationships between the model design matrices and the reliability matrix itself to see how reliability measures are affected locally.

Chapter 2 will summarize reliability theory in the Gauss-Markov model, particularly those results concerning the reliability matrix, inner reliability, and outer reliability . Chapter 3 will present relevant results from the constrained Gauss-Markov model and will address both fixed constraints (constraints with zero variance) and stochastic constraints (constraints with non-zero known variance). Both the full-rank Gauss-Markov model and the rank-deficient Gauss-Markov model will be addressed. Chapter 4 will integrate reliability analysis into the constrained Gauss-Markov model and provide expressions for the reliability matrix, inner reliability, and outer reliability. A simple numerical example will be used to demonstrate the results. Chapter 5 will examine differential relations between the network design matrix (meaning both the observation design matrix and the constraint matrix) and the reliability matrix. In particular, it will express the Jacobian matrix relating these two matrices and analyze its structure. Chapter 6, will apply some of the results from the preceding chapters to two particularly interesting questions in aerial triangulation block design. Finally, Chapter 7 will provide conclusions and directions for future research.

CHAPTER 2

RELIABILITY ANALYSIS IN GAUSS-MARKOV MODELS

2.1. Treatment of a single outlier

We will begin with a development of some of the fundamental results of reliability theory, especially those relevant to the developments to follow. A model for estimating the redundancy of individual observations frequently used in the photogrammetric and geodetic communities was developed by Baarda (1968) for geodetic networks. Since its development, it has been applied to aerial triangulation (Förstner, 1985) and to more general photogrammetric networks in computer vision mensuration applications (Förstner, 1987). Given a Gauss Markov model,

$$\mathbf{y} = \mathbf{A}\xi + \mathbf{e} \qquad \mathbf{e} \sim (\mathbf{0}, \sigma_o^2 \mathbf{P}^{-1}) \tag{2.1}$$

where

- **y** is a *n* x *1* random vector of observations (or, when **A** is the Jacobian of the linearized observation equations, a vector of incremental changes in observations),
- **A** is an *n* x *m* non-random design matrix of rank $q \leq m$ built from the linear relationships between the parameters to be estimated and the observations (again, this is typically the Jacobian matrix defining a local differential relationship between parameters and observations),
- ξ is the *m* x *1* non-random parameter vector (or incremental parameter vector of the linearized observation equations),
- **e** is the *n* x *1* random error vector with first and second moments given, with **P** known but σ_o^2 not necessarily known,

the Weighted LEast Squares Solutions (WLESS) for ξ satisfies the normal equations

$$\mathbf{N}\hat{\boldsymbol{\xi}} = \mathbf{c} \qquad [\mathbf{N},\mathbf{c}] = \mathbf{A}^T\mathbf{P}[\mathbf{A},\mathbf{y}] \tag{2.2}$$

and is guaranteed to exist although it might not be unique depending on the rank of **N**. If we write the estimate $\hat{\xi} = \mathbf{N}_{rs}^{-}\mathbf{c}$ along with dispersion $D\{\hat{\xi}\} = \sigma_o^2\mathbf{N}_{rs}^{-}$, where $\mathbf{N}_{rs}^{-}$ designates any reflexive symmetric generalized inverse of **N**, then the unique predicted residual vector is

$$\tilde{\mathbf{e}} = \mathbf{y} - \mathbf{A}\hat{\boldsymbol{\xi}} = \mathbf{y} - \mathbf{A}\mathbf{N}_{rs}^{-}\mathbf{A}^T\mathbf{P}\mathbf{y} \tag{2.3}$$

with its corresponding (also unique) cofactor matrix

$$\mathbf{Q}_{\tilde{\mathbf{e}}} = \mathbf{P}^{-1} - \mathbf{A}\mathbf{N}_{rs}^{-}\mathbf{A}^T . \tag{2.4}$$

Using (2.4), (2.3) may be compactly written

$$\tilde{\mathbf{e}} = \mathbf{Q}_{\tilde{\mathbf{e}}}\mathbf{P}\mathbf{y} \tag{2.5}$$

so that the matrix $\mathbf{Q}_{\tilde{\mathbf{e}}}\mathbf{P}$ defines a linear mapping from the observation vector to the residual vector. For reasons that will become clear later, the matrix $\mathbf{Q}_{\tilde{\mathbf{e}}}\mathbf{P}$ is often called the "reliability" matrix and designated **R**. From (2.4) we know that the reliability matrix is idempotent and thus $rk(\mathbf{Q}_{\tilde{\mathbf{e}}}\mathbf{P}) = tr(\mathbf{Q}_{\tilde{\mathbf{e}}}\mathbf{P}) = tr(\mathbf{I}_n - \mathbf{A}\mathbf{N}_{rs}^{-}\mathbf{A}^T\mathbf{P}) = tr(\mathbf{I}_n) - rk(\mathbf{N}_{rs}^{-}\mathbf{N}) = n - q$. The sum of the diagonal elements of the reliability matrix sum to the total redundancy of the model. The diagonal elements of **R** can therefore be interpreted as the degree to which the corresponding observation contributes to the redundancy of the model.

The model (2.1) assumes only small random errors (described by the second moment) in the observation vector. If we assume that a single gross error (or outlier) is present in the j^{th} observation then (2.1) must be re-written to account for this outlier. Following Schaffrin (1997) and defining $\eta_j = [0 \ \ldots \ 0 \ \ 1 \ \ 0 \ \ \ldots \ 0]^T$, the new model accounting for the single outlier is

$$\mathbf{y} = \mathbf{A}\xi + \eta_j\xi_o + \mathbf{e} \qquad , \qquad \mathbf{e} \sim (\mathbf{0}, \sigma_o^2\mathbf{P}^{-1}), \tag{2.6}$$

which includes a new parameter, ξ_o, representing the size of the expected outlier in the j^{th} observation. It is important to note that this model may be generalized to describe systematic effects by introducing a

possibly fully occupied matrix **H** before η_j, spreading one or more outliers in a known (i.e. systematic) way throughout the observations (Förstner, 1985, and Snow and Schaffrin, 2003). The corresponding normal equations for (2.6),

$$\begin{bmatrix} \eta_j^T\mathbf{P}\eta_j & \eta_j^T\mathbf{P}\mathbf{A} \\ \mathbf{A}^T\mathbf{P}\eta_j & \mathbf{N} \end{bmatrix}\begin{bmatrix} \hat{\xi}_o^{(j)} \\ \hat{\xi}^{(j)} \end{bmatrix} = \begin{bmatrix} \eta_j^T\mathbf{P}\mathbf{y} \\ \mathbf{c} \end{bmatrix} \tag{2.7}$$

may be analytically solved for the estimate of the outlier as well as the original parameter vector. If we assume that $rk\left[\mathbf{A}, \boldsymbol{\eta}_j\right] = rk\mathbf{A} + 1$ and take into account (2.5) then

$$\begin{aligned} \hat{\xi}_o^{(j)} &= \left(\eta_j^T\mathbf{P}\mathbf{Q}_{\hat{\mathbf{e}}}\mathbf{P}\eta_j\right)^{-1}\left(\eta_j^T\mathbf{P}\mathbf{Q}_{\hat{\mathbf{e}}}\mathbf{P}\mathbf{y}\right) \\ &= \left(\eta_j^T\mathbf{P}\mathbf{R}\eta_j\right)^{-1}\left(\eta_j^T\mathbf{P}\mathbf{R}\mathbf{y}\right) \\ &= \left(\eta_j^T\mathbf{P}\mathbf{R}\eta_j\right)^{-1}\left(\eta_j^T\mathbf{P}\tilde{\mathbf{e}}\right) \end{aligned} \tag{2.8}$$

and,

$$\begin{aligned} \hat{\xi}^{(j)} &= \mathbf{N}_{rs}^{-}\mathbf{c} - \mathbf{N}_{rs}^{-}\mathbf{A}^T\mathbf{P}\eta_j\hat{\xi}_o^{(j)} \\ &= \hat{\xi} - \mathbf{N}_{rs}^{-}\mathbf{A}^T\mathbf{P}\eta_j\left(\eta_j^T\mathbf{P}\mathbf{Q}_{\hat{\mathbf{e}}}\mathbf{P}\eta_j\right)^{-1}\left(\eta_j^T\mathbf{P}\mathbf{Q}_{\hat{\mathbf{e}}}\mathbf{P}\mathbf{y}\right) \\ &= \hat{\xi} - \mathbf{N}_{rs}^{-}\mathbf{A}^T\mathbf{P}\eta_j\left(\eta_j^T\mathbf{P}\mathbf{R}\eta_j\right)^{-1}\left(\eta_j^T\mathbf{P}\mathbf{R}\mathbf{y}\right) \end{aligned} \tag{2.9}$$

The expected size of the outlier is a function of the geometry of the network in the form of the reliability matrix, **R**, and the precision and correlation of the observations contained in **P**, which together create a complex mapping from the observation vector (or residual vector) into the estimated outlier. Furthermore, because the estimate of the outlier is invariant with respect to the chosen reflexive symmetric generalized inverse, it depends only on the internal geometry of the network. To understand the effect of the outlier on the estimated parameters it is helpful to write (2.9) as $\hat{\xi}^{(j)} = \mathbf{N}_{rs}^{-}\mathbf{A}^T\mathbf{P}\left(\mathbf{y} - \eta_j\hat{\xi}_o^{(j)}\right)$ to show that the estimated outlier is simply removed from the observation vector used to estimate the (outlier-free) parameter vector.

If we assume uncorrelated observations in which case **P** is diagonal, the expression for the outlier simplifies to

$$\begin{aligned} \hat{\xi}_o^{(j)} &= \left(\eta_j^T\mathbf{R}\mathbf{y}\right)\Big/\left(\eta_j^T\mathbf{R}\eta_j\right) \\ &= \tilde{\mathbf{e}}_j\Big/\mathbf{R}_{jj} \\ &= \tilde{\mathbf{e}}_j\Big/r_j \end{aligned} \tag{2.10}$$

where r_j is designated the redundancy number of that observation. Now, as the observations are uncorrelated, $\mathbf{R} = \mathbf{Q}_{\hat{\mathbf{e}}}\mathbf{P}$ is not only idempotent, but has the same diagonal elements as $\mathbf{P}^{½}\mathbf{Q}_{\hat{\mathbf{e}}}\mathbf{P}^{½}$ which is symmetric, leading to $0 \le r_j \le 1$. Therefore the expected size of the outlier is larger than the corresponding residual, and r_j can be interpreted as a measure of the degree to which the outlier is "contained within" the corresponding residual. If $r_j = 1$, then the full outlier is determined by the residual and large residuals will flag an observation as an outlier. If, on the other hand, $r_j << 1$ then the outlier in the j^{th} observation is spread among other residuals and is much more difficult to detect and locate. As we saw before, $tr(\mathbf{R}) = tr(\mathbf{Q}_{\hat{\mathbf{e}}}\mathbf{P}) = n - rk(\mathbf{A}) = r := n - q$, and the individual redundancy numbers indicate how each observation contributes to the total redundancy of the model.

With the relations (2.8) and (2.10) defined, Baarda (1968) developed statistical testing procedures for the detection and localization of a single outlier. We may do the same beginning with an analysis of the weighted sum of squared residuals. Following (Schaffrin, 1997),

$$\begin{aligned}\Omega - \Omega^{(j)} &= \left(\eta_j^T \mathbf{P}\mathbf{Q}_{\hat{\mathbf{e}}}\mathbf{P}\eta_j\right)\left(\hat{\xi}_o^{(j)}\right)^2 \\ &= \left(\eta_j^T \mathbf{P}\mathbf{Q}_{\hat{\mathbf{e}}}\mathbf{P}\eta_j\right)^{-1}\left(\eta_j^T \mathbf{P}\mathbf{R}\mathbf{y}\right)^2 \\ &= \left(\eta_j^T \mathbf{P}\mathbf{Q}_{\hat{\mathbf{e}}}\mathbf{P}\eta_j\right)^{-1}\left(\eta_j^T \mathbf{P}\tilde{\mathbf{e}}\right)^2\end{aligned} \tag{2.11}$$

where Ω is the weighted sum of squared residuals resulting from model (2.1) and $\Omega^{(j)}$ is the weighted sum of residuals squared resulting from model (2.6). It is clear that taking into account the outlier in the j^{th} observation reduces the sum of squares by an amount depending, again, on the geometry of the network. In order to determine if this change is statistically significant, we may use $\left(\Omega - \Omega^{(j)}\right)/\sigma_o^2$ as a test statistic if we know, or assume, its distribution. If we assume $\hat{\xi}_o^{(j)} \sim \mathrm{N}\left(\xi_o, \sigma_o^2\left(\eta_j^T \mathbf{P}\mathbf{Q}_{\hat{\mathbf{e}}}\mathbf{P}\eta_j\right)^{-1}\right)$ with expectation and dispersion derived from (2.8), then as a quadratic equation in $\hat{\xi}_o^{(j)}$, $\left(\Omega - \Omega^{(j)}\right)/\sigma_o^2$ is χ^2-distributed with $rk\left(\sigma_o^2\left(\eta_j^T \mathbf{P}\mathbf{Q}_{\hat{\mathbf{e}}}\mathbf{P}\eta_j\right)^{-1}\right) = 1$ degree of freedom and a non-centrality parameter of $2\vartheta_j = \left(\eta_j^T \mathbf{P}\mathbf{Q}_{\hat{\mathbf{e}}}\mathbf{P}\eta_j\right)(\xi_o)^2/\sigma_o^2$ since $\left(\left(\eta_j^T \mathbf{P}\mathbf{Q}_{\hat{\mathbf{e}}}\mathbf{P}\eta_j\right)/\sigma_o^2\right) D\left\{\hat{\xi}_o\right\}$ is idempotent (see, for example, theorems in Searle et al. (1992) and Koch (1999)). Or, by considering $E\left\{x^T \mathbf{B} x\right\} = tr\left(\mathbf{B} D\{x\}\right) + E\{x\}^T \mathbf{B} E\{x\}$ (again from Searle et al. (1992)), we may write the expectation of (2.11) following (Schaffrin, 1997)

$$\begin{aligned}E\left\{\left(\Omega - \Omega^{(j)}\right)/\sigma_o^2\right\} &= 1 + \left(\eta_j^T \mathbf{P}\mathbf{Q}_{\hat{\mathbf{e}}}\mathbf{P}\eta_j\right)(\xi_o)^2/\sigma_o^2 \\ &= 1 + 2\vartheta_j\end{aligned}. \tag{2.12}$$

and arrive at the same χ^2-distribution. Therefore, with these assumptions (all of which depend on the normal distribution of **e**), we may form the null hypothesis $H_o : \xi_o = 0$ under which

$$\Omega/\sigma_o^2 \sim \chi^2(n - rk\mathbf{A}) \qquad \text{and} \qquad \left(\Omega - \Omega^{(j)}\right)/\sigma_o^2 \sim \chi^2(1) \tag{2.13}$$

while under the alternative hypothesis $H_a : \boldsymbol{\xi}_o \neq 0$

$$\Omega^{(j)}/\sigma_o^2 \sim \chi^2(n - rk\mathbf{A} - 1) \qquad \text{and} \qquad \left(\Omega - \Omega^{(j)}\right)/\sigma_o^2 \sim \chi^2\left(1; 2\vartheta_j\right). \tag{2.14}$$

As $2\vartheta_j$ increases, so does the "distance" between the distributions in (2.13) and (2.14). Since $2\vartheta_j$ is determined by $\mathbf{Q}_{\hat{\mathbf{e}}}$ and **P** (and thus **R**), the design of the network as well as the precision of the observations has a direct impact on the detectibility of outliers. $\left(\Omega - \Omega^{(j)}\right)/\sigma_o^2$, as the estimated non-centrality parameter (and note that it may be considered the square of a standardized residual which then has a normal distribution if σ_o^2 is used, or student-t distribution if $\hat{\sigma}_o^2$ is used), must exceed a threshold, δ_o^2 (defined as a function $\delta_o\left(\alpha_o, \beta_o\right)$ of the error probability, α_o, and specified power, $1 - \beta_o$, of a given hypothesis test), for the outlier to be detected. For such an outlier we expect:

$$2\vartheta = \left(\eta_j^T \mathbf{P}\mathbf{Q}_{\hat{\mathbf{e}}}\mathbf{P}\eta_j\right)(\xi_o)^2/\sigma_o^2 > \delta_o^2. \tag{2.15}$$

Rearranging this expression, we may say the outlier must satisfy

$$\xi_o > \delta \cdot \left[\sigma_o\left(\eta_j^T \mathbf{P}\mathbf{Q}_{\hat{\mathbf{e}}}\mathbf{P}\eta_j\right)^{-1/2}\right] \tag{2.16}$$

if it is to be detected by a given hypothesis test. In the case of uncorrelated observations, (1.16) simplifies to

$$\xi_o > \delta \cdot \left[\frac{\sigma_o}{\sqrt{r_j p_j}}\right] \tag{2.17}$$

Equations (2.15) and (2.16) form the basis of "inner reliability" and answer the question – how large must an outlier be before it is detectible by a particular statistical test? Note that the answer depends wholly

upon the geometry of the model, as contained in **R**, and the variances and covariances of the observations, as contained in **P** and σ_o^2. "Outer reliability", on the other hand, is a measure of the effect of an undetectible outlier, say ξ_o just less than the threshold defined in (2.16) on the estimated parameters. It may be computed using (2.2) and (1.9) as follows

$$(\delta\xi)_j = \mathbf{N}_{rs}^{-}\mathbf{A}^T\mathbf{P}\eta_j\xi_o \tag{2.18}$$

Based on (2.18), an appropriate measure of outer reliability is the quadratic form

$$\gamma_j = (\delta\xi)_j^T\,\mathbf{N}(\delta\xi)_j \big/ \sigma_o^2 \tag{2.19}$$

Formula (2.18) shows the outlier's effect on each parameter while (2.19) shows the perturbation of the parameter vector in its squared weighted norm due to the outlier ξ_o. Since the expression for inner reliability (2.15) and the expression for outer reliability (2.17) do not involve estimated parameters or predicted observations, both may be computed from the network design before any observations are made. Inner and outer reliability are thus considered "Phase Zero" design considerations, aiding the photogrammetrist in the design of a network resistant to observational blunders (Kraus, 1999).

The analysis up to this point assumes a single gross error in the observations. In practice, it is possible to test a network adjustment for multiple gross errors applying the test defined in (2.13) and (2.14) to each observation in turn, eliminating the observation that creates the largest change (larger than the threshold) in the sum of squared residuals (2.11). With the supposed outlier eliminated, the adjustment may be run again to achieve a new parameter estimate and tested for outliers again observation by observation. The procedure may be repeated until no observations have estimated outliers larger than an acceptable threshold. Baarda referred to this test of standardized residuals as "data snooping". Triggs, et al. (2000) made the observation that the full iterative procedure is essentially a form of M-estimation with an abruptly vanishing weight function.

2.2 Treatment of grouped, multiple outliers

The analysis above may be generalized to test for outliers in a group of observations (Förstner, 1994, Koch, 1999, Snow and Schaffrin, 2003). This is useful for adjustments in which a measurement blunder might contaminate more than one observation or in which a blunder in one observation would force the elimination of other observations in the group. A misidentified image tie point in a bundle adjustment, for example, would affect the point's *x* and *y* coordinate observations and force the elimination of both *x* and *y* coordinate observations. Analogous to (2.6) we construct a new Gauss-Markov model

$$\mathbf{y} = \mathbf{A}\xi + \mathbf{Z}\xi_o + \mathbf{e} \qquad , \qquad \mathbf{e} \sim \left(\mathbf{0}, \sigma_o^2\mathbf{P}^{-1}\right) \tag{2.20}$$

with $\mathbf{Z} = \left[\eta_i, \cdots, \eta_j, \cdots, \eta_k\right]$. The subscripts identify the *c* observations in which outliers are modeled, so that Z is an *n x c* matrix with rank *c* and $rk\left(\begin{bmatrix}\mathbf{A} & \mathbf{Z}\end{bmatrix}\right) = q + c$. Note that, unlike the additional scalar parameter in (2.6), (2.20) requires an additional *c* x *1* parameter vector for the *c* outliers. The WLESS solutions to (2.19) are

$$\begin{aligned}\hat{\xi}_o^{(c)} &= \left(\mathbf{Z}^T\mathbf{P}\mathbf{Q}_{\tilde{\mathbf{e}}}\mathbf{P}\mathbf{Z}\right)^{-1}\left(\mathbf{Z}^T\mathbf{P}\mathbf{Q}_{\tilde{\mathbf{e}}}\mathbf{P}\mathbf{y}\right) \\ &= \left(\mathbf{Z}^T\mathbf{P}\mathbf{Q}_{\tilde{\mathbf{e}}}\mathbf{P}\mathbf{Z}\right)^{-1}\left(\mathbf{Z}^T\mathbf{P}\tilde{\mathbf{e}}\right)\end{aligned} \tag{2.21}$$

for the estimated outlier in terms of both **y** and the residual vector, $\tilde{\mathbf{e}}$, from model (2.1) and,

$$\hat{\xi}^{(c)} = \mathbf{N}_{rs}^{-}\mathbf{c} - \mathbf{N}_{rs}^{-}\mathbf{A}^T\mathbf{P}\mathbf{Z}\hat{\xi}_o^{(c)} \tag{2.22}$$

for the new parameter vector. Several expressions for the residual vector in (2.20),

$$\begin{aligned}\tilde{\mathbf{e}}^{(c)} &= \mathbf{y} - \mathbf{A}\mathbf{N}_{rs}^{-}\mathbf{c} - \left(\mathbf{Z} - \mathbf{A}\mathbf{N}_{rs}^{-}\mathbf{A}^T\mathbf{P}\mathbf{Z}\right)\hat{\xi}_o^{(c)} \\ &= \tilde{\mathbf{e}} - \left(\mathbf{Z} - \mathbf{A}\mathbf{N}_{rs}^{-}\mathbf{A}^T\mathbf{P}\mathbf{Z}\right)\hat{\xi}_o^{(c)} \\ &= \tilde{\mathbf{e}} - \left(\mathbf{P}^{-1} - \mathbf{A}\mathbf{N}_{rs}^{-}\mathbf{A}^T\right)\mathbf{P}\mathbf{Z}\hat{\xi}_o^{(c)} \\ &= \tilde{\mathbf{e}} - \mathbf{Q}_{\tilde{\mathbf{e}}}\mathbf{P}\mathbf{Z}\hat{\xi}_o^{(c)} \quad ,\end{aligned} \tag{2.23}$$

lead to a formula for the increase in the weighted sum of squared residuals due to the un-modeled outliers

$$\begin{aligned}\Omega - \Omega^{(c)} &= \tilde{\mathbf{e}}^T\mathbf{P}\tilde{\mathbf{e}} - \left(\tilde{\mathbf{e}}^{(c)}\right)^T\mathbf{P}\tilde{\mathbf{e}}^{(c)} \\ &= \left[\hat{\xi}_o^{(c)}\right]^T\mathbf{Z}^T\mathbf{P}\mathbf{Q}_{\tilde{\mathbf{e}}}\mathbf{P}\mathbf{Z}\hat{\xi}_o^{(c)}\end{aligned} \tag{2.24}$$

Using (2.21) the increase may also be written in terms of the original residuals

$$\Omega - \Omega^{(c)} = \tilde{\mathbf{e}}^T\mathbf{P}\mathbf{Z}\left(\mathbf{Z}^T\mathbf{P}\mathbf{Q}_{\tilde{\mathbf{e}}}\mathbf{P}\mathbf{Z}\right)^{-1}\mathbf{Z}^T\mathbf{P}\tilde{\mathbf{e}} \tag{2.25}$$

The particular χ^2 -distribution for this quadratic form (scaled by σ_o^{-2}) may be derived as before, so that

$$\begin{aligned}E\left\{\left(\Omega - \Omega^{(c)}\right)/\sigma_o^2\right\} &= tr\left(\mathbf{P}\mathbf{Q}_{\tilde{\mathbf{e}}}\mathbf{P}\mathbf{Z}\left(\mathbf{Z}^T\mathbf{P}\mathbf{Q}_{\tilde{\mathbf{e}}}\mathbf{P}\mathbf{Z}\right)^{-1}\mathbf{Z}^T\mathbf{P}\mathbf{Q}_{\tilde{\mathbf{e}}}\right) + \\ &\qquad \left(\mathbf{A}\xi + \mathbf{Z}\xi_o\right)^T\left(\mathbf{P}\mathbf{Q}_e\mathbf{P}\mathbf{Z}\left(\mathbf{Z}^T\mathbf{P}\mathbf{Q}_{\tilde{\mathbf{e}}}\mathbf{P}\mathbf{Z}\right)^{-1}\mathbf{Z}^T\mathbf{P}\mathbf{Q}_{\tilde{\mathbf{e}}}\mathbf{P}\right)\left(\mathbf{A}\xi + \mathbf{Z}\xi_o\right)/\sigma_o^2 \\ &= c + \xi_o^T\mathbf{Z}^T\mathbf{P}\mathbf{Q}_{\tilde{\mathbf{e}}}\mathbf{P}\mathbf{Z}\,\xi_o/\sigma_o^2 \\ &= c + 2\vartheta_c\end{aligned} \tag{2.26}$$

Assuming **e** as normally distributed, we conclude that under the null hypothesis $H_o : \xi_o = \mathbf{0}$

$$\Omega/\sigma_o^2 \sim \chi^2\left(n - rk\mathbf{A}\right) \qquad \text{and} \qquad \left(\Omega - \Omega^{(c)}\right)/\sigma_o^2 \sim \chi^2\left(c\right) \tag{2.27}$$

while under the alternative hypothesis $H_a : \xi_o \neq \mathbf{0}$

$$\Omega_j/\sigma_o^2 \sim \chi^2\left(n - rk\mathbf{A} - c\right) \qquad \text{and} \qquad \left(\Omega - \Omega^{(c)}\right)/\sigma_o^2 \sim \chi^2\left(c; 2\vartheta_c\right) \tag{2.28}$$

Again, the non-centrality parameter, $2\vartheta_c = \xi_o^T\left(\mathbf{Z}^T\mathbf{P}\mathbf{Q}_{\tilde{\mathbf{e}}}\mathbf{P}\mathbf{Z}\right)\xi_o/\sigma_o^2$, is a measure of the "distance" between the two functions while the quadratic forms in (2.24) and (2.25) may be used to estimate the distance thus as a test statistic for the presence of an outlying group of observations (Koch, 1999). Note that the inner matrix of the non-centrality parameter in (2.26) uses a *c* x *c* block from the matrix, **PR**, for its representation and, since $D\left\{\hat{\xi}_o^{(c)}\right\} = \sigma_o^2\left(\mathbf{Z}^T\mathbf{P}\mathbf{Q}_{\tilde{\mathbf{e}}}\mathbf{P}\mathbf{Z}\right)^{-1}$, the non-centrality parameter is the inverse-variance-weighted squared norm of the *c* x *1* outlier vector. Förstner (1994) arrived at a similar result and noted that the test statistic allows the observations in the group to be correlated, but loses sharpness if the group is correlated with other observations or groups of observations. The first condition is generally assumed to hold in photogrammetric models where photo point observations are considered independent of other photo point observations. However, most photo point coordinates are the result of inner orientation in which analog stage or digital image coordinates are transformed into the camera coordinate system defined by the fiducial marks. Similarity or affine transformations certainly produce correlations between not only *x* and *y* coordinates of a photo point, but also among *x* and *y* coordinates of different image points. We may, however, assume that in most photogrammetric environments the correlations are small and in practice are rarely taken into account (Kraus, 1999, Mikhail, et al., 2001).

In this more general case in which we must test for an outlying group of observations, we may not isolate the outliers as we isolated the single outlier in (2.11) to obtain the inner reliability expression (2.16) since they are now interlaced in the non-centrality parameter. To get a measure of inner reliability the network designer can not simply compare the size of each standardized residual to the threshold, but instead must form the *c* x *c* block, $\mathbf{Z}^T\mathbf{P}\mathbf{Q}_{\tilde{\mathbf{e}}}\mathbf{P}\mathbf{Z}/\sigma_o^2$, from **PR** and somehow compare the quadratic form (2.24) to the pre-determined threshold δ_o^2 . The L_2, or Frobenius, norm of this block, for example, would

give an indication of the size of the non-centrality parameter and allow a comparison of relative separation formed from different network geometries. Another possible measure is the simple sum of the block elements. We may postulate a single outlier in each of the *c* observations in the group to get an idea of the upper bound of detectibility of each observation within the group.

To determine a measure of outer reliability we may compute the effect of the outliers on the parameter vector by

$$\left(\delta\xi\right)_c = \mathbf{N}_{rs}^{-}\mathbf{A}^T\mathbf{P}\mathbf{Z}\xi_o \tag{2.29}$$

with values for ξ_o that cause $2\vartheta_c = \xi_o^T\left(\mathbf{Z}^T\mathbf{P}\mathbf{Q}_{\hat{\mathbf{e}}}\mathbf{P}\mathbf{Z}\right)\xi_o/\sigma_o^2$ to be just less than the minimum detectible threshold δ^2. Or, as we did when *c* = 1, we may form the measure

$$\begin{aligned}\gamma_c &= \left(\delta\xi\right)_c^T\mathbf{N}\left(\delta\xi\right)_c/\sigma_o^2 \\ &= \xi_o^T\mathbf{Z}^T\mathbf{P}\mathbf{A}\mathbf{N}_{rs}^{-}\mathbf{A}^T\mathbf{P}\mathbf{Z}\xi_o\end{aligned} \tag{2.30}$$

allowing us to see the effect of the outliers on the entire weighted norm of the parameter vector.

2.3. Reliability in the Gauss-Helmert model

Before considering the extended (i.e. the constrained) Gauss-Markov model we should note that, while the Gauss-Markov model has many applications in photogrammetry (e.g. the collinearity bundle adjustment without self-calibration) and geodesy (e.g. a leveling network), we often encounter relations in which the Gauss-Markov model does not apply. Consider the relatively straightforward affine transformation used in inner orientation to transform between photo coordinates and digital image coordinates:

$$\begin{bmatrix} u_i - e_{u_i} \\ v_i - e_{v_i} \end{bmatrix} = \begin{bmatrix} a_{11} & a_{12} & a_{13} \\ a_{21} & a_{22} & a_{23} \end{bmatrix}\begin{bmatrix} x_i - e_{x_i} \\ y_i - e_{v_i} \\ 1 \end{bmatrix} \qquad \begin{bmatrix} e_{u_i} \\ e_{v_i} \\ e_{x_i} \\ e_{v_i} \end{bmatrix} \sim \left(\begin{bmatrix} 0 \\ 0 \\ 0 \\ 0 \end{bmatrix}, \sigma_o^2\begin{bmatrix} \mathbf{P}_{uv}^{-1} & 0 \\ 0 & \mathbf{P}_{xy}^{-1} \end{bmatrix}\right)$$

where (*u* , *v*) represents an image point (line and sample) and (*x* , *y*) represent the corresponding photo coordinates (the coordinates in the frame defined by the fiducial marks). Both of the points should be treated as observations corrupted with random error and both are modeled to reflect that fact. However, this relation is not compatible with the Gauss-Markov model because of the non-linear relationship between the observations and the parameters (the transform coefficients a_{ij}). The Gauss-Helmert (also mixed or condition equations with parameters) model

$$\mathbf{w} = \mathbf{B}\mathbf{y} = \mathbf{A}\xi + \mathbf{B}\mathbf{e} \qquad\qquad \mathbf{e} \sim \left(\mathbf{0}, \sigma_o^2\mathbf{P}^{-1}\right) \tag{2.31}$$

is often used for these relations in which for this particular example **w** is a *2p* x *1* vector of linear combinations of the random vector, **y**, **A** is a 2*p* x *6* non-random matrix, B is a 2*p* x *2p* non-random matrix and *p* is the number of points measured. The WLESS to (2.31) is

$$\hat{\xi} = \left(\mathbf{A}^T\left(\mathbf{B}\mathbf{P}^{-1}\mathbf{B}^T\right)^{-1}\mathbf{A}\right)^{-1}\mathbf{A}^T\left(\mathbf{B}\mathbf{P}^{-1}\mathbf{B}^T\right)^{-1}\mathbf{w} \tag{2.32}$$

with dispersion

$$D\{\hat{\xi}\} = \sigma_o^2\left(\mathbf{A}^T\left(\mathbf{B}\mathbf{P}^{-1}\mathbf{B}^T\right)^{-1}\mathbf{A}\right)^{-1}. \tag{2.33}$$

These solutions are very similar to (2.1) and, in fact, the Gauss-Helmert model may be transformed into the Gauss-Markov with the appropriate variable substitutions (Koch, 1999). In particular, from (2.1) $\sigma_o^2\mathbf{P}^{-1} = D\{\mathbf{y}\} = \Sigma_{yy}$ so that we may re-write (2.2) as $\left(\mathbf{A}^T\Sigma_{yy}^{-1}\mathbf{A}\right)\hat{\xi} = \mathbf{A}^T\Sigma_{yy}^{-1}\mathbf{y}$. Now in the Gauss-Helmert model, $D\{\mathbf{w}\} = \Sigma_{ww} = \sigma_o^2\mathbf{B}\mathbf{P}^{-1}\mathbf{B}^T = \mathbf{B}\Sigma_{yy}\mathbf{B}^T$, so that we transform (2.26) into a Gauss-Markov model

$$\mathbf{w} = \mathbf{A}\xi + \mathbf{e}_w \qquad\qquad \mathbf{e}_w \sim \left(\mathbf{0}, \sigma_o^2\left(\mathbf{B}\mathbf{P}^{-1}\mathbf{B}^T\right)\right). \tag{2.34}$$

and the WLESS agrees with (2.32) and (2.33). In practice, linearizing non-linear relations as was done in (2.31) with respect to all parameters to be estimated (whose Jacobian is **A**) and the observations (whose

Jacobian is **B**) leads directly to the Gauss Helmert model if $\mathbf{B} \neq \mathbf{I}_n$ and to the Gauss Markov model if **B** is the identity matrix (Leick, 1995, Pope, 1972). The ability to transform the Gauss-Helmert model to a Gauss-Markov model allows estimation of the parameter vector and its covariance matrix. However, the transformation from (2.31) to (2.34) makes the true observation residuals, $\tilde{\mathbf{e}}$, in $\tilde{\mathbf{e}}_w = \mathbf{B}\tilde{\mathbf{e}}$, unrecoverable. To recover $\tilde{\mathbf{e}}$, note that the normal equations of (2.31) which lead to (2.32) also provide a solution to the Lagrange vector $\hat{\lambda} = -\left(\mathbf{B}\mathbf{P}^{-1}\mathbf{B}^T\right)^{-1}\left(\mathbf{w} - \mathbf{A}\hat{\xi}\right)$. One Lagrange-Euler necessary condition, $\mathbf{P}\tilde{\mathbf{e}} - \mathbf{B}^T\hat{\lambda} \doteq \mathbf{0}$, allows the observation residual vector to be computed directly as

$$\begin{aligned}\tilde{\mathbf{e}} &= \mathbf{P}^{-1}\mathbf{B}^T\left(\mathbf{B}\mathbf{P}^{-1}\mathbf{B}^T\right)^{-1}\left(\mathbf{w} - \mathbf{A}\hat{\xi}\right)\\ &= \mathbf{P}^{-1}\mathbf{B}^T\left(\mathbf{B}\mathbf{P}^{-1}\mathbf{B}^T\right)^{-1}\left(\mathbf{I} - \mathbf{A}\left(\mathbf{A}^T\left(\mathbf{B}\mathbf{P}^{-1}\mathbf{B}^T\right)^{-1}\mathbf{A}\right)^{-1}\mathbf{A}^T\left(\mathbf{B}\mathbf{P}^{-1}\mathbf{B}^T\right)^{-1}\right)\mathbf{w} \qquad (2.35)\\ &= \mathbf{P}^{-1}\mathbf{B}^T\bar{\mathbf{P}}\left(\mathbf{I} - \mathbf{A}\bar{\mathbf{N}}^{-1}\mathbf{A}^T\bar{\mathbf{P}}\right)\mathbf{w} \quad ,\end{aligned}$$

with $\bar{\mathbf{N}} = \mathbf{A}^T\left(\mathbf{B}\mathbf{P}^{-1}\mathbf{B}^T\right)^{-1}\mathbf{A}$ and $\bar{\mathbf{P}} = \left(\mathbf{B}\mathbf{P}^{-1}\mathbf{B}^T\right)^{-1}$. The residual cofactor matrix may be computed from (2.35),

$$\mathbf{Q}_{\tilde{e}} = \mathbf{P}^{-1}\mathbf{B}^T\bar{\mathbf{P}}\left(\mathbf{I} - \mathbf{A}\bar{\mathbf{N}}^{-1}\mathbf{A}^T\bar{\mathbf{P}}\right)\mathbf{B}\mathbf{P}^{-1}, \qquad (2.36)$$

which, combined with (2.35), allows us to express, as we did for the Gauss-Markov model, a transformation from the observation vector to the residual vector in terms of the residual cofactor matrix:

$$\tilde{\mathbf{e}} = \mathbf{Q}_{\tilde{\mathbf{e}}}\mathbf{P}\mathbf{y}\,. \qquad (2.37)$$

In obvious analogy to (2.5), we now have a reliability matrix, **R**, for the Gauss-Helmert model. We extend the model (2.31) to include the possibility of multiple outliers

$$\mathbf{w} = \mathbf{A}\xi + (\mathbf{B}\mathbf{Z})\,\xi_o + \mathbf{B}\mathbf{e} \qquad \mathbf{e} \sim \left(\mathbf{0}, \sigma_o^2\mathbf{P}^{-1}\right) \qquad (2.38)$$

and, with the reliability matrix defined in (2.37), we may use formulas (2.21) – (2.28) to test for outliers in model (2.31).

We will not address the Gauss-Helmert model further, except to note the numerous photogrammetric operations (affine transforms for inner orientation, three-dimensional similarity transforms for absolute orientation, coplanarity conditions for relative orientation, least-squares matches of gray scale patches in automated orientation procedures, and more) that require the Gauss-Helmert model.

CHAPTER 3

THE GAUSS-MARKOV MODEL WITH STOCHASTIC AND FIXED CONSTRAINTS

We will consider two types of constraints on the Gauss Markov (GM) model: stochastic and fixed. Stochastic constraints may be considered as additional observation equations in the GM model – expressing observations as a (non-)linear function of the model parameters - which differ from the "original" observation equations only in that they are considered to come from another measurement source entirely. Therefore, the observations typically are uncorrelated with the "original" observations and exhibit a perhaps significantly different covariance matrix. Examples of external observations that may be modeled as stochastic constraints in a photogrammetric bundle adjustment include but are certainly not limited to:

i. GPS observations in the form of Cartesian coordinates of ground points or baselines between two ground points,
ii. GPS observations of exposure centers,
iii. total station observations of distance, azimuth, or angle between two points,
iv. relationships between ground points or between ground points and orientation parameters arising from the implicit scene geometry such as four or more points known to lie in a plane,
v. inertial navigation system (INS) observations of platform orientation, and
vi. photo-coordinate observations from additional imagery from another source (e.g. air-borne frame camera imagery "constraining" space-borne pushbroom array imagery).

Stochastic constraints are also treated as additional uncorrelated observations used to "update" a parameter estimate (see for example, Leick, 1995).

Fixed constraint equations, unlike stochastic constraints which are modeled with random error, must be satisfied exactly by the estimated parameter vector. This type of constraint may result from any of the examples cited previously by ignoring the random errors associated with the observations. In many cases, fixed constraints are used to provide datum information to an otherwise rank-deficient model or to test hypotheses concerning parameter estimates.

3.1 Background and summary of results

Stochastic constraints on model parameters extend the Gauss-Markov model as follows,

$$\begin{bmatrix}\mathbf{y}\\ \mathbf{z}\end{bmatrix} = \begin{bmatrix}\mathbf{A}\\ \mathbf{K}\end{bmatrix}\xi + \begin{bmatrix}\mathbf{e}_y\\ \mathbf{e}_z\end{bmatrix} \qquad \begin{bmatrix}\mathbf{e}_y\\ \mathbf{e}_z\end{bmatrix} \sim \left(\begin{bmatrix}\mathbf{0}\\ \mathbf{0}\end{bmatrix}, \sigma_o^2 \begin{bmatrix}\mathbf{P}_y^{-1} & \mathbf{0}\\ \mathbf{0} & \mathbf{P}_z^{-1}\end{bmatrix}\right) \tag{3.1}$$

where

- $\mathbf{y}$, $\mathbf{A}$, and ξ remain unchanged from model (2.1),
- $\mathbf{e}_y$ is the unknown random error vector with second moment $\sigma_o^2\mathbf{P}_y^{-1}$ (equivalent to $\mathbf{e}$ and $\mathbf{P}$ in model (2.1)),
- $\mathbf{z}$ is an l x 1 random vector of observations related to the constraint equations (or, when $\mathbf{K}$ is the Jacobian of the linearized constraint equations, a vector of incremental changes in observations),
- $\mathbf{K}$ is an l x m non-random design matrix, typically of rank l, built from the linear relationships between the parameters to be estimated and the constraint observations (again, this is typically the Jacobian matrix defining a local differential relationship between parameters and observations), and
- $\mathbf{e}_z$ is the l x 1 unknown random error vector with first and second moments given, with the positive definite matrix $\mathbf{P}_z$ known and σ_o^2 not necessarily known.

When written this way, model (3.1) emphasizes the structural equivalency of the stochastic constraint equations with the original observation equations while at the same time partitioning them so that the effects of constraints on (3.1) may be analyzed and tested for consistency. The two sets of equations share a standard variance component (often considered unity, though this isn't required), have distinct cofactor matrices, and are uncorrelated. From here forward, we will refer to the "original" observation equations (contained in $\mathbf{y}$, $\mathbf{A}$ and $\mathbf{e}_y$) as the base equations, the base partition, or the base observations. The stochastic or fixed constraints we refer to as simply the constraints with their nature being clear from the context.

The WLESS principle requires us to make the Lagrange target function

$$\Phi = (\mathbf{y} - \mathbf{A}\xi)^T \mathbf{P}_y (\mathbf{y} - \mathbf{A}\xi) + \mathbf{e}_z \mathbf{P}_z \mathbf{e}_z - 2\lambda(\mathbf{z} - \mathbf{K}\xi - \mathbf{e}_z) \tag{3.2}$$

stationary with respect to $\xi,\ \lambda,\ \text{and}\ e_z$ yielding the normal equations

$$\begin{bmatrix} \mathbf{N} & \mathbf{K}^T \\ \mathbf{K} & -\mathbf{P}_z^{-1} \end{bmatrix} \begin{bmatrix} \hat{\xi}_s \\ \hat{\lambda}_s \end{bmatrix} = \begin{bmatrix} \mathbf{c} \\ \mathbf{z} \end{bmatrix} \tag{3.3}$$

and the weighted least squares solution to (3.1). If the target function (3.2) is modified so that the second sum of residuals is zero, the resulting normal equations are valid in the case of fixed constraints, i.e. constraints in which $\mathbf{P}_z^{-1} \to \mathbf{0}$. In this case, (3.3) becomes

$$\begin{bmatrix} \mathbf{N} & \mathbf{K}^T \\ \mathbf{K} & \mathbf{0} \end{bmatrix} \begin{bmatrix} \hat{\xi}_f \\ \hat{\lambda}_f \end{bmatrix} = \begin{bmatrix} \mathbf{c} \\ \mathbf{z} \end{bmatrix} \tag{3.4}$$

Solutions for the constrained parameter vectors and their dispersion matrices are developed by eliminating $\hat{\lambda}_s$ and $\hat{\lambda}_f$ from (3.3) and (3.4) respectively. The solutions of both (3.3) and (3.4) depend upon the rank of $\mathbf{A}$ and $\mathbf{K}$ so we will consider the following four cases, all more or less occurring in practice, for the normal equations in both (3.3) and (3.4). After examining each case and summarizing solutions to the normal equations, we will look at a simple but practical example of an adjustment of a small trilateration network.

Case 1: $rk(\mathbf{N}) = q = m$, $rk\left(\begin{bmatrix} \mathbf{A}^T & \mathbf{K}^T \end{bmatrix}\right) = m$. The base equations alone are sufficient to estimate the parameters, while the additional constraints serve to strengthen the solution by improving the precision of the estimate, $D\{\hat{\xi}_s\}$ or $D\{\hat{\xi}_f\}$, and/or increasing the reliability of the observations (we shall investigate this possibility in the next chapter). These and other relevant expressions are summarized in Tables 3.1 and 3.2 below. Derivations of these expressions are readily found in the literature (Koch,1999, Leick, 1995). Because the base partition is sufficient to estimate a unique parameter vector, all the expressions in Tables 3.1 and 3.2 may be written in terms of the unconstrained estimate $\hat{\xi} = \mathbf{N}^{-1}\mathbf{c}$. A close look at the results in the tables shows in this case, the fixed constraint results are fully equivalent with the stochastic constraint results when $\mathbf{P}_z^{-1} \to \mathbf{0}$. The one expression that may not be used interchangeably is (3.3) since it requires the non-existent $\mathbf{P}_z$. However, (3.2) is valid and correctly produces $\bar{\mathbf{e}}_z = \mathbf{0}$. The same restriction applies to the two formulas in (3.15).

Case 2: $rk(\mathbf{N}) = q < m$, $rk\left(\begin{bmatrix} \mathbf{A}^T & \mathbf{K}^T \end{bmatrix}\right) = m$, $rk\mathbf{A} + rk\mathbf{K} = q + l > m$. The base observations are not sufficient to uniquely estimate the parameter vector (in photogrammetric and geodetic applications this is usually due to the lack of a datum) while the constraints add more than enough information to estimate the parameter vector – that is, the constraints not only add datum information, they add redundant model information. While it is possible to estimate the parameter vector from the base observations by the choice of an appropriate reflexive symmetric generalized inverse of $\mathbf{N}$ (see Case 3 below), the resulting estimate will be biased by the choice of datum implied by the generalized inverse. Now, while any subset of the *m-q* constraints (since $\mathbf{K}$ has full row rank) will serve to define the datum without invalidating the base normal equations (that is, maintaining $\mathbf{N}\hat{\xi}_s = \mathbf{c}$ and $\mathbf{N}\hat{\xi}_f = \mathbf{c}$), the remaining redundant constraints on the

parameter vector do indeed invalidate the base normal equations ($\mathbf{N}\hat{\xi}_s \neq \mathbf{c}$ and $\mathbf{N}\hat{\xi}_f \neq \mathbf{c}$), perturbing both the residual vector and its covariance matrix. For this reason it is not possible to analytically show the change from the unconstrained results to the constrained results as we did in Case 1. This is true even if we introduce the generalized inverse into the expressions in Tables 3.1 and 3.2 because the chosen generalized-inverse will, in general, be inconsistent with the datum specified by the constraints. However, there are conditions in which replacing $\mathbf{N}^{-1}$ with $\mathbf{N}_{rs}^{-}$ in the expressions is consistent. Case 4 examines these conditions.

Case 3: $rk(\mathbf{N}) = q < m$, $rk\left(\begin{bmatrix}\mathbf{A}^T & \mathbf{K}^T\end{bmatrix}\right) = m$, $rk\mathbf{A} + rk\mathbf{K} = q + l = m$. The base observations are not sufficient to uniquely estimate the parameter vector while the constraints add exactly enough information to uniquely estimate the parameter vector. These restrictions may be considered a special case of Case 2. The restrictions on $\mathbf{K}$ – that $\Re\left(\mathbf{K}^T\right) \oplus \Re\left(\mathbf{A}^T\right) = \mathbb{R}^m$ - along with the introduction of the null-space spanning *m* x (*m*-*q*) matrix $\mathbf{E}^{\mathbf{T}}$ ($\mathbf{A}\mathbf{E}^T = \mathbf{0}$ and thus $\mathbf{N}\mathbf{E}^T = \mathbf{0}$) result in the relationships

$$\begin{aligned}\left(\mathbf{N} + \mathbf{K}^T\mathbf{P}_z\mathbf{K}\right)\mathbf{E}^T &= \mathbf{K}^T\mathbf{P}_z\mathbf{K}\mathbf{E}^T \\ \left(\mathbf{N} + \mathbf{K}^T\mathbf{P}_z\mathbf{K}\right)\mathbf{E}^T\left(\mathbf{K}\mathbf{E}^T\right)^{-1} &= \mathbf{K}^T\mathbf{P}_z \\ \mathbf{E}^T\left(\mathbf{K}\mathbf{E}^T\right)^{-1} &= \left(\mathbf{N} + \mathbf{K}^T\mathbf{P}_z\mathbf{K}\right)^{-1}\mathbf{K}^T\mathbf{P}_z\end{aligned} \tag{3.5}$$

which may be used to simplify the expressions in Tables 3.3 and 3.4. By setting $\mathbf{P}_z = \mathbf{I}_{m-q}$, the relations may be used for the fixed constraint case. In particular, introducing the third and fourth equalities into the expressions in Table 3.3 and 3.4 result in the new expressions in Tables 3.5 and 3.6. If $\mathbf{z} = \mathbf{0}$ then the stochastic results in this case are identical to Case 2. The constraints in this case are often called the minimal constraints and while they "select" a particular parameter vector from the general (particular plus homogenous) solution, they do not disturb the residual vector nor its covariance matrix since $\bar{\mathbf{e}}_y = \left(\mathbf{P}_y^{-1} - \mathbf{A}\mathbf{N}_{rs}^{-}\mathbf{A}^T\right)\mathbf{P}_y\mathbf{y}$ and $\mathbf{Q}_{\bar{\mathbf{e}}_y} = \mathbf{P}_y^{-1} - \mathbf{A}\mathbf{N}_{rs}^{-}\mathbf{A}^T$ are invariant with respect to the choice of generalized inverse – or equivalently, to the choice of $\mathbf{K}$. This is different from both Cases 1 and 2 where $\bar{\mathbf{e}}_y$ is indeed disturbed by the additional constraints. Minimal constraints therefore will not affect the observation reliability and will only be considered in the context of filling the rank-deficiency of the normal equations. In fact, minimal constraints are addressed in Chapter 2 by the use of a reflexive symmetric generalized inverse.

Case 4: $rk(\mathbf{N}) = q < m$, $rk\left(\begin{bmatrix}\mathbf{A}^T & \mathbf{K}^T\end{bmatrix}\right) = q$. The constraints do not add any datum-defining information but do provide additional redundancy to the estimable parameters. Note that the constrained residual vectors (3.10, 3.11, 3.12, 3.13, and 3.23, 3.24, 3.25) and their covariance matrices (3.14, 3.15, 3.16 and 3.26) are invariant with respect to the choice of generalized inverse of $\mathbf{N}$ because the rows of $\mathbf{K}$ are elements of the column space of $\mathbf{A}^{\mathbf{T}}$ (that is, $\Re\left(\mathbf{K}^T\right) \subset \Re\left(\mathbf{A}^T\right)$). While this violates the conditions in Case 2, in particular the assumptions $rk\left(\begin{bmatrix}\mathbf{A}^T & \mathbf{K}^T\end{bmatrix}\right) = m$ and $rk\mathbf{A} + rk\mathbf{K} = q + l > m$, it occurs often enough in practice to be examined. As we will see in the trilateration example later in this chapter, this can occur in practice when constraints which do not provide datum information are added to the Gauss-Markov model. Under the conditions of Case 4, therefore, the expressions in Tables 3.1 and 3.2 are valid even when a reflexive symmetric generalized inverse is used in place of the full-rank normal equation inverse.

Value	Formula(s) : Case 1-Full-rank N, Stochastic Constraints	
$\hat{\xi}_s$	$\mathbf{N}^{-1}\mathbf{c}+\mathbf{N}^{-1}\mathbf{K}^T\left(\mathbf{P}_z^{-1}+\mathbf{K}\mathbf{N}^{-1}\mathbf{K}^T\right)^{-1}\left(\mathbf{z}-\mathbf{K}\mathbf{N}^{-1}\mathbf{c}\right)$	(3.6)
	$\hat{\xi}+\mathbf{N}^{-1}\mathbf{K}^T\left(\mathbf{P}_z^{-1}+\mathbf{K}\mathbf{N}^{-1}\mathbf{K}^T\right)^{-1}\left(\mathbf{z}-\mathbf{K}\hat{\xi}\right)$	(3.7)
$D\{\hat{\xi}_s\}$	$\sigma_o^2\left(\mathbf{N}^{-1}-\mathbf{N}^{-1}\mathbf{K}^T\left(\mathbf{P}_z^{-1}+\mathbf{K}\mathbf{N}^{-1}\mathbf{K}^T\right)^{-1}\mathbf{K}\mathbf{N}^{-1}\right)$	(3.8)
	$D\left\{\hat{\xi}\right\}-\sigma_o^2\mathbf{N}^{-1}\mathbf{K}^T\left(\mathbf{P}_z^{-1}+\mathbf{K}\mathbf{N}^{-1}\mathbf{K}^T\right)^{-1}\mathbf{K}\mathbf{N}^{-1}$	(3.9)
$\overline{\mathbf{e}}_y$	$\mathbf{y}-\mathbf{A}\hat{\xi}_s=\mathbf{y}-\mathbf{A}\mathbf{N}^{-1}\mathbf{c}-\mathbf{A}\mathbf{N}^{-1}\mathbf{K}^T\left(\mathbf{P}_z^{-1}+\mathbf{K}\mathbf{N}^{-1}\mathbf{K}^T\right)^{-1}\left(\mathbf{z}-\mathbf{K}\mathbf{N}^{-1}\mathbf{c}\right)$	(3.10)
	$\mathbf{Q}_{\overline{\mathbf{e}}_y}\mathbf{P}_y\mathbf{y}+\mathbf{Q}_{\overline{\mathbf{e}}_y\overline{\mathbf{e}}_z}\left(\mathbf{K}\mathbf{N}^{-1}\mathbf{K}^T\right)^{-1}\mathbf{z}$	(3.11)
$\overline{\mathbf{e}}_z$	$\mathbf{z}-\mathbf{K}\hat{\xi}_s=\mathbf{z}-\mathbf{K}\mathbf{N}^{-1}\mathbf{c}-\mathbf{K}\mathbf{N}^{-1}\mathbf{K}^T\left(\mathbf{P}_z^{-1}+\mathbf{K}\mathbf{N}^{-1}\mathbf{K}^T\right)^{-1}\left(\mathbf{z}-\mathbf{K}\mathbf{N}^{-1}\mathbf{c}\right)$ $=\left(I_l-\mathbf{K}\mathbf{N}^{-1}\mathbf{K}^T\left(\mathbf{P}_z^{-1}+\mathbf{K}\mathbf{N}^{-1}\mathbf{K}^T\right)^{-1}\right)\left(\mathbf{z}-\mathbf{K}\mathbf{N}^{-1}\mathbf{c}\right)$	(3.12)
	$\mathbf{z}-\mathbf{K}\hat{\xi}_s=\left(\mathbf{I}_l+\mathbf{K}^T\mathbf{N}^{-1}\mathbf{K}\mathbf{P}_z\right)^{-1}\left(\mathbf{z}-\mathbf{K}\mathbf{N}^{-1}\mathbf{c}\right)$	(3.13)
$\mathbf{Q}_{\overline{\mathbf{e}}_y}$	$\mathbf{P}_y^{-1}-\mathbf{A}\mathbf{N}^{-1}\mathbf{A}^T+\mathbf{A}\mathbf{N}^{-1}\mathbf{K}^T\left(\mathbf{P}_z^{-1}+\mathbf{K}\mathbf{N}^{-1}\mathbf{K}^T\right)^{-1}\mathbf{K}\mathbf{N}^{-1}\mathbf{A}^T$	(3.14)
$\mathbf{Q}_{\overline{\mathbf{e}}_z}$	$\mathbf{P}_z^{-1}-\mathbf{K}\mathbf{N}^{-1}\mathbf{K}^T+\mathbf{K}\mathbf{N}^{-1}\mathbf{K}^T\left(\mathbf{P}_z^{-1}+\mathbf{K}\mathbf{N}^{-1}\mathbf{K}^T\right)^{-1}\mathbf{K}\mathbf{N}^{-1}\mathbf{K}^T$	(3.15)
	$\mathbf{P}_z^{-1}-\left(\mathbf{I}_l+\mathbf{K}\mathbf{N}^{-1}\mathbf{K}^T\mathbf{P}_z\right)^{-1}\mathbf{K}\mathbf{N}^{-1}\mathbf{K}^T$ $\left(\mathbf{P}_z+\mathbf{P}_z\mathbf{K}\mathbf{N}^{-1}\mathbf{K}^T\mathbf{P}_z\right)^{-1}$	
$\mathbf{Q}_{\overline{\mathbf{e}}_y\overline{\mathbf{e}}_z}$	$-\mathbf{A}\mathbf{N}^{-1}\mathbf{K}^T+\mathbf{A}\mathbf{N}^{-1}\mathbf{K}^T\left(\mathbf{P}_z^{-1}+\mathbf{K}\mathbf{N}^{-1}\mathbf{K}^T\right)^{-1}\mathbf{K}\mathbf{N}^{-1}\mathbf{K}^T$	(3.16)
	$-\mathbf{A}\mathbf{N}^{-1}\mathbf{K}^T\left(\mathbf{I}_l+\mathbf{P}_z\mathbf{K}\mathbf{N}^{-1}\mathbf{K}^T\right)^{-1}$	
Ω_s	$\overline{\mathbf{e}}_y^T\mathbf{P}_y\overline{\mathbf{e}}_y+\overline{\mathbf{e}}_z^T\mathbf{P}_z\overline{\mathbf{e}}_z$	(3.17)
	$\mathbf{y}^T\mathbf{P}_y\mathbf{y}-\mathbf{y}^T\mathbf{P}_y\mathbf{A}\mathbf{N}^{-1}\mathbf{c}+(\mathbf{z}-\mathbf{K}\mathbf{N}^{-1}\mathbf{c})^T\left(\mathbf{P}_z^{-1}+\mathbf{K}\mathbf{N}^{-1}\mathbf{K}^T\right)^{-1}(\mathbf{z}-\mathbf{K}\mathbf{N}^{-1}\mathbf{c})$ $\Omega+(\mathbf{z}-\mathbf{K}\mathbf{N}^{-1}\mathbf{c})^T\left(\mathbf{P}_z^{-1}+\mathbf{K}\mathbf{N}^{-1}\mathbf{K}^T\right)^{-1}(\mathbf{z}-\mathbf{K}\mathbf{N}^{-1}\mathbf{c})$	(3.18)
$\hat{\sigma}_o^2$	$\Omega_s/(n-m+l)$	(3.19)

Table 3.1. Case 1: full-rank **N**, stochastic constraint results, *rk*(**K**)= *l*.

Value	Formula(s) : Case 1-Full-rank N, Fixed Constraints	
$\hat{\xi}_f$	$\mathbf{N}^{-1}\mathbf{c}+\mathbf{N}^{-1}\mathbf{K}^T\left(\mathbf{K}\mathbf{N}^{-1}\mathbf{K}^T\right)^{-1}\left(\mathbf{z}-\mathbf{K}\mathbf{N}^{-1}\mathbf{c}\right)$	(3.20)
	$\hat{\xi}+\mathbf{N}^{-1}\mathbf{K}^T\left(\mathbf{K}\mathbf{N}^{-1}\mathbf{K}^T\right)^{-1}\left(\mathbf{z}-\mathbf{K}\hat{\xi}\right)$	(3.21)
$D\{\hat{\xi}_f\}$	$\sigma_o^2\left(\mathbf{N}^{-1}-\mathbf{N}^{-1}\mathbf{K}^T\left(\mathbf{K}\mathbf{N}^{-1}\mathbf{K}^T\right)^{-1}\mathbf{K}\mathbf{N}^{-1}\right)$	(3.22)
$\overline{\mathbf{e}}_y$	$\mathbf{y}-\mathbf{A}\hat{\xi}_f$	(3.23)
	$\mathbf{y}-\mathbf{A}\mathbf{N}^{-1}\mathbf{c}-\mathbf{A}\mathbf{N}^{-1}\mathbf{K}^T\left(\mathbf{K}\mathbf{N}^{-1}\mathbf{K}^T\right)^{-1}\left(\mathbf{z}-\mathbf{K}\mathbf{N}^{-1}\mathbf{c}\right)$	(3.24)
	$\mathbf{Q}_{\overline{\mathbf{e}}_y}\mathbf{P}_y\mathbf{y}-\mathbf{A}\mathbf{N}^{-1}\mathbf{K}^T\left(\mathbf{K}\mathbf{N}^{-1}\mathbf{K}^T\right)^{-1}\mathbf{z}$	(3.25)
$\mathbf{Q}_{\overline{\mathbf{e}}_y}$	$\mathbf{P}_y^{-1}-\mathbf{A}\mathbf{N}^{-1}\mathbf{A}^T+\mathbf{A}\mathbf{N}^{-1}\mathbf{K}^T\left(\mathbf{K}\mathbf{N}^{-1}\mathbf{K}^T\right)^{-1}\mathbf{K}\mathbf{N}^{-1}\mathbf{A}^T$	(3.26)
Ω_f	$\overline{\mathbf{e}}_y^T\mathbf{P}_y\overline{\mathbf{e}}_y$	(3.27)
	$\mathbf{y}^T\mathbf{P}_y\mathbf{y}-\mathbf{y}^T\mathbf{P}_y\mathbf{A}\mathbf{N}^{-1}\mathbf{c}+(\mathbf{z}-\mathbf{K}\mathbf{N}^{-1}\mathbf{c})^T\left(\mathbf{K}\mathbf{N}^{-1}\mathbf{K}^T\right)^{-1}(\mathbf{z}-\mathbf{K}\mathbf{N}^{-1}\mathbf{c})$ $\Omega+(\mathbf{z}-\mathbf{K}\mathbf{N}^{-1}\mathbf{c})^T\left(\mathbf{K}\mathbf{N}^{-1}\mathbf{K}^T\right)^{-1}(\mathbf{z}-\mathbf{K}\mathbf{N}^{-1}\mathbf{c})$	(3.28)
$\hat{\sigma}_o^2$	$\Omega_f/(n-m+l)$	(3.29)

Table 3.2. Case 1: full-rank **N**, fixed constraint results, *rk*(**K**)=*l*

Value	Formula(s) : Case 2-Rank-deficient N, Stochastic Constraints	
$\hat{\xi}_s$	$\left(\mathbf{N}+\mathbf{K}^T\mathbf{P}_z\mathbf{K}\right)^{-1}\left(\mathbf{c}+\mathbf{K}^T\mathbf{P}_z\mathbf{z}\right)$	(3.30)
$D\{\hat{\xi}_s\}$	$\sigma_o^2\left(\mathbf{N}+\mathbf{K}^T\mathbf{P}_z\mathbf{K}\right)^{-1}$	(3.31)
$\overline{\mathbf{e}}_y$	$\mathbf{y}-\mathbf{A}\hat{\xi}_s=\mathbf{y}-\mathbf{A}\left(\mathbf{N}+\mathbf{K}^T\mathbf{P}_z\mathbf{K}\right)^{-1}\left(\mathbf{c}+\mathbf{K}^T\mathbf{P}_z\mathbf{z}\right)$	(3.32)
$\overline{\mathbf{e}}_z$	$\mathbf{z}-\mathbf{K}\hat{\xi}_s=\mathbf{z}-\mathbf{K}\left(\mathbf{N}+\mathbf{K}^T\mathbf{P}_z\mathbf{K}\right)^{-1}\left(\mathbf{c}+\mathbf{K}^T\mathbf{P}_z\mathbf{z}\right)$	(3.33)
$\begin{bmatrix}\mathbf{Q}_{\overline{\mathbf{e}}_y} & \mathbf{Q}_{\overline{\mathbf{e}}_y\overline{\mathbf{e}}_z}\\ \mathbf{Q}_{\overline{\mathbf{e}}_z\overline{\mathbf{e}}_y} & \mathbf{Q}_{\overline{\mathbf{e}}_z}\end{bmatrix}$	$\begin{bmatrix}\mathbf{P}_y^{-1}-\mathbf{A}\left(\mathbf{N}+\mathbf{K}^T\mathbf{P}_z\mathbf{K}\right)^{-1}\mathbf{A}^T & -\mathbf{A}\left(\mathbf{N}+\mathbf{K}^T\mathbf{P}_z\mathbf{K}\right)^{-1}\mathbf{K}^T\\ -\mathbf{K}\left(\mathbf{N}+\mathbf{K}^T\mathbf{P}_z\mathbf{K}\right)^{-1}\mathbf{A}^T & \mathbf{P}_z^{-1}-\mathbf{K}\left(\mathbf{N}+\mathbf{K}^T\mathbf{P}_z\mathbf{K}\right)^{-1}\mathbf{K}^T\end{bmatrix}$	(3.34)
Ω_s	$\overline{\mathbf{e}}_y^T\mathbf{P}_y\overline{\mathbf{e}}_y+\overline{\mathbf{e}}_z^T\mathbf{P}_z\overline{\mathbf{e}}_z$	(3.35)
$\hat{\sigma}_o^2$	$\Omega_s/(n-m+l)$	(3.36)

Table 3.3. Case 2: rank-deficient **N**, stochastic constraint results.

Value	Formula(s) : Case 2-Rank-deficient N, Fixed Constraints
$\hat{\xi}_f$	$\left(\mathbf{N}+\mathbf{K}^T\mathbf{K}\right)^{-1}\mathbf{c}+\left(\mathbf{N}+\mathbf{K}^T\mathbf{K}\right)^{-1}\mathbf{K}^T\left(\mathbf{K}\left(\mathbf{N}+\mathbf{K}^T\mathbf{K}\right)^{-1}\mathbf{K}^T\right)^{-1}\left(\mathbf{z}-\mathbf{K}\left(\mathbf{N}+\mathbf{K}^T\mathbf{K}\right)^{-1}\mathbf{c}\right)$ (3.37)
$D\{\hat{\xi}_f\}$	$\sigma_o^2\left(\left(\mathbf{N}+\mathbf{K}^T\mathbf{K}\right)^{-1}-\left(\mathbf{N}+\mathbf{K}^T\mathbf{K}\right)^{-1}\mathbf{K}^T\left(\mathbf{K}\left(\mathbf{N}+\mathbf{K}^T\mathbf{K}\right)^{-1}\mathbf{K}^T\right)^{-1}\mathbf{K}\left(\mathbf{N}+\mathbf{K}^T\mathbf{K}\right)^{-1}\right)$ (3.38)
$\overline{\mathbf{e}}_y$	$\mathbf{y}-\mathbf{A}\hat{\xi}_f$ (3.39) $\mathbf{y}-\mathbf{A}\left(\mathbf{N}+\mathbf{K}^T\mathbf{K}\right)^{-1}\mathbf{c}-\mathbf{A}\left(\mathbf{N}+\mathbf{K}^T\mathbf{K}\right)^{-1}\mathbf{K}^T\left(\mathbf{K}\left(\mathbf{N}+\mathbf{K}^T\mathbf{K}\right)^{-1}\mathbf{K}^T\right)^{-1}\left(\mathbf{z}-\mathbf{K}\left(\mathbf{N}+\mathbf{K}^T\mathbf{K}\right)^{-1}\mathbf{c}\right)$ (3.40) $\mathbf{Q}_{\overline{\mathbf{e}}_y}\mathbf{P}_y\mathbf{y}-\mathbf{A}\left(\mathbf{N}+\mathbf{K}^T\mathbf{K}\right)^{-1}\mathbf{K}^T\left(\mathbf{K}\left(\mathbf{N}+\mathbf{K}^T\mathbf{K}\right)^{-1}\mathbf{K}^T\right)^{-1}\mathbf{z}$ (3.41)
$\mathbf{Q}_{\overline{\mathbf{e}}_y}$	$\mathbf{P}_y^{-1}-\mathbf{A}\left(\mathbf{N}+\mathbf{K}^T\mathbf{K}\right)^{-1}\mathbf{A}^T+\mathbf{A}\left(\mathbf{N}+\mathbf{K}^T\mathbf{K}\right)^{-1}\mathbf{K}^T\left(\mathbf{K}\left(\mathbf{N}+\mathbf{K}^T\mathbf{K}\right)^{-1}\mathbf{K}^T\right)^{-1}\mathbf{K}\left(\mathbf{N}+\mathbf{K}^T\mathbf{K}\right)^{-1}\mathbf{A}^T$ (3.42)
Ω_f	$\overline{\mathbf{e}}_y^T\mathbf{P}_y\overline{\mathbf{e}}_y$ (3.43) $\mathbf{y}^T\mathbf{P}_y\mathbf{y}-\mathbf{c}^T\left(\mathbf{N}+\mathbf{K}^T\mathbf{K}\right)^{-1}\mathbf{c}-\mathbf{z}^T\mathbf{z}+\left(\mathbf{z}-\hat{\lambda}\right)^T\mathbf{K}\left(\mathbf{N}+\mathbf{K}^T\mathbf{K}\right)^{-1}\mathbf{K}^T\left(\mathbf{z}-\hat{\lambda}\right)$ with $\left(\mathbf{z}-\hat{\lambda}\right)=\left(\mathbf{K}\left(\mathbf{N}+\mathbf{K}^T\mathbf{K}\right)^{-1}\mathbf{K}^T\right)^{-1}\left(\mathbf{z}-\mathbf{K}\left(\mathbf{N}+\mathbf{K}^T\mathbf{K}\right)^{-1}\mathbf{c}\right)$ (3.44)
$\hat{\sigma}_o^2$	$\Omega_f/(n-m+l)$ (3.45)

Table 3.4. Case 2: rank-deficient **N**, fixed constraint results.

Value	Formula(s) : Case 3-Rank-deficient N, Stochastic Minimum Constraints
$\hat{\xi}$	$\left(\mathbf{N}+\mathbf{K}^T\mathbf{P}_z\mathbf{K}\right)^{-1}\mathbf{c}+\mathbf{E}^T\left(\mathbf{K}\mathbf{E}^T\right)^{-1}\mathbf{z}$ (3.46)
$D\{\hat{\xi}\}$	$\sigma_o^2\left(\mathbf{N}+\mathbf{K}^T\mathbf{P}_z\mathbf{K}\right)^{-1} \quad \in\left\{\mathbf{N}_s^- \mid \mathbf{N}\mathbf{N}_s^-\mathbf{N}=\mathbf{N},\ \mathbf{N}_s^-=\left(\mathbf{N}_s^-\right)^T\right\}$ (3.47)
$\tilde{\mathbf{e}}_y$	$\mathbf{y}-\mathbf{A}\hat{\xi}$ (3.48) $\mathbf{y}-\mathbf{A}\left(\mathbf{N}+\mathbf{K}^T\mathbf{P}_z\mathbf{K}\right)^{-1}\mathbf{c}$ (3.49)
$\tilde{\mathbf{e}}_z$	$\mathbf{z}-\mathbf{K}\hat{\xi}$ (3.50) $\mathbf{z}-\mathbf{K}\left(\mathbf{N}+\mathbf{K}^T\mathbf{P}_z\mathbf{K}\right)^{-1}\mathbf{c}+\mathbf{K}\mathbf{E}^T\left(\mathbf{K}\mathbf{E}^T\right)^{-1}\mathbf{z}=\mathbf{0}$ (3.51)
$\begin{bmatrix}\mathbf{Q}_{\tilde{\mathbf{e}}_y} & \mathbf{Q}_{\tilde{\mathbf{e}}_y\tilde{\mathbf{e}}_z}\\ \mathbf{Q}_{\tilde{\mathbf{e}}_z\tilde{\mathbf{e}}_y} & \mathbf{Q}_{\tilde{\mathbf{e}}_z}\end{bmatrix}$	$\begin{bmatrix}\mathbf{P}_y^{-1} & \mathbf{0}\\ \mathbf{0} & \mathbf{P}_z^{-1}\end{bmatrix}-\begin{bmatrix}\mathbf{A}\left(\mathbf{N}+\mathbf{K}^T\mathbf{P}_z\mathbf{K}\right)^{-1}\mathbf{A}^T & \mathbf{0}\\ \mathbf{0} & \mathbf{P}_z^{-1}\end{bmatrix}=\begin{bmatrix}\mathbf{P}_y^{-1}-\mathbf{A}\left(\mathbf{N}+\mathbf{K}^T\mathbf{P}_z\mathbf{K}\right)^{-1}\mathbf{A}^T & \mathbf{0}\\ \mathbf{0} & \mathbf{0}\end{bmatrix}$ (3.52)
Ω	$\tilde{\mathbf{e}}_y^T\mathbf{P}_y\tilde{\mathbf{e}}_y$ (3.53)
$\hat{\sigma}_o^2$	$\Omega/(n-q)$ (3.54)

Table 3.5. Case 3 rank-deficient **N**, minimum stochastic constraint results.

Value	Formula(s) : Case 3-Rank-deficient N, Fixed Minimum Constraints
$\hat{\xi}$	$\left(\mathbf{N}+\mathbf{K}^T\mathbf{K}\right)^{-1}\mathbf{c}+\mathbf{E}^T\left(\mathbf{K}\mathbf{E}^T\right)^{-1}\mathbf{z}$ (3.55)
$D\{\hat{\xi}\}$	$\sigma_o^2\left(\mathbf{N}+\mathbf{K}^T\mathbf{K}\right)^{-1}\mathbf{N}\left(\mathbf{N}+\mathbf{K}^T\mathbf{K}\right)^{-1} \in \left\{\mathbf{N}_{rs}^- \mid \mathbf{N}\mathbf{N}_{rs}^-\mathbf{N}=\mathbf{N}\ ,\ \mathbf{N}_{rs}^-\mathbf{N}\mathbf{N}_{rs}^-=\mathbf{N}_{rs}^-\ ,\ \mathbf{N}_{rs}^-=\left(\mathbf{N}_{rs}^-\right)^T\right\}$ (3.56)
	$\sigma_o^2\left(\left(\mathbf{N}+\mathbf{K}^T\mathbf{K}\right)^{-1}-\mathbf{E}^T\left(\mathbf{E}\mathbf{K}^T\mathbf{K}\mathbf{E}^T\right)^{-1}\mathbf{E}\right)$ (3.57)
$\tilde{\mathbf{e}}_y$	$\mathbf{y}-\mathbf{A}\hat{\xi}$ (3.58)
$\mathbf{Q}_{\hat{\mathbf{e}}_y}$	$\mathbf{P}_y^{-1}-\mathbf{A}\left(\mathbf{N}+\mathbf{K}^T\mathbf{K}\right)^{-1}\mathbf{A}^T$ (3.59)
Ω	$\tilde{\mathbf{e}}_y^T\mathbf{P}_y\tilde{\mathbf{e}}_y$ (3.60)
$\hat{\sigma}_o^2$	$\Omega/(n-q)$ (3.61)

Table 3.6. Case 3: rank-deficient **N**, minimum fixed constraint results

3.2 Trilateration example

To show how constraints might be applied in practice, some results from (2.5 – 2.61) may be applied to a simple but illustrative example. We consider a five station trilateration network (Figure 3.1) with eight distance observations (made with some type of EDM) among the five stations. This two-dimensional network, like many photogrammetric and geodetic networks, is datum-deficient. It lacks a point of origin and orientation, resulting in a rank-deficiency of three in the design matrix. Furthermore, the constraints do not provide information to fix any of the three orientation parameters. With only the information given in Figure 1, this network meets the conditions of Case 4.

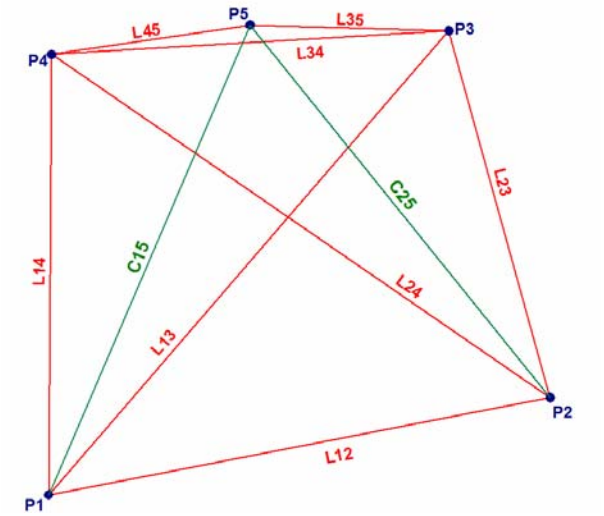

Distance Observations (meters)
L45 = 34.94
L35 = 34.61
L23 = 66.52
L34 = 69.29
L12 = 89.00
L14 = 76.97
L24 = 105.53
L13 = 106.95

Constraint Observations (meters)
C15 = 89.3085
C25 = 83.5083

Base Observations variance
σ_o^2 0.0001 meters

Constraint variance
σ_o^2 0.0004 meters

Initial Point Approximations (X,Y, meters)
P1 = 100 , 100
P2 = 187 , 117
P3 = 117 , 181
P4 = 110 , 177
P5 = 135 , 182

Figure 3.1. Five station trilateration network with constraints.

The eight non-linear observation equations relating parameters to observations are $\rho_{ij}^2=\left(x_j-x_i\right)^2+\left(y_j-y_i\right)^2$ for points $i,j=1...5$. The total differentials of these equations, $d\rho_{ij}=\frac{\left(x_i-x_j\right)}{\rho_{ij}}dx_i+\frac{\left(x_j-x_i\right)}{\rho_{ij}}dx_j+\frac{\left(y_i-y_j\right)}{\rho_{ij}}dy_i+\frac{\left(y_j-y_i\right)}{\rho_{ij}}dy_j$, allow us to construct the (rank-deficient) *8x10* design matrix, while the *8x1* observation vector is formed as $y_k=L_{ij}-\rho_{ij}^o$ where *k*

represents any of the eight observations shown in the figure in the order listed in the figure. All of the point coordinates (absent the datum definition) are over-determined except point P5. Perhaps the simplest way to define the datum is to fix the *x* and *y* coordinates of P1 and the *x* coordinate of P2. To do this we define the parameter vector as $\xi^T = \begin{bmatrix} dx_1 & dy_1 & dx_2 & dy_2 & \cdots & dx_5 & dy_5 \end{bmatrix}$ and partition it as $\xi^T = \begin{bmatrix} x_1 & y_1 & x_2 & \xi_2^T \end{bmatrix} = \begin{bmatrix} \xi_1^T & \xi_2^T \end{bmatrix}$ so that the generalized inverse would take the form $\begin{bmatrix} \mathbf{N}_{11} & \mathbf{N}_{12} \\ \mathbf{N}_{21} & \mathbf{N}_{22} \end{bmatrix}^- = \begin{bmatrix} \mathbf{0} & \mathbf{0} \\ \mathbf{0} & \mathbf{N}_{22}^{-1} \end{bmatrix}$ and the unconstrained solution $\xi_1^o = \mathbf{0}$ and $\hat{\xi}_2 = \mathbf{N}_{22}^{-1}\mathbf{c}_2$. Using the Gauss-Markov results in Chapter 1 we find the relevant unconstrained solutions:

$\hat{\xi}_2^T = \begin{bmatrix} -0.0059 & -0.2939 & 0.1230 & -0.4610 & -0.0294 & 0.1084 & 0.0465 \end{bmatrix}$

with dispersion matrix

$$D\left\{\hat{\xi}_2\right\} = \sigma_o^2 \begin{bmatrix} 0.246 & - & - & - & - & - & - \\ -0.201 & 0.177 & - & - & - & - & - \\ 0.185 & -0.154 & 0.146 & - & - & - & - \\ -0.183 & 0.158 & -0.139 & 0.148 & - & - & - \\ -0.003 & 0.005 & -0.003 & 0.006 & 0.009 & - & - \\ -0.203 & 0.178 & -0.155 & 0.160 & 0.006 & 0.186 & - \\ 0.130 & -0.130 & 0.104 & -0.074 & 0.011 & -0.161 & 1.002 \end{bmatrix}.$$

The residual vector $\tilde{\mathbf{e}}^T = \begin{bmatrix} 0 & 0 & -0.0013 & -0.0015 & -0.0013 & -0.0011 & 0.0018 & -0.0017 \end{bmatrix}$ shows the effect of zero redundancy in the measurements to P5. The weighted sum of squared residuals is estimated at 0.122, while the reliability numbers of the observations, $r \equiv vecdiag(\mathbf{R}) = \begin{bmatrix} 0 & 0 & 0.13 & 0.17 & 0.11 & 0.10 & 0.25 & 0.24 \end{bmatrix}^T$, reveal zero reliability of these same two observations L45 and L35 – that is, errors in these two observations would be completely absorbed by the coordinates of P5 and could not be detected with the previously described tests. In the language of Förstner (1994) outliers or blunders in these observations would go *undetected* while observation L14 would be the least *locatable* of the observations with a redundancy of 0.10. In terms of inner reliability, it is typical to establish a threshold of $\delta_o = 4$, corresponding to an error probability of $\alpha = 1\%$ (implying that we are willing to accept all observations less than 2.56 standard deviations away from the mean), and a power $\beta = 93\%$. Therefore, from (2.17) each of the observations must be $\begin{bmatrix} \infty & \infty & 11.1 & 9.7 & 12.0 & 12.6 & 8.0 & 8.2 \end{bmatrix}$ times larger than σ_o or its estimate, $\hat{\sigma}_o$, to be detected in such a test. Errors in the first two observations may not be detected at all. With an average redundancy of 0.12 per observation and no reliability number greater than 0.25, this network would be considered unreliable without constraints.

If an undetectible error in L14 did occur, one that was, say, 12.0 times larger than the square root of the variance (0.02 meters), then applying (2.18), we obtain $\left[\delta\hat{\xi}^{(j)}\right]^T = \begin{bmatrix} 0 & 0 & 0 & 0 & -0.03 & -0.03 & -0.02 & 0.21 & 0.04 & 0.04 \end{bmatrix}$ and see that the outlier affects all coordinates except those of the fixed point P1 and the partially fixed P2. However, we see significant changes in the *y* coordinate of P4.

The constraints take the same form as the observation equations. Considering the random errors we use the expressions in Table 1 and see that the changes to the parameter vector $\left(\hat{\xi}_2 - \hat{\xi}_{2_s}\right)^T = \begin{bmatrix} 0.0014 & 0.0001 & 0.0006 & -0.0032 & -0.0011 & 0.0021 & -0.0692 \end{bmatrix}$ are uniformly small (millimeter or less) except in the *y* coordinate of P5. This was the weakest parameter in the unconstrained solution with a variance of 1.002 m^2 which with the addition of the stochastic constraints improved to 0.032 m^2. However, the weighted sum of squared residuals increases almost five-fold to 0.677. If we do

not consider the random error associated with the constraint equations we use the expressions in Table 2 to estimate the parameter vector and obtain the change $\left(\hat{\xi}_2 - \hat{\xi}_{2_f}\right)^T = \begin{bmatrix} 0.0041 & -0.0021 & 0.0027 & -0.0055 & -0.0012 & 0.0000 & -0.0720 \end{bmatrix}$ in the parameter vector along with the dispersion of the weak parameter which improves to 0.0006 m^2. This is to be expected considering the assumed strength of the constraints. As in the stochastic case the addition of the fixed constraints increased the weighted sum of squared residuals to 0.720.

It is important to note that, although we adjusted the network to the observations, we could have analyzed the reliability of the network based only on the model and the initial values of the parameters. In the next chapter we will look into the change in reliability of the observations when these constraints are taken into account.

CHAPTER 4

ANALYTICAL RELIABILITY IN CONSTRAINED GAUSS-MARKOV MODELS

Having examined important concepts first from reliability analysis in the Gauss Markov model and then summarized results from the constrained Gauss Markov model, we are ready to integrate the two concepts to produce expressions for the reliability matrix, inner reliability, and outer reliability in the constrained Gauss Markov model. Again we have two general forms to consider: stochastic and fixed constraints and within these forms we must consider both full-rank and rank-deficient design matrices. We will not address Case 3 (the case of minimum constraints can be naturally handled by the choice of $\mathbf{N}_{rs}^{-}$ in the rank deficient Gauss-Markov model) and will concern ourselves with estimable parameters only so that Case 4 reduces to Case 1. For both forms we begin with the reliability matrix (defined consistently as the matrix which maps the observation vector to the predicted residual vector) and use it in expressions with which to test the outlier hypothesis and expressions for inner and outer reliability. Expression of the reliability matrices is straightforward since the residual dispersion matrices were defined in the previous chapter. However, in order to fully develop expressions for inner and outer reliability we must start with the equivalent of expression (2.6) in which a presumed outlier in the base observation vector (or possible in the stochastic constraints) is modeled as an additional parameter and integrate it first with the normal equations of the stochastically constrained Gauss-Markov model (3.3) and then with those of the fully constrained Gauss-Markov model (3.4).

4.1. Reliability considering stochastic constraints

The reliability matrix for the stochastically constrained Gauss-Markov model, both with full-rank and with rank-deficiency, may be formed by writing (3.10) and (3.13) in terms of (3.14)-(3.16)

$$\begin{bmatrix}\bar{\mathbf{e}}_y\\ \bar{\mathbf{e}}_z\end{bmatrix}=\begin{bmatrix}\mathbf{P}_y^{-1}-\mathbf{A}\left(\mathbf{N}+\mathbf{K}^T\mathbf{P}_z\mathbf{K}\right)^{-1}\mathbf{A}^T & -\mathbf{A}\left(\mathbf{N}+\mathbf{K}^T\mathbf{P}_z\mathbf{K}\right)^{-1}\mathbf{K}^T\\ -\mathbf{K}\left(\mathbf{N}+\mathbf{K}^T\mathbf{P}_z\mathbf{K}\right)^{-1}\mathbf{A}^T & \mathbf{P}_z^{-1}-\mathbf{K}\left(\mathbf{N}+\mathbf{K}^T\mathbf{P}_z\mathbf{K}\right)^{-1}\mathbf{K}^T\end{bmatrix}\begin{bmatrix}\mathbf{P}_y & \mathbf{0}\\ \mathbf{0} & \mathbf{P}_z\end{bmatrix}\begin{bmatrix}\mathbf{y}\\ \mathbf{z}\end{bmatrix}$$
$$=\begin{bmatrix}\mathbf{Q}_{\tilde{e}_y} & \mathbf{Q}_{\tilde{e}_y\tilde{e}_z}\\ \mathbf{Q}_{\tilde{e}_z\tilde{e}_y} & \mathbf{Q}_{\tilde{e}_z}\end{bmatrix}\begin{bmatrix}\mathbf{P}_y & \mathbf{0}\\ \mathbf{0} & \mathbf{P}_z\end{bmatrix}\begin{bmatrix}\mathbf{y}\\ \mathbf{z}\end{bmatrix}=\begin{bmatrix}\bar{\mathbf{R}}_y & \bar{\mathbf{R}}_{yz}\\ \bar{\mathbf{R}}_{zy} & \bar{\mathbf{R}}_z\end{bmatrix}\begin{bmatrix}\mathbf{y}\\ \mathbf{z}\end{bmatrix} \tag{4.1}$$

in which the $\bar{\mathbf{R}}_y$ and $\bar{\mathbf{R}}_{yz}$ blocks map the observations into the base residuals and the $\bar{\mathbf{R}}_{zy}$ and $\bar{\mathbf{R}}_z$ blocks map the observations into the constraint residuals. Under the conditions of Case 2, we may go no farther. However, if the model meets the conditions of Case 1 (where all the parameters are estimable and $\mathbf{N}_{rs}^{-}=\mathbf{N}^{-1}$) or Case 4 (in which we are working only with the estimable part of the parameters, defined by $\xi_{est}\equiv\mathbf{N}_{rs}^{-}\mathbf{A}^T\mathbf{P}_y\mathbf{A}\xi$), we may factor out the unconstrained reliability matrix, $\mathbf{R}$, and write

$$\begin{bmatrix}\bar{\mathbf{R}}_y & \bar{\mathbf{R}}_{yz}\\ \bar{\mathbf{R}}_{zy} & \bar{\mathbf{R}}_z\end{bmatrix}=\begin{bmatrix}\mathbf{R} & \mathbf{0}\\ \mathbf{0} & \mathbf{0}\end{bmatrix}+\begin{bmatrix}\delta\mathbf{R}_y & \delta\mathbf{R}_{yz}\\ \delta\mathbf{R}_{zy} & \delta\mathbf{R}_z\end{bmatrix} \tag{4.2}$$

where several formulas are available the changes

$$\begin{aligned}\delta\mathbf{R}_y &= \mathbf{A}\mathbf{N}_{rs}^{-}\mathbf{K}^T\left(\mathbf{P}_z^{-1}+\mathbf{K}\mathbf{N}_{rs}^{-}\mathbf{K}^T\right)^{-1}\mathbf{K}\mathbf{N}_{rs}^{-}\mathbf{A}^T\mathbf{P}_y\\ &= \mathbf{A}\mathbf{N}_{rs}^{-}\mathbf{K}^T\mathbf{P}_z\left(\mathbf{I}_l+\mathbf{K}\mathbf{N}_{rs}^{-}\mathbf{K}^T\mathbf{P}_z\right)^{-1}\mathbf{K}\mathbf{N}_{rs}^{-}\mathbf{A}^T\mathbf{P}_y\,.\\ &= \mathbf{A}\mathbf{N}_{rs}^{-}\mathbf{K}^T\mathbf{P}_z\mathbf{K}\left(\mathbf{N}+\mathbf{K}^T\mathbf{P}_z\mathbf{K}\right)^{-1}\mathbf{A}^T\mathbf{P}_y\end{aligned}$$

$$\delta\mathbf{R}_z = \mathbf{I}_l - \mathbf{K}\mathbf{N}_{rs}^{-}\mathbf{K}^T\mathbf{P}_z + \mathbf{K}\mathbf{N}_{rs}^{-}\mathbf{K}^T\left(\mathbf{P}_z^{-1} + \mathbf{K}\mathbf{N}_{rs}^{-}\mathbf{K}^T\right)^{-1}\mathbf{K}\mathbf{N}_{rs}^{-}\mathbf{K}^T\mathbf{P}_z$$

$$= \left(\mathbf{I}_l + \mathbf{K}\mathbf{N}_{rs}^{-}\mathbf{K}^T\mathbf{P}_z\right)^{-1}$$

$$\delta\mathbf{R}_{yz} = -\mathbf{A}\mathbf{N}_{rs}^{-}\mathbf{K}^T\mathbf{P}_z + \mathbf{A}\mathbf{N}_{rs}^{-}\mathbf{K}^T\left(\mathbf{P}_z^{-1} + \mathbf{K}\mathbf{N}_{rs}^{-}\mathbf{K}^T\right)^{-1}\mathbf{K}\mathbf{N}_{rs}^{-}\mathbf{K}^T\mathbf{P}_z$$

$$= -\mathbf{A}\mathbf{N}_{rs}^{-}\mathbf{K}^T\mathbf{P}_z\left(\mathbf{I}_l + \mathbf{K}\mathbf{N}_{rs}^{-}\mathbf{K}^T\mathbf{P}_z\right)^{-1}$$

$$\delta\mathbf{R}_{zy} = -\mathbf{K}\mathbf{N}_{rs}^{-}\mathbf{A}^T\mathbf{P}_y + \mathbf{K}\mathbf{N}_{rs}^{-}\mathbf{K}^T\left(\mathbf{P}_z^{-1} + \mathbf{K}\mathbf{N}_{rs}^{-}\mathbf{K}^T\right)^{-1}\mathbf{K}\mathbf{N}_{rs}^{-}\mathbf{A}^T\mathbf{P}_y$$

$$= -\left(\mathbf{I}_l + \mathbf{K}\mathbf{N}_{rs}^{-}\mathbf{K}^T\mathbf{P}_z\right)^{-1}\mathbf{K}\mathbf{N}_{rs}^{-}\mathbf{A}^T\mathbf{P}_y$$

From the changes $\delta\mathbf{R}_y$ it seems that since $\delta\mathbf{R}_y$ is positive semi-definite the constraints increase the redundancy and reliability of the model. Note that this does not necessarily mean that every the redundancy of every observation is increases. It is clear, too, that as the constraints become more precise, that is as $\mathbf{P}_z^{-1}$ decreases, reliability for **y** increases, but not for **z**. Finally, we note that the reliability matrix must map both the observation vector, **y**, and the constraining observations, **z**, into the residuals $\bar{\mathbf{e}}_y$. We do not consider the residuals $\bar{\mathbf{e}}_z$ here because model (4.1) assumes that outliers are present only in the base observations. We will fully derive the reliability matrix for the fixed constraint model in the next section, but notice here that as $\mathbf{P}_z^{-1}$ approaches **0**, $\delta\mathbf{R}_z$ and $\delta\mathbf{R}_{zy}$ also approach **0** as we would expect since the fixed constraints are satisfied exactly, not leaving room for any effect through outliers. Considering the trace elements of $\begin{bmatrix}\bar{\mathbf{R}}_y & \bar{\mathbf{R}}_{yz}\\ \bar{\mathbf{R}}_{zy} & \bar{\mathbf{R}}_z\end{bmatrix}$ and their relationship to redundancy, we may show from (4.1) that the constrained reliability matrix is idempotent and therefore,

$$tr\left(\begin{bmatrix}\bar{\mathbf{R}}_y & \bar{\mathbf{R}}_{yz}\\ \bar{\mathbf{R}}_{zy} & \bar{\mathbf{R}}_z\end{bmatrix}\right) = tr\left(\begin{bmatrix}\mathbf{I}_n & \mathbf{0}\\ \mathbf{0} & \mathbf{I}_l\end{bmatrix}\right) - rk\left(\begin{bmatrix}\mathbf{A}\left(\mathbf{N}+\mathbf{K}^T\mathbf{P}_z\mathbf{K}\right)^{-1}\mathbf{A}^T\mathbf{P}_y & \mathbf{A}\left(\mathbf{N}+\mathbf{K}^T\mathbf{P}_z\mathbf{K}\right)^{-1}\mathbf{K}^T\mathbf{P}_z\\ \mathbf{K}\left(\mathbf{N}+\mathbf{K}^T\mathbf{P}_z\mathbf{K}\right)^{-1}\mathbf{A}^T\mathbf{P}_y & \mathbf{K}\left(\mathbf{N}+\mathbf{K}^T\mathbf{P}_z\mathbf{K}\right)^{-1}\mathbf{K}^T\mathbf{P}_z\end{bmatrix}\right) = n+l-q.$$ Thus $tr\left(\bar{\mathbf{R}}_y\right) < n-q+l$ so that the additional redundancy coming from the constraints is spread among the constraints as well as the base observations. If $\left(\mathbf{N}+\mathbf{K}^T\mathbf{P}_z\mathbf{K}\right)$ is singular (Case 4), then we may use (4.2) to arrive at the same results.

With the extended reliability matrix defined we are now in a position to revisit the extended Gauss-Markov model, written to accommodate a group of *c* outliers – because most photogrammetric observations involve image points or lines with at least two observations per measurement – in the base observations as additional parameters

$$\begin{bmatrix}\mathbf{y}\\ \mathbf{z}\end{bmatrix} = \begin{bmatrix}\mathbf{A}\\ \mathbf{K}\end{bmatrix}\xi + \begin{bmatrix}\mathbf{Z}\\ \mathbf{0}\end{bmatrix}\xi_0 + \begin{bmatrix}\mathbf{e}_y\\ \mathbf{e}_z\end{bmatrix} \qquad \begin{bmatrix}\mathbf{e}_y\\ \mathbf{e}_z\end{bmatrix} \sim \left(\begin{bmatrix}\mathbf{0}\\ \mathbf{0}\end{bmatrix}, \sigma_o^2\begin{bmatrix}\mathbf{P}_y^{-1} & \mathbf{0}\\ \mathbf{0} & \mathbf{P}_z^{-1}\end{bmatrix}\right), \tag{4.3}$$

with **Z** and ξ_o as defined in (2.20), and the outliers assumed to be in the base observations. The WLESS is the solution to the normal equations

$$\begin{bmatrix}\mathbf{Z}^T\mathbf{P}_y\mathbf{Z} & \mathbf{Z}^T\mathbf{P}_y\mathbf{A} & \mathbf{0}\\ \mathbf{A}^T\mathbf{P}_y\mathbf{Z} & \mathbf{N} & \mathbf{K}^T\\ \mathbf{0} & \mathbf{K} & -\mathbf{P}_z^{-1}\end{bmatrix}\begin{bmatrix}\hat{\xi}_o^{(Z)}\\ \hat{\xi}_s^{(Z)}\\ \hat{\lambda}_s\end{bmatrix} = \begin{bmatrix}\mathbf{Z}^T\mathbf{P}_y\mathbf{y}\\ \mathbf{A}^T\mathbf{P}_y\mathbf{y}\\ \mathbf{z}\end{bmatrix} = \begin{bmatrix}\mathbf{Z}^T\mathbf{P}_y\mathbf{y}\\ \mathbf{c}\\ \mathbf{z}\end{bmatrix}. \tag{4.4}$$

From here we follow the same path as with the Gauss-Markov model: First find the WLESS to the unknown parameters and the corresponding residual vectors and then find the increase in the weighted sum of squared residuals when the outlier is not modeled. This increase will provide a test statistic to determine

if a group of observations should be treated as outliers. From the second and third parts of the normal equations we find $\hat{\lambda}_s = -\mathbf{P}_z\left(\mathbf{z} - \mathbf{K}\hat{\xi}_s^{(Z)}\right)$ and $\left(\mathbf{A}^T\mathbf{P}_y\mathbf{Z}\right)\hat{\xi}_o^{(Z)} + \left(\mathbf{N} + \mathbf{K}^T\mathbf{P}_z\mathbf{K}\right)\hat{\xi}_s^{(Z)} = \mathbf{c} + \mathbf{K}^T\mathbf{P}_z\mathbf{z}$, leading to the estimate for the parameter vector

$$\begin{aligned}\hat{\xi}_s^{(Z)} &= \left(\mathbf{N} + \mathbf{K}^T\mathbf{P}_z\mathbf{K}\right)^{-1}\left(\mathbf{c} + \mathbf{K}^T\mathbf{P}_z\mathbf{z} - \mathbf{A}^T\mathbf{P}_y\mathbf{Z}\hat{\xi}_o^{(Z)}\right)\\ &= \left(\mathbf{N} + \mathbf{K}^T\mathbf{P}_z\mathbf{K}\right)^{-1}\left(\mathbf{c} + \mathbf{K}^T\mathbf{P}_z\mathbf{z}\right) - \left(\mathbf{N} + \mathbf{K}^T\mathbf{P}_z\mathbf{K}\right)^{-1}\mathbf{A}^T\mathbf{P}_y\mathbf{Z}\hat{\xi}_o^{(Z)} \qquad (4.5)\\ &= \hat{\xi}_s - \left(\mathbf{N} + \mathbf{K}^T\mathbf{P}_z\mathbf{K}\right)^{-1}\mathbf{A}^T\mathbf{P}_y\mathbf{Z}\hat{\xi}_o^{(Z)}\end{aligned}$$

which is equivalent in form to (2.22) and shows the change in the parameter vector due to the effects of the outliers. Conditions in Case 1 or Case 4 allow us to expand (4.5) to

$$\hat{\xi}_s^{(Z)} = \hat{\xi}_s - \left(\mathbf{N}_{rs}^- - \mathbf{N}_{rs}^-\mathbf{K}\left(\mathbf{P}_z^{-1} + \mathbf{K}\mathbf{N}_{rs}^-\mathbf{K}^T\right)^{-1}\mathbf{K}^T\mathbf{N}_{rs}^-\right)\mathbf{A}^T\mathbf{P}_y\mathbf{Z}\hat{\xi}_o^{(Z)}. \qquad (4.6)$$

Likewise, an estimate for the outlier may be written

$$\hat{\xi}_o^{(Z)} = \left(\mathbf{Z}^T\mathbf{P}_y\mathbf{Z} - \mathbf{Z}^T\mathbf{P}_y\mathbf{A}\left(\mathbf{N} + \mathbf{K}^T\mathbf{P}_z\mathbf{K}\right)^{-1}\mathbf{A}^T\mathbf{P}_y\mathbf{Z}\right)^{-1}\left(\mathbf{Z}^T\mathbf{P}_y\mathbf{y} - \mathbf{Z}^T\mathbf{P}_y\mathbf{A}\left(\mathbf{N} + \mathbf{K}^T\mathbf{P}_z\mathbf{K}\right)^{-1}\left(\mathbf{c} + \mathbf{K}^T\mathbf{P}_z\mathbf{z}\right)\right) \qquad (4.7)$$

or more simply, using $\begin{bmatrix}\mathbf{Q}_{\bar{\mathbf{e}}_y} & \mathbf{Q}_{\bar{\mathbf{e}}_y\bar{\mathbf{e}}_z}\\ \mathbf{Q}_{\bar{\mathbf{e}}_z\bar{\mathbf{e}}_y} & \mathbf{Q}_{\bar{\mathbf{e}}_z}\end{bmatrix}$ from (3.34)

$$\begin{aligned}\hat{\xi}_o^{(Z)} &= \left(\begin{bmatrix}\mathbf{Z}^T & \mathbf{0}\end{bmatrix}\begin{bmatrix}\mathbf{P}_y & \mathbf{0}\\ \mathbf{0} & \mathbf{P}_z\end{bmatrix}\begin{bmatrix}\mathbf{Q}_{\bar{\mathbf{e}}_y} & \mathbf{Q}_{\bar{\mathbf{e}}_y\bar{\mathbf{e}}_z}\\ \mathbf{Q}_{\bar{\mathbf{e}}_z\bar{\mathbf{e}}_y} & \mathbf{Q}_{\bar{\mathbf{e}}_z}\end{bmatrix}\begin{bmatrix}\mathbf{P}_y & \mathbf{0}\\ \mathbf{0} & \mathbf{P}_z\end{bmatrix}\begin{bmatrix}\mathbf{Z}\\ \mathbf{0}\end{bmatrix}\right)^{-1}\left(\begin{bmatrix}\mathbf{Z}^T & \mathbf{0}\end{bmatrix}\begin{bmatrix}\mathbf{P}_y & \mathbf{0}\\ \mathbf{0} & \mathbf{P}_z\end{bmatrix}\begin{bmatrix}\mathbf{Q}_{\bar{\mathbf{e}}_y} & \mathbf{Q}_{\bar{\mathbf{e}}_y\bar{\mathbf{e}}_z}\\ \mathbf{Q}_{\bar{\mathbf{e}}_z\bar{\mathbf{e}}_y} & \mathbf{Q}_{\bar{\mathbf{e}}_z}\end{bmatrix}\begin{bmatrix}\mathbf{P}_y & \mathbf{0}\\ \mathbf{0} & \mathbf{P}_z\end{bmatrix}\begin{bmatrix}\mathbf{y}\\ \mathbf{z}\end{bmatrix}\right)\\ &= \left(\mathbf{Z}^T\mathbf{P}_y\mathbf{Q}_{\bar{\mathbf{e}}_y}\mathbf{P}_y\mathbf{Z}\right)^{-1}\left(\mathbf{Z}^T\mathbf{P}_y\mathbf{Q}_{\bar{\mathbf{e}}_y}\mathbf{P}_y\mathbf{y} + \mathbf{Z}^T\mathbf{P}_y\mathbf{Q}_{\bar{\mathbf{e}}_y\bar{\mathbf{e}}_z}\mathbf{P}_z\mathbf{z}\right) \qquad (4.8)\\ &= \left(\mathbf{Z}^T\mathbf{P}_y\bar{\mathbf{R}}_y\mathbf{Z}\right)^{-1}\left(\mathbf{Z}^T\mathbf{P}_y\bar{\mathbf{R}}_y\mathbf{y} + \mathbf{Z}^T\mathbf{P}_y\bar{\mathbf{R}}_{yz}\mathbf{z}\right)\end{aligned}$$

which is in form equivalent to (2.21). The difference between (2.21) and (4.8) lies in the definition of the reliability matrix and the influence of the constraining observations. Note that, since we modeled the outlier in the base observations only, the last *l* rows of the combined reliability matrix, $\begin{bmatrix}\bar{\mathbf{R}}_{zy} & \bar{\mathbf{R}}_z\end{bmatrix}$ do not enter into the estimation of the outlier. We may relax this assumption and model for outliers in both the base partition and in the stochastic constraints (which is not inappropriate given the shared variance component). In this case (4.3) may be treated as a partitioned Gauss-Markov model using results from Chapter 2. It is also important to remember that while $\bar{\mathbf{R}}_y\mathbf{y} \neq \bar{\mathbf{e}}_y$ and $\bar{\mathbf{R}}_{yz}\mathbf{z} \neq \bar{\mathbf{e}}_z$, (4.7) is consistent with (3.1), (3.4), and (4.1) since $\bar{\mathbf{R}}_y\mathbf{y} + \bar{\mathbf{R}}_{yz}\mathbf{z} = \bar{\mathbf{e}}_y$.

The change in the weighted sum of squared residuals may now be expressed as

$$\begin{aligned}\Omega_s - \Omega_s^{(Z)} &= \begin{bmatrix}\bar{\mathbf{e}}_y^T & \bar{\mathbf{e}}_z^T\end{bmatrix}\begin{bmatrix}\mathbf{P}_y & \mathbf{0}\\ \mathbf{0} & \mathbf{P}_z\end{bmatrix}\begin{bmatrix}\bar{\mathbf{e}}_y\\ \bar{\mathbf{e}}_z\end{bmatrix} - \left[\left(\mathbf{y} - \mathbf{A}\hat{\xi}_s^{(Z)} - \mathbf{Z}\hat{\xi}_o^{(Z)}\right)^T \;\middle|\; \left(\mathbf{z} - \mathbf{K}\hat{\xi}_s^{(Z)}\right)^T\right]\begin{bmatrix}\mathbf{P}_y & \mathbf{0}\\ \mathbf{0} & \mathbf{P}_z\end{bmatrix}\begin{bmatrix}\mathbf{y} - \mathbf{A}\hat{\xi}_s^{(Z)} - \mathbf{Z}\hat{\xi}_s^{(Z)}\\ \mathbf{z} - \mathbf{K}\hat{\xi}_s^{(Z)}\end{bmatrix}\\ &= \left[\hat{\xi}_o^{(Z)}\right]^T\begin{bmatrix}\mathbf{Z}^T & \mathbf{0}\end{bmatrix}\begin{bmatrix}\mathbf{P}_y & \mathbf{0}\\ \mathbf{0} & \mathbf{P}_z\end{bmatrix}\begin{bmatrix}\mathbf{Q}_{\bar{\mathbf{e}}_y} & \mathbf{Q}_{\bar{\mathbf{e}}_y\bar{\mathbf{e}}_z}\\ \mathbf{Q}_{\bar{\mathbf{e}}_z\bar{\mathbf{e}}_y} & \mathbf{Q}_{\bar{\mathbf{e}}_z}\end{bmatrix}\begin{bmatrix}\mathbf{P}_y & \mathbf{0}\\ \mathbf{0} & \mathbf{P}_z\end{bmatrix}\begin{bmatrix}\mathbf{Z}\\ \mathbf{0}\end{bmatrix}\hat{\xi}_o^{(Z)}\end{aligned}$$

or

$$\begin{aligned}\Omega_s - \Omega_s^{(Z)} &= \left[\hat{\xi}_o^{(Z)}\right]^T\mathbf{Z}^T\mathbf{P}_y\mathbf{Q}_{\bar{\mathbf{e}}_y}\mathbf{P}_y\mathbf{Z}\hat{\xi}_o^{(Z)}\\ &= \left[\hat{\xi}_o^{(Z)}\right]^T\mathbf{Z}^T\mathbf{P}_y\bar{\mathbf{R}}_y\mathbf{Z}\hat{\xi}_o^{(Z)}\end{aligned}, \qquad (4.9)$$

in a form identical to the unconstrained Gauss-Markov model with the differences again encapsulated in the estimate of the outlier and the reliability matrix. We may also write the change in the sum of squared residuals in terms of the original residuals themselves

$$\Omega_s - \Omega_s^{(Z)} = \left(\bar{\mathbf{R}}_y\mathbf{y} + \bar{\mathbf{R}}_{yz}\mathbf{z}\right)^T \mathbf{P}_y\mathbf{Z}\left(\mathbf{Z}^T\mathbf{P}_y\mathbf{Q}_{\bar{\mathbf{e}}_y}\mathbf{P}_y\mathbf{Z}\right)^{-1}\mathbf{Z}^T\mathbf{P}_y\left(\bar{\mathbf{R}}_y\mathbf{y} + \bar{\mathbf{R}}_{yz}\mathbf{z}\right)$$
$$= \bar{\mathbf{e}}_y^T\mathbf{P}_y\mathbf{Z}\left(\mathbf{Z}^T\mathbf{P}_y\mathbf{Q}_{\bar{\mathbf{e}}_y}\mathbf{P}_y\mathbf{Z}\right)^{-1}\mathbf{Z}^T\mathbf{P}_y\bar{\mathbf{e}}_y$$

As before, we use the expectation of (3.9),

$$E\left\{\left(\Omega_s - \Omega_s^{(Z)}\right)\Big/\sigma_o^2\right\} = c + \xi_o^T\mathbf{Z}^T\mathbf{P}_y\mathbf{Q}_{\bar{\mathbf{e}}_y}\mathbf{P}_y\mathbf{Z}\,\xi_o\Big/\sigma_o^2 = c + 2\vartheta_Z \tag{4.10}$$

to find the redundancy and non-centrality of the distribution of $\left(\Omega_s - \Omega_s^{(Z)}\right)\Big/\sigma_o^2$. It is important to note here that the non-centrality parameter involves only $\bar{\mathbf{R}}_y$ but that our estimate of the outlier requires the first full *n* rows of the extended reliability matrix, that is $\bar{\mathbf{R}}_{yz}$ in addition. From (3.8) and (3.9), and assuming both $\mathbf{e_y}$ and $\mathbf{e_z}$ are normally distributed, we may find under the hypothesis $H_o : \xi_o = \mathbf{0}$ that

$$\Omega_s\Big/\sigma_o^2 \sim \chi^2\left(n - rk(\mathbf{A}) + rk(\mathbf{K})\right) \quad \text{and} \quad \left(\Omega_s - \Omega_s^{(Z)}\right)\Big/\sigma_o^2 \sim \chi^2(c) \tag{4.11}$$

while under the alternative hypothesis $H_a : \xi_o \neq \mathbf{0}$

$$\Omega_s\Big/\sigma_o^2 \sim \chi^2\left(n - rk(\mathbf{A}) + rk(\mathbf{K}) - c\right) \quad \text{and} \quad \left(\Omega_s - \Omega_s^{(Z)}\right)\Big/\sigma_o^2 \sim \chi^2\left(c; 2\vartheta_j\right) \tag{4.12}$$

Aside from the increase in degrees of freedom due to the inclusion of constraints and the change in the expression for the sum of squared residuals, these tests are identical to the outlier tests in the Gauss-Markov model detailed in Chapter 2. With **R** replaced by $\bar{\mathbf{R}}_y$, the discussion of inner reliability in the Gauss-Markov model applies to the constrained model. Outer reliability may be computed accordingly, depending on which stochastic constraint case applies. For example, using (2.30)

$$\delta\hat{\xi}_s = \hat{\xi}_s - \hat{\xi}_s^{(Z)} = \left(\mathbf{N} + \mathbf{K}^T\mathbf{P}_z\mathbf{K}\right)^{-1}\left(\mathbf{A}^T\mathbf{P}_y\mathbf{Z}\hat{\xi}_o^{(Z)}\right) \quad . \tag{4.13}$$

we see the effects on the constrained estimate when **N** has full rank and/or **N** is rank-deficient but **K** provides sufficient information to remove the rank-deficiency (Cases 1, 2, or 3).

4.2. Reliability considering fixed constraints

We begin by describing the reliability matrix of the constrained model in Cases 1 and 4. Beginning with (3.25) from Table 3.2,

$$\begin{aligned}\bar{\mathbf{e}}_y &= \mathbf{y} - \mathbf{A}\mathbf{N}_{rs}^-\mathbf{A}^T\mathbf{P}_y\mathbf{y} - \mathbf{A}\mathbf{N}_{rs}^-\mathbf{K}^T\left(\mathbf{K}\mathbf{N}_{rs}^-\mathbf{K}^T\right)^{-1}\left(\mathbf{z} - \mathbf{K}\mathbf{N}_{rs}^-\mathbf{A}^T\mathbf{P}_y\mathbf{y}\right)\\ &= \left(\mathbf{P}_y^{-1} - \mathbf{A}\mathbf{N}_{rs}^-\mathbf{A}^T + \mathbf{A}\mathbf{N}_{rs}^-\mathbf{K}^T\left(\mathbf{K}\mathbf{N}_{rs}^-\mathbf{K}^T\right)^{-1}\mathbf{K}\mathbf{N}_{rs}^-\mathbf{A}^T\right)\mathbf{P}_y\mathbf{y} - \mathbf{A}\mathbf{N}^{-1}\mathbf{K}^T\left(\mathbf{K}\mathbf{N}_{rs}^-\mathbf{K}^T\right)^{-1}\mathbf{z}\ ,\end{aligned} \tag{4.14}$$

we may extract part of the partitioned reliability matrix and write it in terms of the unconstrained reliability matrix, **R**,

$$\begin{aligned}\left[\bar{\mathbf{R}}_y \quad \bar{\mathbf{R}}_{yz}\right] &= \left[\mathbf{I}_n - \mathbf{A}\mathbf{N}_{rs}^-\mathbf{A}^T\mathbf{P}_y + \mathbf{A}\mathbf{N}_{rs}^-\mathbf{K}^T\left(\mathbf{K}\mathbf{N}_{rs}^-\mathbf{K}^T\right)^{-1}\mathbf{K}\mathbf{N}_{rs}^-\mathbf{A}^T\mathbf{P}_y \;\Big|\; -\mathbf{A}\mathbf{N}_{rs}^-\mathbf{K}^T\left(\mathbf{K}\mathbf{N}_{rs}^-\mathbf{K}^T\right)^{-1}\right]\\ &= \left[\mathbf{R} \quad \mathbf{0}\right] + \left[\delta\bar{\mathbf{R}}_y \quad \delta\bar{\mathbf{R}}_{yz}\right]\end{aligned} \tag{4.15}$$

with

$$\delta\bar{\mathbf{R}}_y = \mathbf{A}\mathbf{N}_{rs}^-\mathbf{K}^T\left(\mathbf{K}\mathbf{N}_{rs}^-\mathbf{K}^T\right)^{-1}\mathbf{K}\mathbf{N}_{rs}^-\mathbf{A}^T\mathbf{P}_y$$

$$\delta\bar{\mathbf{R}}_{yz} = -\mathbf{A}\mathbf{N}_{rs}^-\mathbf{K}^T\left(\mathbf{K}\mathbf{N}_{rs}^-\mathbf{K}^T\right)^{-1}$$

in obvious analogy to (4.2) if $\mathbf{P}_z^{-1} \to \mathbf{0}$. The full reliability then reads

$$\begin{bmatrix}\bar{\mathbf{R}}_y & \bar{\mathbf{R}}_{yz}\\ \bar{\mathbf{R}}_{zy} & \bar{\mathbf{R}}_z\end{bmatrix} = \begin{bmatrix}\mathbf{R} & \mathbf{0}\\ \mathbf{0} & \mathbf{0}\end{bmatrix} + \begin{bmatrix}\delta\mathbf{R}_y & \delta\mathbf{R}_{yz}\\ \mathbf{0} & \mathbf{0}\end{bmatrix} \tag{4.16}$$

which is consistent with (2.4) in that it leads to $\overline{\mathbf{e}}_z = \mathbf{0}$ and, thus maps the **z** vector to itself with no "contamination" from the observation vector, **y**. Furthermore, $\overline{\mathbf{R}}_y$ is idempotent and $tr\left(\overline{\mathbf{R}}_y\right) = n - q + l$, indicating that the redundancy of the model is spread among the diagonal elements of $\overline{\mathbf{R}}_y$.

The WLESS to the extended Gauss-Markov model with fixed constraints and a single group of *c* outliers

$$\begin{aligned} \mathbf{y} &= \mathbf{A}\xi + \mathbf{Z}\xi_0 + \mathbf{e}_y \qquad\qquad \mathbf{e}_y \sim \left(\mathbf{0}, \sigma_o^2 \mathbf{P}_y^{-1}\right) \\ \mathbf{z} &= \mathbf{K}\xi \end{aligned} \tag{4.17}$$

is the solution to the normal equations

$$\begin{bmatrix} \mathbf{Z}^T\mathbf{P}_y\mathbf{Z} & \mathbf{Z}^T\mathbf{P}_y\mathbf{A} & \mathbf{0} \\ \mathbf{A}^T\mathbf{P}_y\mathbf{Z} & \mathbf{N} & \mathbf{K}^T \\ \mathbf{0} & \mathbf{K} & \mathbf{0} \end{bmatrix} \begin{bmatrix} \hat{\xi}_o^{(Z)} \\ \hat{\xi}_f^{(Z)} \\ \hat{\lambda} \end{bmatrix} = \begin{bmatrix} \mathbf{Z}^T\mathbf{P}_y\mathbf{y} \\ \mathbf{A}^T\mathbf{P}_y\mathbf{y} \\ \mathbf{z} \end{bmatrix} = \begin{bmatrix} \mathbf{Z}^T\mathbf{P}_y\mathbf{y} \\ \mathbf{c} \\ \mathbf{z} \end{bmatrix}$$

From the second and third normal equations $\hat{\lambda} = -\left(\mathbf{K}\mathbf{N}_{rs}^-\mathbf{K}^T\right)^{-1}\left(\mathbf{z} - \mathbf{K}\mathbf{N}_{rs}^-\mathbf{c} + \mathbf{K}\mathbf{N}_{rs}^-\mathbf{A}^T\mathbf{P}_y\mathbf{Z}\hat{\xi}_o^{(Z)}\right)$ which by substitution into the second normal equation leads to the parameter estimate

$$\begin{aligned} \hat{\xi}_f^{(Z)} &= \mathbf{N}_{rs}^-\left(\mathbf{c} + \mathbf{K}^T\left(\mathbf{K}\mathbf{N}_{rs}^-\mathbf{K}^T\right)^{-1}\left(\mathbf{z} - \mathbf{K}\mathbf{N}_{rs}^-\mathbf{c} + \mathbf{K}\mathbf{N}_{rs}^-\mathbf{A}^T\mathbf{P}_y\mathbf{Z}\hat{\xi}_o^{(Z)}\right) - \mathbf{A}^T\mathbf{P}_y\mathbf{Z}\hat{\xi}_o^{(Z)}\right) \\ &= \mathbf{N}_{rs}^-\mathbf{c} + \mathbf{N}_{rs}^-\mathbf{K}^T\left(\mathbf{K}\mathbf{N}_{rs}^-\mathbf{K}^T\right)^{-1}\left(\mathbf{z} - \mathbf{K}\mathbf{N}_{rs}^-\mathbf{c}\right) + \\ &\qquad \left(\mathbf{N}_{rs}^-\mathbf{K}^T\left(\mathbf{K}\mathbf{N}_{rs}^-\mathbf{K}^T\right)^{-1}\mathbf{K}\mathbf{N}_{rs}^-\mathbf{A}^T\mathbf{P}_y\mathbf{Z} - \mathbf{N}_{rs}^-\mathbf{A}^T\mathbf{P}_y\mathbf{Z}\right)\hat{\xi}_o^{(Z)} \\ &= \hat{\xi}_f - \left(\mathbf{N}_{rs}^-\mathbf{A}^T\mathbf{P}_y\mathbf{Z} - \mathbf{N}_{rs}^-\mathbf{K}^T\left(\mathbf{K}\mathbf{N}_{rs}^-\mathbf{K}^T\right)^{-1}\mathbf{K}\mathbf{N}_{rs}^-\mathbf{A}^T\mathbf{P}_y\mathbf{Z}\right)\hat{\xi}_o^{(Z)} \\ &= \hat{\xi}_f - \mathbf{N}_{rs}^-\left(\mathbf{I}_m - \mathbf{K}^T\left(\mathbf{K}\mathbf{N}_{rs}^-\mathbf{K}^T\right)^{-1}\mathbf{K}\mathbf{N}_{rs}^-\right)\mathbf{A}^T\mathbf{P}_y\mathbf{Z}\hat{\xi}_o^{(Z)} \end{aligned} \tag{4.18}$$

which again is in form similar to (1.22) but with an extra term. The change in the parameter vector estimate may be defined explicitly as

$$\delta\hat{\xi}_f^{(Z)} = \hat{\xi}_f - \hat{\xi}_f^{(Z)} = \mathbf{N}_{rs}^-\left(\mathbf{I}_m - \mathbf{K}^T\left(\mathbf{K}\mathbf{N}_{rs}^-\mathbf{K}^T\right)^{-1}\mathbf{K}\mathbf{N}_{rs}^-\right)\mathbf{A}^T\mathbf{P}_y\mathbf{Z}\hat{\xi}_o^{(Z)} \tag{4.19}$$

Substituting (4.18) in the first part of the normal equations leads to

$$\begin{aligned} &\left(\mathbf{Z}^T\mathbf{P}_y\mathbf{Z} - \mathbf{Z}^T\mathbf{P}_y\mathbf{A}\mathbf{N}_{rs}^-\mathbf{A}^T\mathbf{P}_y\mathbf{Z} + \mathbf{Z}^T\mathbf{P}_y\mathbf{A}\mathbf{N}_{rs}^-\mathbf{K}^T\left(\mathbf{K}\mathbf{N}_{rs}^-\mathbf{K}^T\right)^{-1}\mathbf{K}\mathbf{N}_{rs}^-\mathbf{A}^T\mathbf{P}_y\mathbf{Z}\right)\hat{\xi}_o^{(Z)} \\ &\qquad = \mathbf{Z}^T\mathbf{P}_y\mathbf{y} - \mathbf{Z}^T\mathbf{P}_y\mathbf{A}\hat{\xi}_f \end{aligned} \tag{4.20}$$

or, more simply by taking into account (3.26), (3.20), and the non-trivial part of the reliability matrix, $\begin{bmatrix}\overline{\mathbf{R}}_y & \overline{\mathbf{R}}_{yz}\end{bmatrix}$,

$$\begin{aligned} \hat{\xi}_o^{(Z)} &= \left(\mathbf{Z}^T\mathbf{P}_y\mathbf{Q}_{\overline{\mathbf{e}}_y}\mathbf{P}_y\mathbf{Z}\right)^{-1}\left(\mathbf{Z}^T\mathbf{P}_y\mathbf{Q}_{\overline{\mathbf{e}}_y}\mathbf{P}_y\mathbf{y} - \mathbf{Z}^T\mathbf{P}_y\mathbf{A}\mathbf{N}_{rs}^-\mathbf{K}^T\left(\mathbf{K}\mathbf{N}_{rs}^-\mathbf{K}^T\right)^{-1}\mathbf{z}\right) \\ &= \left(\mathbf{Z}^T\mathbf{P}_y\overline{\mathbf{R}}_y\mathbf{Z}\right)^{-1}\left(\mathbf{Z}^T\mathbf{P}_y\right)\begin{bmatrix}\overline{\mathbf{R}}_y & \overline{\mathbf{R}}_{yz}\end{bmatrix}\begin{bmatrix}\mathbf{y} \\ \mathbf{z}\end{bmatrix} \end{aligned} \tag{4.21}$$

which differs in form from the unconstrained Gauss-Markov model only by consideration of the constraining vector, **z**. It may also be useful to write the outlier estimate in terms of the residual vector from the original normal equations (4.4) using (3.25), respectively (4.14),

$$\hat{\xi}_o^{(Z)} = \left(\mathbf{Z}^T\mathbf{P}_y\mathbf{Q}_{\overline{\mathbf{e}}_y}\mathbf{P}_y\mathbf{Z}\right)^{-1}\left(\mathbf{Z}^T\mathbf{P}_y\overline{\mathbf{e}}_y\right) \tag{4.22}$$

The residual vector in the model with estimated outliers is

$$
\begin{aligned}
\overline{\mathbf{e}}^{(Z)} &= \mathbf{y} - \mathbf{A}\hat{\xi}_f^{(Z)} - \mathbf{Z}\hat{\xi}_o^{(Z)} \\
&= \mathbf{y} - \mathbf{A}\hat{\xi}_f - \left(-\mathbf{A}\mathbf{N}^{-1}\mathbf{K}^T\left(\mathbf{K}\mathbf{N}^{-1}\mathbf{K}^T\right)^{-1}\mathbf{K}\mathbf{N}^{-1}\mathbf{A}^T\mathbf{P}_y\mathbf{Z} + \mathbf{A}\mathbf{N}^{-1}\mathbf{A}^T\mathbf{P}_y\mathbf{Z} - \mathbf{Z}\right)\hat{\xi}_o^{(Z)} \\
&= \overline{\mathbf{e}}_y - \left(\mathbf{P}_y^{-1} - \mathbf{A}\mathbf{N}^{-1}\mathbf{A}^T + \mathbf{A}\mathbf{N}^{-1}\mathbf{K}^T\left(\mathbf{K}\mathbf{N}^{-1}\mathbf{K}^T\right)^{-1}\mathbf{K}\mathbf{N}^{-1}\mathbf{A}^T\right)\mathbf{P}_y\mathbf{Z}\hat{\xi}_o^{(Z)} \\
&= \overline{\mathbf{e}}_y - \mathbf{Q}_{\overline{\mathbf{e}}_y}\mathbf{P}_y\mathbf{Z}\hat{\xi}_o^{(Z)} \quad ,
\end{aligned}
\tag{4.23}
$$

implying that the change in the residual vector resulting from the addition of the outlier parameter is $\delta\overline{\mathbf{e}}^{(Z)} = \overline{\mathbf{e}}_y - \overline{\mathbf{e}}^{(Z)} = \mathbf{Q}_{\overline{\mathbf{e}}_y}\mathbf{P}_y\hat{\xi}_o^{(Z)}$. As in the case of stochastic constraints, these results show a strong similarity to the Gauss-Markov model with the primary differences encapsulated in the definition of $\mathbf{Q}_{\overline{\mathbf{e}}_y}, \hat{\xi}_o^{(j)}, \text{ and } \overline{\mathbf{e}}_y$. Using the results from (1.24), we may write the reduction in the sum of squared residuals resulting from the included outlier as

$$
\begin{aligned}
\Omega - \Omega^{(Z)} &= \left[\hat{\xi}_o^{(Z)}\right]^T\mathbf{Z}^T\mathbf{P}_y\mathbf{Q}_{\hat{e}_y}\mathbf{P}_y\mathbf{Z}\hat{\xi}_o^{(Z)} \\
&= \overline{\mathbf{e}}_y^T\mathbf{P}_y\mathbf{Z}\left(\mathbf{Z}^T\mathbf{P}_y\mathbf{Q}_{\hat{e}_y}\mathbf{P}_y\mathbf{Z}\right)^{-1}\mathbf{Z}^T\mathbf{P}_y\overline{\mathbf{e}}_y \quad .
\end{aligned}
\tag{4.24}
$$

In order to use $\left(\Omega - \Omega^{(Z)}\right)\Big/\sigma_o^2$ as a test statistic as before we need the expectation and dispersion of $\hat{\xi}_o^{(Z)}$. From (3.21)

$$
\begin{aligned}
E\left\{\hat{\xi}_o\right\} &= \left(\mathbf{Z}^T\mathbf{P}_y\mathbf{Q}_{\overline{\mathbf{e}}_y}\mathbf{P}_y\mathbf{Z}\right)^{-1}\left(\mathbf{Z}^T\mathbf{P}_y\mathbf{Q}_{\overline{\mathbf{e}}_y}\mathbf{P}_y\left(\mathbf{A}\xi + \mathbf{Z}\xi_o\right) - \mathbf{Z}^T\mathbf{P}_y\mathbf{A}\mathbf{N}_{rs}^-\mathbf{K}^T\left(\mathbf{K}\mathbf{N}_{rs}^-\mathbf{K}^T\right)^{-1}\mathbf{z}\right) \\
&= \xi_o + \left(\mathbf{Z}^T\mathbf{P}_y\mathbf{Q}_{\overline{\mathbf{e}}_y}\mathbf{P}_y\mathbf{Z}\right)^{-1}\left(\mathbf{Z}^T\mathbf{P}_y\mathbf{A}\xi - \mathbf{Z}^T\mathbf{P}_y\mathbf{A}\mathbf{N}_{rs}^-\mathbf{A}^T\mathbf{P}_y\mathbf{A}\xi + \mathbf{Z}^T\mathbf{P}_y\mathbf{A}\mathbf{N}_{rs}^-\mathbf{K}^T\left(\mathbf{K}\mathbf{N}_{rs}^-\mathbf{K}^T\right)^{-1}\left(\mathbf{K}\mathbf{N}_{rs}^-\mathbf{A}^T\mathbf{P}_y\mathbf{A}\xi - \mathbf{z}\right)\right) \\
&= \xi_o + \left(\mathbf{Z}^T\mathbf{P}_y\mathbf{Q}_{\overline{\mathbf{e}}_y}\mathbf{P}_y\mathbf{Z}\right)^{-1}\left(\mathbf{Z}^T\mathbf{P}_y\mathbf{A}\xi - \mathbf{Z}^T\mathbf{P}_y\mathbf{A}\xi + \mathbf{Z}^T\mathbf{P}_y\mathbf{A}\mathbf{N}_{rs}^-\mathbf{K}^T\left(\mathbf{K}\mathbf{N}_{rs}^-\mathbf{K}^T\right)^{-1}\left(\mathbf{K}\xi - \mathbf{z}\right)\right) \\
&= \xi_o
\end{aligned}
$$

while $D\left\{\hat{\xi}_o^{(Z)}\right\} = \sigma_o^2\left(\mathbf{Z}^T\mathbf{P}_y\mathbf{Q}_{\overline{\mathbf{e}}_y}\mathbf{P}_y\mathbf{Z}\right)^{-1}$ is also determined from (3.22). Assuming a normal distribution for $\mathbf{e}_y$ in the model (3.10) and thus a normal distribution for $\hat{\xi}_o^{(Z)}$, we may use the same theorems from Searle (1992) as before to find the degrees of freedom and non-centrality of the χ^2-distribution of (3.24)

$$
E\left\{\left(\Omega_s - \Omega_s^{(Z)}\right)\Big/\sigma_o^2\right\} = c + \xi_o^T\mathbf{Z}^T\mathbf{P}\mathbf{Q}_{\overline{\mathbf{e}}_y}\mathbf{P}_y\mathbf{Z}\,\xi_o\Big/\sigma_o^2 = c + 2\vartheta_Z \tag{4.25}
$$

It is important to note here that while the combined reliability matrix (3.16) plays a role in the change of the weighted sum of squared residuals (3.24) through $\overline{\mathbf{e}}_y$, only $\overline{\mathbf{R}}_y$ is used to determine the non-centrality parameter. We see no difference in basic form from the Gauss-Markov model with stochastic constraints and so we use the result described in (3.11) and (3.12) but with the outlier expression from (3.21) or (3.22). Inner and outer reliability may be evaluated as in the case of stochastic constraints but with the appropriate formulas for the reliability matrix and parameter vector estimates.

4.3 Trilateration example continued

We continue with the example begun in Section 2.3 to demonstrate how reliability is affected by the addition of stochastic or fixed constraints. We remember that the reliability numbers (or the diagonal of the reliability matrix) of the observations in the absence of constraints was

$r = vecdiag(\mathbf{R}) = \begin{bmatrix}0 & 0 & 0.13 & 0.17 & 0.11 & 0.10 & 0.25 & 0.24\end{bmatrix}^T$. We may compute the change in reliability due to the addition of the stochastic constraining distance observations C15 and C25 (see Figure 1) by applying (3.2) to find

$vecdiag\left(\delta\overline{\mathbf{R}}_y\right) = r_s - r = \begin{bmatrix}0.37 & 0.30 & 0.01 & 0.25 & 0.77 & 0.04 & 0.08 & 0.01\end{bmatrix}^T$. Notice that the elements of $vecdiag\left(\delta\overline{\mathbf{R}}_y\right)$ sum to 1.82 while the elements of $tr\left(\overline{\mathbf{R}}_z\right) = 0.18$ indicate that some of the additional

redundancy provided by the constraints is used to predict $\bar{\mathbf{e}}_z$. As we expected, the observations that share parameters with the constraints are affected the most, with observations L45 and L25 receiving all of their redundancy contribution from the constraints. The average redundancy of the network increases to a more acceptable value of 0.35.

Likewise, we may use (3.16) to compute the change in reliability due to the addition of fixed constraints to find $vecdiag\left(\delta\bar{\mathbf{R}}_y\right) = r_f - r = \begin{bmatrix} 0.39 & 0.32 & 0.01 & 0.26 & 0.87 & 0.05 & 0.09 & 0.01 \end{bmatrix}^T$ which shows the full redundancy increase of two provided by the constraints (since none of the redundancy is used to compute errors in **z**) and thus a slight improvement over the stochastic results. Notice that, with the constraints, observation L12 now has a very strong redundancy, only 13% below 1.0 in the fixed case. The average redundancy with these fixed constraints rises to 0.38.

CHAPER 5

DIFFERENTIAL RELIABILITY

In the previous chapter we derived a method to analytically look at the change in reliability of a model as constraints are added using only the current network geometry contained in the non-random design matrices **A** and **K**. In the case of purely linear models, in which the elements of the design matrices are constant (such as in leveling networks) we have a fairly complete picture of the network's reliability. However, in linearized models, in which the elements of the design matrices – now Jacobian matrices of the observations and constraint equations – depend upon the initial approximations (or "seed" values) of the parameters, we do not yet have a complete picture. The reliability matrix of the network also depends on seed values but we do not yet know how sensitive the reliability numbers are to small changes in seed values. Knowing this would aid in network design, allowing the practitioner to build redundancy into the network to stabilize the reliability matrix..

In this chapter we will develop a familiar measure that tells us the sensitivity of any given reliability number to changes in both **A** and **K** design matrices. We may consider the reliability matrices from (2.5), (4.2), and (4.16) as matrix functions of **A** and/or **K**, and construct the Jacobian matrix of these functions with respect to the design matrices. Large values in this Jacobian matrix indicate high sensitivities to the corresponding design matrix element. Throughout this section we will rely heavily upon the results from Magnus and Neudecker (1999).

5.1 Differential reliability in the Gauss-Markov model

In linearized models (including most geodetic and photogrammetric models) the elements of **A** are computed from the parameter "seed" values (we do not use the expression "estimates" to avoid confusion with the stochastic estimates resulting from the various models) $\boldsymbol{\Xi}^o$ in a first order Taylor series approximation – only the incremental changes of the estimated $\boldsymbol{\xi}$ in (2.1), (3.1), and (4.3) are considered random. These "seed" values, which may represent interior and exterior orientation parameters, ground point coordinates, ground-line parameters etc., have an effect on model reliability by changing the values in **A**. Incremental model changes, *d***A**, which occur due to incremental changes in seed values, cause incremental changes in the reliability matrix. The effects on the reliability matrix can be examined for a given *d***A** and large changes, especially on the diagonal elements of **R**, would indicate which seed values (which, of course, correspond to parameter values) have large effects on the reliability (either positively or negatively) of particular observations. This information might also be used to guide the addition of observations or constraints to control these parameters.

We will follow the approach of Magnus and Neudecker (1999) to compute a Jacobian matrix without trying to differentiate the complicated n^2 elements of **R**. First, we compute the differential of **R** and $\bar{\mathbf{R}}_y$ with respect to **A**, then vectorize the resulting matrix to obtain the expression

$$d\left(vec(\mathbf{R})\right) = J(\mathbf{R})d\left(vec(\mathbf{A})\right). \tag{5.1}$$

From this relation, J(**R**) follows as the Jacobian of *vec***R** with respect to *vec*(**A**)$^{\boldsymbol{T}}$.

Considering the Gauss-Markov model, the explicit relationship between the reliability matrix and the design matrix may be written

$$\mathbf{R} = \mathbf{I}_n - \mathbf{A}\mathbf{N}_{rs}^{-}\mathbf{A}^T\mathbf{P} \tag{5.2}$$

noting that the reliability matrix is non-linear in **A** and that $\mathbf{N}_{rs}^{-}$ is also a function of **A**. If we denote differential changes in a generic matrix, **M**, as *d***M**, then from the total derivative we find

$$d\mathbf{R} = -d\mathbf{A}\left(\mathbf{N}_{rs}^{-}\mathbf{A}^T\mathbf{P}\right) - \mathbf{A}\left(d\mathbf{N}_{rs}^{-}\right)\mathbf{A}^T\mathbf{P} - \mathbf{A}\mathbf{N}_{rs}^{-}d\mathbf{A}^T\mathbf{P}. \tag{5.3}$$

Expression (5.2) is invariant with respect to the choice of generalized inverse, but (5.3) requires $d\mathbf{N}_{rs}^{-}$ as a function of *d***A**.

5.1.1 The differential of reflexive symmetric generalized inverses

Before we derive a general expression for $d\mathbf{N}_{rs}^{-}$ we mention two specific generalized inverses, $\mathbf{N}^{-1}$, available when $\mathbf{N}$ is non-singular, and $\mathbf{N}^{+}$, the Moore-Penrose (or pseudo-) inverse (Magnus and Neudecker, 1999, Koch, 1999, Golub and Van Loan, 1996).

If $\mathbf{N}$ has full-rank then $d\mathbf{N}_{rs}^{-} = d\mathbf{N}^{-1}$ and, since $\mathbf{N}\mathbf{N}^{-1} = \mathbf{I}$ we may write $d\mathbf{N}\mathbf{N}^{-1} + \mathbf{N}d\mathbf{N}^{-1} = \mathbf{0}$ and write $d\mathbf{N}^{-1}$ in terms of $d\mathbf{N}$,

$$d\mathbf{N}^{-1} = -\mathbf{N}^{-1}d\mathbf{N}\mathbf{N}^{-1} \tag{5.4}$$

which may in turn be written in terms of $d\mathbf{A}$ since $d\mathbf{N} = d\mathbf{A}^T\mathbf{P}\mathbf{A} + \mathbf{A}^T\mathbf{P}\,d\mathbf{A}$. The second case is somewhat more involved but has been addressed by Magnus and Neudecker (1999, pages 152-154). Their derivation of $d\mathbf{N}^{+}$ makes use of the symmetry properties of projections involving the pseudo-inverse, namely $\mathbf{N}^{+}\mathbf{N} = \left(\mathbf{N}^{+}\mathbf{N}\right)^T$ and $\mathbf{N}\mathbf{N}^{+} = \left(\mathbf{N}\mathbf{N}^{+}\right)^T$, to arrive at the expression

$$d\mathbf{N}^{+} = -\mathbf{N}^{+}d\mathbf{N}\mathbf{N}^{+} + \left(\mathbf{N}^{+}\right)^2 d\mathbf{N}\left(I_m - \mathbf{N}\mathbf{N}^{+}\right) + \left(I_m - \mathbf{N}\mathbf{N}^{+}\right)d\mathbf{N}\left(\mathbf{N}^{+}\right)^2 \quad . \tag{5.5}$$

Either (5.4) or (5.5), may be substituted into (5.3) .

To compute $d\mathbf{N}_{rs}^{-}$ we express $\mathbf{N}_{rs}^{-}$ in terms of minimum constraints as described in Chapter 3 (Case 3, fixed constraints),

$$\begin{aligned}\mathbf{N}_{rs}^{-} &= \left(\mathbf{N} + \mathbf{K}^T\mathbf{K}\right)^{-1}\mathbf{N}\left(\mathbf{N} + \mathbf{K}^T\mathbf{K}\right)^{-1} \\ &= \left(\mathbf{N} + \mathbf{K}^T\mathbf{K}\right)^{-1} - \left(\mathbf{N} + \mathbf{K}^T\mathbf{K}\right)^{-1}\mathbf{K}^T\mathbf{K}\left(\mathbf{N} + \mathbf{K}^T\mathbf{K}\right)^{-1}\end{aligned} \tag{5.6}$$

To simplify notation in the expressions to follow, we let $\mathbf{N}_K = \left(\mathbf{N} + \mathbf{K}^T\mathbf{K}\right)$. Now we may write the differential of the generalized inverse in terms of $d\mathbf{N}_K^{-1}$ and $d\mathbf{K}$,

$$d\mathbf{N}_{rs}^{-} = d\mathbf{N}_K^{-1} - d\mathbf{N}_K^{-1}\mathbf{K}^T\mathbf{K}\mathbf{N}_K^{-1} - \mathbf{N}_K^{-1}\mathbf{K}^T\mathbf{K}\,d\mathbf{N}_K^{-1} - \mathbf{N}_K^{-1}\left(d\mathbf{K}^T\mathbf{K} + \mathbf{K}^T d\mathbf{K}\right)\mathbf{N}_K^{-1} \tag{5.7}$$

Since $\mathbf{N}_K\mathbf{N}_K^{-1} = \mathbf{I}_m$, $d\mathbf{N}_K\mathbf{N}_K^{-1} + \mathbf{N}_K d\mathbf{N}_K^{-1} = \mathbf{0}$ which may be rearranged to obtain

$$d\mathbf{N}_K^{-1} = -\mathbf{N}_K^{-1}d\mathbf{N}_K\mathbf{N}_K^{-1}. \tag{5.8}$$

If we expand the differential $d\mathbf{N}_K = d\mathbf{N} + d\mathbf{K}^T\mathbf{K} + \mathbf{K}d\mathbf{K}^T$ and insert it into (5.8) then

$$d\mathbf{N}_K^{-1} = -\mathbf{N}_K^{-1}d\mathbf{N}\mathbf{N}_K^{-1} - \mathbf{N}_K^{-1}\left(d\mathbf{K}^T\mathbf{K} + \mathbf{K}^T d\mathbf{K}\right)\mathbf{N}_K^{-1} \tag{5.9}$$

Expression (5.9) may be substituted into (5.7) to obtain

$$\begin{aligned}d\mathbf{N}_{rs}^{-} &= -\mathbf{N}_K^{-1}d\mathbf{N}_K\mathbf{N}_K^{-1} + \mathbf{N}_K^{-1}d\mathbf{N}_K\mathbf{N}_K^{-1}\mathbf{K}^T\mathbf{K}\mathbf{N}_K^{-1} + \mathbf{N}_K^{-1}\mathbf{K}^T\mathbf{K}\mathbf{N}_K^{-1}d\mathbf{N}_K\mathbf{N}_K^{-1} - \mathbf{N}_K^{-1}\left(d\mathbf{K}^T\mathbf{K} + \mathbf{K}^T d\mathbf{K}\right)\mathbf{N}_K^{-1} \\ &= -\mathbf{N}_K^{-1}d\mathbf{N}\mathbf{N}_K^{-1} + \mathbf{N}_K^{-1}d\mathbf{N}_K\mathbf{N}_K^{-1}\mathbf{K}^T\mathbf{K}\mathbf{N}_K^{-1} + \mathbf{N}_K^{-1}\mathbf{K}^T\mathbf{K}\mathbf{N}_K^{-1}d\mathbf{N}_K\mathbf{N}_K^{-1} - 2\mathbf{N}_K^{-1}\left(d\mathbf{K}^T\mathbf{K} + \mathbf{K}^T d\mathbf{K}\right)\mathbf{N}_K^{-1} \\ &= -\mathbf{N}_K^{-1}d\mathbf{N}\mathbf{N}_K^{-1} + \mathbf{N}_K^{-1}d\mathbf{N}_K\mathbf{E}^T\left(\mathbf{E}\mathbf{K}^T\mathbf{K}\mathbf{E}^T\right)^{-1}\mathbf{E} + \mathbf{E}^T\left(\mathbf{E}\mathbf{K}^T\mathbf{K}\mathbf{E}^T\right)^{-1}\mathbf{E}d\mathbf{N}_K\mathbf{N}_K^{-1} - 2\mathbf{N}_K^{-1}\left(d\mathbf{K}^T\mathbf{K} + \mathbf{K}^T d\mathbf{K}\right)\mathbf{N}_K^{-1}\end{aligned}$$

Or, written entirely in terms of $d\mathbf{N}$ and $d\mathbf{K}$

$$\begin{aligned}d\mathbf{N}_{rs}^{-} = {} & \mathbf{N}_K^{-1}d\mathbf{N}\mathbf{N}_K^{-1} - 2\mathbf{N}_K^{-1}\left(d\mathbf{N} + d\mathbf{K}^T\mathbf{K} + \mathbf{K}^T d\mathbf{K}\right)\mathbf{N}_K^{-1} \\ & + \mathbf{N}_K^{-1}\left(d\mathbf{N} + d\mathbf{K}^T\mathbf{K} + \mathbf{K}^T d\mathbf{K}\right)\mathbf{E}^T\left(\mathbf{E}\mathbf{K}^T\mathbf{K}\mathbf{E}^T\right)^{-1}\mathbf{E} \\ & + \mathbf{E}^T\left(\mathbf{E}\mathbf{K}^T\mathbf{K}\mathbf{E}^T\right)^{-1}\mathbf{E}\left(d\mathbf{N} + d\mathbf{K}^T\mathbf{K} + \mathbf{K}^T d\mathbf{K}\right) \\ = {} & \mathbf{N}_K^{-1}d\mathbf{N}\mathbf{N}_K^{-1} - \mathbf{N}_K^{-1}\left(d\mathbf{N} + \mathbf{K}^T d\mathbf{K}\right)\mathbf{N}_{rs}^{-} - \mathbf{N}_{rs}^{-}\left(d\mathbf{N} + d\mathbf{K}^T\mathbf{K}\right)\mathbf{N}_K^{-1}\end{aligned} \tag{5.10}$$

We may also, of course, express (5.10) in terms of $d\mathbf{A}$. Note that (5.10) has a form similar to the form of the differential for the pseudo-inverse in (5.5). By replacing $\mathbf{K}$ with $\mathbf{E}$ in (5.10) we could write (5.5) in

terms of $\mathbf{E}$, noting that $\left(\mathbf{I}_m - \mathbf{N}\mathbf{N}^+\right) = \left(\mathbf{I}_m - \mathbf{N}\mathbf{N}_E^{-1}\right) = \mathbf{E}^T\left(\mathbf{E}\mathbf{N}_E^{-1}\right) = \mathbf{E}^T\left(\mathbf{E}\mathbf{E}^T\right)^{-1}\mathbf{E}$ and that $\mathbf{E}\mathbf{N} = \mathbf{0} \rightarrow d\mathbf{E}\mathbf{N} = -\mathbf{E}d\mathbf{N}$.

5.1.2 Full-rank Gauss-Markov model

We may substitute (5.4) into (5.3) to obtain the total differential of $\mathbf{R}$ in $\mathbf{A}$

$$d\mathbf{R} = -d\mathbf{A}\mathbf{N}^{-1}\mathbf{A}^T\mathbf{P} - \mathbf{A}\mathbf{N}^{-1}d\mathbf{A}^T\mathbf{P} + \mathbf{A}\mathbf{N}^{-1}\left(d\mathbf{A}^T\mathbf{P}\mathbf{A} + \mathbf{A}^T\mathbf{P}d\mathbf{A}\right)\mathbf{N}^{-1}\mathbf{A}^T\mathbf{P}. \tag{5.11}$$

Unlike scalar or vector differentials in which the Jacobian matrix is explicit in the total derivative, we must write (5.11) in the form of (5.1) in order to express the Jacobian matrix, $J(\mathbf{R})$. Our goal then is to vectorize each of the four terms of (5.11) with respect to $d\mathbf{A}$ to achieve this explicit representation. Beginning with the first two terms of (5.11)

$$vec\left(d\mathbf{A}\mathbf{N}^{-1}\mathbf{A}^T\mathbf{P}\right) = \left(\mathbf{P}\mathbf{A}\mathbf{N}^{-1} \otimes \mathbf{I}_n\right)d(vec\mathbf{A})$$

and

$$\begin{aligned} vec\left(\mathbf{A}\mathbf{N}^{-1}d\mathbf{A}^T\mathbf{P}\right) &= \left(\mathbf{P} \otimes \mathbf{A}\mathbf{N}^{-1}\right)\mathbf{K}_{nm}d(vec\mathbf{A}) \\ &= \mathbf{K}_{n^2}\left(\mathbf{A}\mathbf{N}^{-1} \otimes \mathbf{P}\right)d(vec\mathbf{A}) \end{aligned}.$$

with $\mathbf{K}_{nm}$ and $\mathbf{K}_{n^2}$ as "commutation" matrices (cf. Appendix B). The third and fourth terms become

$$\begin{aligned} vec\left(\mathbf{A}\mathbf{N}^{-1}d\mathbf{A}^T\mathbf{P}\mathbf{A}\mathbf{N}^{-1}\mathbf{A}^T\mathbf{P}\right) &= \left(\mathbf{P}\mathbf{A}\mathbf{N}^{-1}\mathbf{A}^T\mathbf{P} \otimes \mathbf{A}\mathbf{N}^{-1}\right)\mathbf{K}_{nm}d(vec\mathbf{A}) \\ &= \mathbf{K}_{n^2}\left(\mathbf{A}\mathbf{N}^{-1} \otimes \mathbf{P}\mathbf{A}\mathbf{N}^{-1}\mathbf{A}^T\mathbf{P}\right)d(vec\mathbf{A}) \end{aligned},$$

and

$$vec\left(\mathbf{A}\mathbf{N}^{-1}\mathbf{A}^T\mathbf{P}d\mathbf{A}\mathbf{N}^{-1}\mathbf{A}^T\mathbf{P}\right) = \left(\mathbf{P}\mathbf{A}\mathbf{N}^{-1} \otimes \mathbf{A}\mathbf{N}^{-1}\mathbf{A}^T\mathbf{P}\right)d(vec\mathbf{A}).$$

Combining these terms results in an expression for $d(vec\mathbf{R})$

$$\begin{aligned} d(vec\mathbf{R}) &= -\left[\mathbf{P}\mathbf{A}\mathbf{N}^{-1} \otimes \left(\mathbf{I}_n - \mathbf{A}\mathbf{N}^{-1}\mathbf{A}^T\mathbf{P}\right) + \mathbf{K}_{n^2}\left(\mathbf{A}\mathbf{N}^{-1} \otimes \mathbf{P}\left(\mathbf{I}_n - \mathbf{A}\mathbf{N}^{-1}\mathbf{A}^T\mathbf{P}\right)\right)\right]d(vec\mathbf{A}) \\ &= -\left[\mathbf{P}\mathbf{A}\mathbf{N}^{-1} \otimes \mathbf{Q}_{\tilde{\mathbf{e}}}\mathbf{P} + \mathbf{K}_{n^2}\left(\mathbf{A}\mathbf{N}^{-1} \otimes \mathbf{P}\mathbf{Q}_{\tilde{\mathbf{e}}}\mathbf{P}\right)\right]d(vec\mathbf{A}) \end{aligned} \tag{5.12}$$

from which we conclude that the Jacobian of $\mathbf{R}$ with respect to $\mathbf{A}$ is

$$\begin{aligned} J(\mathbf{R}) &= \underbrace{\left[\left(\mathbf{P} \otimes \mathbf{I}_n\right) + \mathbf{K}_{n^2}\left(\mathbf{I}_n \otimes \mathbf{P}\right)\right]}_{nn\ \mathrm{x}\ nn}\underbrace{\left[\mathbf{A}\mathbf{N}^{-1} \otimes \left(\mathbf{I}_n - \mathbf{A}\mathbf{N}^{-1}\mathbf{A}^T\mathbf{P}\right)\right]}_{nn\ \mathrm{x}\ nm} \\ &= \underbrace{\left[\left(\mathbf{P} \otimes \mathbf{I}_n\right)\left(\mathbf{I}_n + \mathbf{K}_{n^2}\right)\right]}_{nn\ \mathrm{x}\ nn}\underbrace{\left[\mathbf{A}\mathbf{N}^{-1} \otimes \mathbf{Q}_{\tilde{\mathbf{e}}}\mathbf{P}\right]}_{nn\ \mathrm{x}\ nm} \end{aligned}. \tag{5.13}$$

Again, we should be clear that (5.10) models the changes in the n^2 elements of *vec*$\mathbf{R}$ with respect to changes in the *nm* elements of *vec*$\mathbf{A}$ – but not to changes in the parameter seed values that are used to compute the elements of *vec*$\mathbf{A}$. Since the elements of the (*nm* x *1*) vector $d(vec\mathbf{A}) = vec(d\mathbf{A})$ are functions of the *m* seed values, Ξ^o, we may relate $dvec(\mathbf{A})$ to $d\Xi^o$ by identifying the Jacobian of *vec*$\mathbf{A}$ with respect to Ξ^o, $d(vec\mathbf{A}) = J(\mathbf{A})d\Xi^o$. We may approach this directly by examining each element of $d\mathbf{A}$, which are related to $d\Xi^o$ as follows

$$da_{ij} = \frac{\partial a_{ij}}{\partial \Xi_1^o}d\Xi_1^o + \frac{\partial a_{ij}}{\partial \Xi_2^o}d\Xi_2^o + \ldots + \frac{\partial a_{ij}}{\partial \Xi_m^o}d\Xi_m^o \tag{5.14}$$

for $i = 1..n$ and $j = 1..m$. We may compactly write these elements as the *nm* x *1* vector *d*(*vec*$\mathbf{A}$)

$$d(vec\mathbf{A}) = \underbrace{\left[\frac{\partial(vec\mathbf{A})}{\partial \Xi_1^o} \quad \frac{\partial(vec\mathbf{A})}{\partial \Xi_2^o} \quad \ldots \quad \frac{\partial(vec\mathbf{A})}{\partial \Xi_m^o}\right]}_{mn\ \mathrm{x}\ m}d\Xi^o = \frac{\partial(vec\mathbf{A})}{\left(\partial \Xi^o\right)^T}d\Xi^o. \tag{5.15}$$

If we designate $\mathbf{f}\left(\Xi^o\right)$ as the vector of approximate non-linear observations, then $d\mathbf{f} = \mathbf{A}d\Xi^o$ and each element of $\mathbf{A}$, $a_{ij} = \dfrac{\partial \mathbf{f}_i}{\partial \Xi^o_j}$, for $i = 1..n$ and $j = 1..m$. By substituting these elements into (5.15) we recognize the matrix $\left[\dfrac{\partial(vec\mathbf{A})}{\partial \Xi^o_1} \quad \dfrac{\partial(vec\mathbf{A})}{\partial \Xi^o_2} \quad \cdots \quad \dfrac{\partial(vec\mathbf{A})}{\partial \Xi^o_m}\right]$ as the Hessian matrix of **f** with respect to the vector of seed values, Ξ^o, with elements arranged in the particular order

$$\begin{aligned} \underset{nm \text{ x } m}{\mathbf{H}} &= \left[vec\left(\frac{\partial^2 \mathbf{f}}{\left[\partial \Xi^o\right]^T \partial \Xi^o_1}\right) \quad vec\left(\frac{\partial^2 \mathbf{f}}{\left[\partial \Xi^o\right]^T \partial \Xi^o_2}\right) \quad \cdots \quad vec\left(\frac{\partial^2 \mathbf{f}}{\left[\partial \Xi^o\right]^T \partial \Xi^o_m}\right)\right] \\ &= \left[\frac{\partial(vec\mathbf{A})}{\partial \Xi^o_1} \quad \frac{\partial(vec\mathbf{A})}{\partial \Xi^o_2} \quad \cdots \quad \frac{\partial(vec\mathbf{A})}{\partial \Xi^o_m}\right] . \end{aligned} \tag{5.16}$$

Since (5.12) is written in terms of $d(vec\mathbf{A})$, we may express the elements of (5.15) directly through (5.16) as

$$d(vec\mathbf{A}) = \mathbf{H}d\Xi^o . \tag{5.17}$$

Forming the required Hessian matrix can be tedious. In the case of the collinearity equations with three unknowns of interior orientation, six unknowns of exterior orientation, and three ground coordinate unknowns, this requires 144 second partial derivatives of the collinearity equations. Indeed, if it were easy to form, it would almost certainly be used more often in the Taylor series expansion and iteration procedure in a pure Newton approach rather than the analytical approximation of a **H** with **N** in the Gauss-Newton approach (cf. Triggs, et al., 2000). While symbolic mathematics software may relieve the burden somewhat, numerical differentiation is straightforward and also effective (Lanczos, 1956). We will use this approach to compute the Hessian matrix (4.16) in the numerical work to follow.

5.1.3 Rank-deficient Gauss-Markov model

We may substitute (5.10) into (5.3) to obtain

$$\begin{aligned} d\mathbf{R} = &-d\mathbf{A}\left(\mathbf{N}_{rs}^{-}\mathbf{A}^T\mathbf{P}\right) + \mathbf{A}\mathbf{N}_K^{-1}d\mathbf{N}\mathbf{N}_K^{-1}\mathbf{A}^T\mathbf{P} \\ &- 2\mathbf{A}\mathbf{N}_K^{-1}\left(d\mathbf{N} + d\mathbf{K}^T\mathbf{K} + \mathbf{K}^T d\mathbf{K}\right)\mathbf{N}_K^{-1}\mathbf{A}^T\mathbf{P} \\ &- \mathbf{A}\mathbf{N}_K^{-1}\left(d\mathbf{N} + d\mathbf{K}^T\mathbf{K} + \mathbf{K}^T d\mathbf{K}\right)\mathbf{E}^T\left(\mathbf{E}\mathbf{K}^T\mathbf{K}\mathbf{E}^T\right)^{-1}\mathbf{E}\mathbf{A}^T\mathbf{P} \\ &- \mathbf{A}\mathbf{E}^T\left(\mathbf{E}\mathbf{K}^T\mathbf{K}\mathbf{E}^T\right)^{-1}\mathbf{E}\left(d\mathbf{N} + d\mathbf{K}^T\mathbf{K} + \mathbf{K}^T d\mathbf{K}\right)\mathbf{A}^T\mathbf{P} \\ &- \mathbf{A}\mathbf{N}_{rs}^{-}d\mathbf{A}^T\mathbf{P} \end{aligned} \tag{5.18}$$

This expression may be simplified because of the condition $\mathbf{A}\mathbf{E}^T = \mathbf{0}$. Furthermore, by substituting $\mathbf{N}_{rs}^{-} = \left(\mathbf{N} + \mathbf{K}^T\mathbf{K}\right)^{-1}\mathbf{N}\left(\mathbf{N} + \mathbf{K}^T\mathbf{K}\right)^{-1}$ and $d\mathbf{N} = d\mathbf{A}^T\mathbf{P}\mathbf{A} + \mathbf{A}^T\mathbf{P}\,d\mathbf{A}$ into expression (5.18) and taking into account the relations $\mathbf{N}\mathbf{N}_K^{-1}\mathbf{A}^T = \mathbf{A}^T$ and $\mathbf{K}\mathbf{N}_K^{-1}\mathbf{A}^T = \mathbf{0}$ we finally arrive at an expression for *d***R** in terms of *d***A**,

$$\begin{aligned} d\mathbf{R} &= -d\mathbf{A}\left(\mathbf{N}_K^{-1}\mathbf{N}\mathbf{N}_K^{-1}\mathbf{A}^T\mathbf{P}\right) - \mathbf{A}\mathbf{N}_K^{-1}d\mathbf{N}\mathbf{N}_K^{-1}\mathbf{A}^T\mathbf{P} + 2\mathbf{A}\mathbf{N}_K^{-1}d\mathbf{N}\mathbf{N}_K^{-1}\mathbf{A}^T\mathbf{P} - \mathbf{A}\mathbf{N}_K^{-1}\mathbf{N}\mathbf{N}_K^{-1}d\mathbf{A}^T\mathbf{P} \\ &= -d\mathbf{A}(\mathbf{N}_K^{-1}\mathbf{A}^T\mathbf{P}) + \mathbf{A}\mathbf{N}_K^{-1}d\mathbf{N}\mathbf{N}_K^{-1}\mathbf{A}^T\mathbf{P} - \mathbf{A}\mathbf{N}_K^{-1}d\mathbf{A}^T\mathbf{P} \\ &= -d\mathbf{A}(\mathbf{N}_K^{-1}\mathbf{A}^T\mathbf{P}) - \mathbf{A}\mathbf{N}_K^{-1}d\mathbf{A}^T\mathbf{P} + \mathbf{A}\mathbf{N}_K^{-1}\left(d\mathbf{A}^T\mathbf{P}\mathbf{A} + \mathbf{A}^T\mathbf{P}\,d\mathbf{A}\right)\mathbf{N}_K^{-1}\mathbf{A}^T\mathbf{P} \end{aligned} \tag{5.19}$$

Note that (5.19) is made identical to (5.11) by replacing $\mathbf{N}_K = \left(\mathbf{N} + \mathbf{K}^T\mathbf{K}\right)$ with **N**. Therefore, we may apply the results from the previous section to obtain an expression for the Jacobian of **R** with respect to **A**,

$$d(vec\mathbf{R}) = -\left[\mathbf{P}\mathbf{A}\mathbf{N}_K^{-1} \otimes \left(\mathbf{I}_n - \mathbf{A}\mathbf{N}_K^{-1}\mathbf{A}^T\mathbf{P}\right) + \mathbf{K}_{n^2}\left(\mathbf{A}\mathbf{N}_K^{-1} \otimes \mathbf{P}\left(\mathbf{I}_n - \mathbf{A}\mathbf{N}_K^{-1}\mathbf{A}^T\mathbf{P}\right)\right)\right] d(vec\mathbf{A}) \tag{5.20}$$

and

$$\begin{aligned} J(\mathbf{R}) &= \left[\underbrace{\left(\mathbf{P} \otimes \mathbf{I}_n\right)\left(\mathbf{I}_n + \mathbf{K}_{n^2}\right)}_{nn \text{ x } nn}\right]\left[\underbrace{\mathbf{A}\mathbf{N}_K^{-1} \otimes \left(\mathbf{I}_n - \mathbf{A}\mathbf{N}_K^{-1}\mathbf{A}^T\mathbf{P}\right)}_{nn \text{ x } nm}\right] \\ &= \left[\underbrace{\left(\mathbf{P} \otimes \mathbf{I}_n\right)\left(\mathbf{I}_n + \mathbf{K}_{n^2}\right)}_{nn \text{ x } nn}\right]\left[\underbrace{\mathbf{A}\mathbf{N}_K^{-1} \otimes \left(\mathbf{Q}_{\tilde{\mathbf{e}}}\mathbf{P}\right)}_{nn \text{ x } nm}\right] \end{aligned}. \tag{5.21}$$

5.2. Constrained Gauss-Markov model

5.2.1 Stochastic constraints

We may extend (5.11) to include stochastic constraints in Cases 1,2, and 4 as follows

$$\begin{aligned} d\mathbf{R} = &-\begin{bmatrix} d\mathbf{A} \\ d\mathbf{K} \end{bmatrix}\left(\mathbf{N} + \mathbf{K}^T\mathbf{P}_z\mathbf{K}\right)^{-1}\begin{bmatrix}\mathbf{A}^T & \mathbf{K}^T\end{bmatrix}\begin{bmatrix}\mathbf{P}_y & \mathbf{0} \\ \mathbf{0} & \mathbf{P}_z\end{bmatrix} - \begin{bmatrix}\mathbf{A} \\ \mathbf{K}\end{bmatrix}\left(\mathbf{N} + \mathbf{K}^T\mathbf{P}_z\mathbf{K}\right)^{-1}\begin{bmatrix}d\mathbf{A}^T & d\mathbf{K}^T\end{bmatrix}\begin{bmatrix}\mathbf{P}_y & \mathbf{0} \\ \mathbf{0} & \mathbf{P}_z\end{bmatrix} \\ &+ \begin{bmatrix}\mathbf{A} \\ \mathbf{K}\end{bmatrix}\left(\mathbf{N} + \mathbf{K}^T\mathbf{P}_z\mathbf{K}\right)^{-1}\left(\begin{bmatrix}d\mathbf{A}^T & d\mathbf{K}^T\end{bmatrix}\begin{bmatrix}\mathbf{P}_y & \mathbf{0} \\ \mathbf{0} & \mathbf{P}_z\end{bmatrix}\begin{bmatrix}\mathbf{A} \\ \mathbf{K}\end{bmatrix} + \begin{bmatrix}\mathbf{A}^T & \mathbf{K}^T\end{bmatrix}\begin{bmatrix}\mathbf{P}_y & \mathbf{0} \\ \mathbf{0} & \mathbf{P}_z\end{bmatrix}\begin{bmatrix}d\mathbf{A} \\ d\mathbf{K}\end{bmatrix}\right) \\ &\cdot\left(\mathbf{N} + \mathbf{K}^T\mathbf{P}_z\mathbf{K}\right)^{-1}\begin{bmatrix}\mathbf{A}^T & \mathbf{K}^T\end{bmatrix}\begin{bmatrix}\mathbf{P}_y & \mathbf{0} \\ \mathbf{0} & \mathbf{P}_z\end{bmatrix} \end{aligned} \tag{5.22}$$

or, with $\bar{\mathbf{R}}$ partitioned as in (3.1),

$$\begin{aligned} d\begin{bmatrix}\bar{\mathbf{R}}_y & \bar{\mathbf{R}}_{yz} \\ \bar{\mathbf{R}}_{zy} & \bar{\mathbf{R}}_z\end{bmatrix} = & \\ &-\begin{bmatrix} d\mathbf{A}\left(\mathbf{N} + \mathbf{K}^T\mathbf{P}_z\mathbf{K}\right)^{-1}\mathbf{A}^T\mathbf{P}_y & d\mathbf{A}\left(\mathbf{N} + \mathbf{K}^T\mathbf{P}_z\mathbf{K}\right)^{-1}\mathbf{K}^T\mathbf{P}_z \\ d\mathbf{K}\left(\mathbf{N} + \mathbf{K}^T\mathbf{P}_z\mathbf{K}\right)^{-1}\mathbf{A}^T\mathbf{P}_y & d\mathbf{K}\left(\mathbf{N} + \mathbf{K}^T\mathbf{P}_z\mathbf{K}\right)^{-1}\mathbf{K}^T\mathbf{P}_z \end{bmatrix} \\ &-\begin{bmatrix} \mathbf{A}\left(\mathbf{N} + \mathbf{K}^T\mathbf{P}_z\mathbf{K}\right)^{-1}d\mathbf{A}^T\mathbf{P}_y & \mathbf{A}\left(\mathbf{N} + \mathbf{K}^T\mathbf{P}_z\mathbf{K}\right)^{-1}d\mathbf{K}^T\mathbf{P}_z \\ \mathbf{K}\left(\mathbf{N} + \mathbf{K}^T\mathbf{P}_z\mathbf{K}\right)^{-1}d\mathbf{A}^T\mathbf{P}_y & \mathbf{K}\left(\mathbf{N} + \mathbf{K}^T\mathbf{P}_z\mathbf{K}\right)^{-1}d\mathbf{K}^T\mathbf{P}_z \end{bmatrix} \\ &+\begin{bmatrix}\mathbf{A}\left(\mathbf{N} + \mathbf{K}^T\mathbf{P}_z\mathbf{K}\right)^{-1} \\ \mathbf{K}\left(\mathbf{N} + \mathbf{K}^T\mathbf{P}_z\mathbf{K}\right)^{-1}\end{bmatrix}\left[d\mathbf{A}^T\mathbf{P}_y\mathbf{A} + d\mathbf{K}^T\mathbf{P}_z\mathbf{K} + \mathbf{A}^T\mathbf{P}_y d\mathbf{A} + \mathbf{K}^T\mathbf{P}_z d\mathbf{K}\right]\left(\mathbf{N} + \mathbf{K}^T\mathbf{P}_z\mathbf{K}\right)^{-1}\left[\mathbf{A}^T\mathbf{P}_y \;\middle|\; \mathbf{K}^T\mathbf{P}_z\right] \end{aligned} \tag{5.23}$$

Although we could vectorize the entire expression (5.23), for now we focus primarily on the trace elements of $d\bar{\mathbf{R}}_y$, that is the differential changes in the reliability numbers (or blocks of reliability values in the case of grouped observations) of the base observations. In analogy to (5.8) and (5.9), but with the two additional terms in $d\mathbf{K}$ and $d\mathbf{K}^T$, we may vectorize the upper-left block of (5.23) to obtain

$$
\begin{aligned}
d\left(vec\bar{\mathbf{R}}_y\right) &= -\left[\mathbf{P}_y\mathbf{A}\left(\mathbf{N}+\mathbf{K}^T\mathbf{P}_z\mathbf{K}\right)^{-1}\otimes\left(\mathbf{I}_n-\mathbf{A}\left(\mathbf{N}+\mathbf{K}^T\mathbf{P}_z\mathbf{K}\right)^{-1}\mathbf{A}^T\mathbf{P}_y\right)\right]d(vec\mathbf{A}) \\
&\quad -\mathbf{K}_{n^2}\left[\mathbf{A}\left(\mathbf{N}+\mathbf{K}^T\mathbf{P}_z\mathbf{K}\right)^{-1}\otimes\mathbf{P}_y\left(\mathbf{I}_n-\mathbf{A}\left(\mathbf{N}+\mathbf{K}^T\mathbf{P}_z\mathbf{K}\right)^{-1}\mathbf{A}^T\mathbf{P}_y\right)\right]d(vec\mathbf{A}) \\
&\quad +\left[\mathbf{P}_y\mathbf{A}\left(\mathbf{N}+\mathbf{K}^T\mathbf{P}_z\mathbf{K}\right)^{-1}\otimes\mathbf{A}\left(\mathbf{N}+\mathbf{K}^T\mathbf{P}_z\mathbf{K}\right)^{-1}\mathbf{K}^T\mathbf{P}_z\right]d(vec\mathbf{K}) \\
&\quad +\mathbf{K}_{n^2}\left[\mathbf{A}\left(\mathbf{N}+\mathbf{K}^T\mathbf{P}_z\mathbf{K}\right)^{-1}\otimes\mathbf{P}_y\mathbf{A}\left(\mathbf{N}+\mathbf{K}^T\mathbf{P}_z\mathbf{K}\right)^{-1}\mathbf{K}^T\mathbf{P}_z\right]d(vec\mathbf{K}) \\
&= -\left(\mathbf{P}_y\otimes\mathbf{I}_n\right)\left(\mathbf{I}_n+\mathbf{K}_{n^2}\right)\left[\mathbf{A}\left(\mathbf{N}+\mathbf{K}^T\mathbf{P}_z\mathbf{K}\right)^{-1}\otimes\left(\mathbf{I}_n-\mathbf{A}\left(\mathbf{N}+\mathbf{K}^T\mathbf{P}_z\mathbf{K}\right)^{-1}\mathbf{A}^T\mathbf{P}_y\right)\right]d(vec\mathbf{A}) \\
&\quad +\left(\mathbf{P}_y\otimes\mathbf{I}_n\right)\left(\mathbf{I}_{n^2}+\mathbf{K}_{n^2}\right)\left[\mathbf{A}\left(\mathbf{N}+\mathbf{K}^T\mathbf{P}_z\mathbf{K}\right)^{-1}\otimes\mathbf{A}\left(\mathbf{N}+\mathbf{K}^T\mathbf{P}_z\mathbf{K}\right)^{-1}\mathbf{K}^T\mathbf{P}_z\right]d(vec\mathbf{K})
\end{aligned}
\tag{5.24}
$$

Or, to simplify (5.24) we may write it in terms of the cofactor matrix of residuals, $\mathbf{Q}_{\bar{\mathbf{e}}_y}$ and $\mathbf{Q}_{\bar{\mathbf{e}}_z\bar{\mathbf{e}}_y}$ from (3.34),

$$
\begin{aligned}
d\left(vec\bar{\mathbf{R}}_y\right) &= -\left[\mathbf{P}_y\mathbf{A}\left(\mathbf{N}+\mathbf{K}^T\mathbf{P}_z\mathbf{K}\right)^{-1}\otimes\mathbf{Q}_{\bar{\mathbf{e}}_y}\mathbf{P}_y\right]d(vec\mathbf{A})-\mathbf{K}_{n^2}\left[\mathbf{A}\left(\mathbf{N}+\mathbf{K}^T\mathbf{P}_z\mathbf{K}\right)^{-1}\otimes\mathbf{P}_y\mathbf{Q}_{\bar{\mathbf{e}}_y\bar{\mathbf{e}}_z}\mathbf{P}_z\right]d(vec\mathbf{A}) \\
&\quad -\left[\mathbf{P}_y\mathbf{A}\left(\mathbf{N}+\mathbf{K}^T\mathbf{P}_z\mathbf{K}\right)^{-1}\otimes\mathbf{Q}_{\bar{\mathbf{e}}_y\bar{\mathbf{e}}_z}\mathbf{P}_z\right]d(vec\mathbf{K})-\mathbf{K}_{n^2}\left[\mathbf{A}\left(\mathbf{N}+\mathbf{K}^T\mathbf{P}_z\mathbf{K}\right)^{-1}\otimes\mathbf{P}_y\mathbf{Q}_{\bar{\mathbf{e}}_y\bar{\mathbf{e}}_z}\mathbf{P}_z\right]d(vec\mathbf{K}) \\
&= -\left(\mathbf{P}_y\otimes\mathbf{I}_n\right)\left(\mathbf{I}_n+\mathbf{K}_{n^2}\right)\left[\mathbf{A}\left(\mathbf{N}+\mathbf{K}^T\mathbf{P}_z\mathbf{K}\right)^{-1}\otimes\left(\left(\mathbf{Q}_{\bar{\mathbf{e}}_y}\mathbf{P}_y\right)d(vec\mathbf{A})+\left(\mathbf{Q}_{\bar{\mathbf{e}}_y\bar{\mathbf{e}}_z}\mathbf{P}_z\right)d(vec\mathbf{K})\right)\right]
\end{aligned}
\tag{5.25}
$$

The Jacobian follows and the discussion leading to (5.17) may be applied to write $d(vec\mathbf{K})$ in terms of $d\Xi^o$.

5.2.2 Fixed Constraints

Again, we concentrate on $d\bar{\mathbf{R}}_y$ and begin with that part of (4.15) expressing the reliability of the base observations in Cases 1 and 4: $\bar{\mathbf{R}}_y=\mathbf{I}_n-\mathbf{A}\mathbf{N}_{rs}^-\mathbf{A}^T\mathbf{P}_y+\mathbf{A}\mathbf{N}_{rs}^-\mathbf{K}^T\left(\mathbf{K}\mathbf{N}_{rs}^-\mathbf{K}^T\right)^{-1}\mathbf{K}\mathbf{N}_{rs}^-\mathbf{A}^T\mathbf{P}_y$. The differential $d\bar{\mathbf{R}}_y$ with respect to *d***A** and *d***K** could be derived directly from this expression. However, we recall that a fixed constraint may be expressed as a stochastic constraint in which $\mathbf{P}_z^{-1}\rightarrow\mathbf{0}$ so that, rather than computing the differential of (4.15) and vectorizing the result, we may rewrite (5.25) in a form involving $\mathbf{P}_z^{-1}$. In Case 1 we find

$$
d\left(vec\bar{\mathbf{R}}_y\right)=-\left(\mathbf{P}_y\otimes\mathbf{I}_n\right)\left(\mathbf{I}_n+\mathbf{K}_{n^2}\right)\left[\mathbf{A}\left(\mathbf{N}_{rs}^--\mathbf{N}_{rs}^-\mathbf{K}^T\left(\mathbf{K}\mathbf{N}_{rs}^-\mathbf{K}^T\right)^{-1}\mathbf{K}\mathbf{N}_{rs}^-\right)\otimes\left(\mathbf{Q}_{\bar{\mathbf{e}}_y}\mathbf{P}_y\right)d(vec\mathbf{A})\right]\ , \tag{5.26}
$$

which is expressed in terms of $\mathbf{Q}_{\bar{\mathbf{e}}_y}$ from (3.26). Note that the last terms of (5.24) and (5.25), those in *d*(*vec***K**), reduce to zero due to the relation $\mathbf{A}\mathbf{N}_{rs}^-\mathbf{K}^T\left(\mathbf{P}_z^{-1}+\left(\mathbf{K}\mathbf{N}_{rs}^-\mathbf{K}^T\right)^{-1}\mathbf{P}_z^{-1}\right)\rightarrow\mathbf{0}$ as $\mathbf{P}_z^{-1}\rightarrow\mathbf{0}$. Case 2 may be addressed by replacing $\mathbf{N}_{rs}^-$ with $\left(\mathbf{N}+\mathbf{K}^T\mathbf{K}\right)^{-1}$ and using (3.42) for $\mathbf{Q}_{\bar{\mathbf{e}}_y}$. Case 4 may be addressed by replacing $\mathbf{N}_{rs}^-$ with $\left(\mathbf{N}+\mathbf{K}^T\mathbf{K}\right)_{rs}^{-1}$.

5.3 Trilateration Example Continued

To demonstrate how the differential relations derived in the preceding sections may be used in a simple network, we look again to the trilateration example from Section 3.2. For the unconstrained network and the Gauss-Markov model, we may use formulas (5.12), (5.13), (5.16), and (5.17) to compute incremental changes in the redundancy of the distance observations when incremental changes occur in the *x*, *y* coordinates of P1, P2, P3, P4, and P5. Figure 5.1 graphs incremental changes to the redundancy numbers (the diagonal elements of each $d\mathbf{R}$) of the distance observations in our network observation caused by a 1-meter shift in both *x* and *y* coordinates of points P1 and P2. These numbers indicate that changes in P1 – which was not estimated and helped establish the datum – cause large (relative to the other points) changes to all of the observations, in effect shifting the redundancy of the network to different observations. Note that the zero-redundancy observations are not affected by either movement in point coordinates. Figure 5.2 shows similar changes cause by movement of P3 and P4. P5 is not shown because it has no effect on the redundancy numbers.

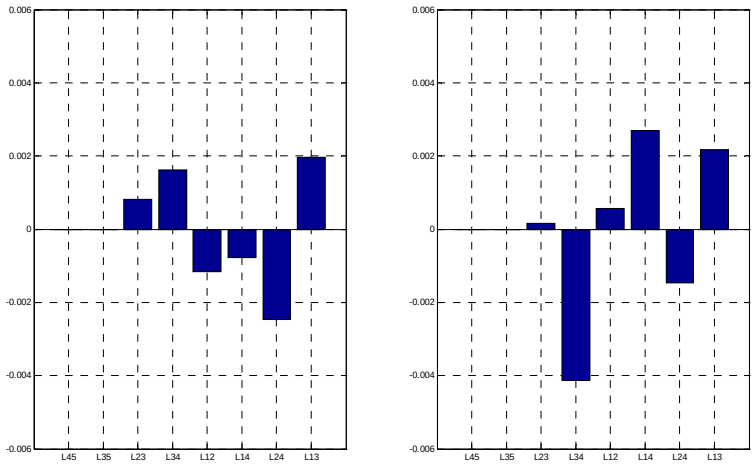

Figure 5.1. Change in distance observation redundancy numbers based on a 1-meter change in the *x* and *y* coordinates of P1 (left) and P2 (right).

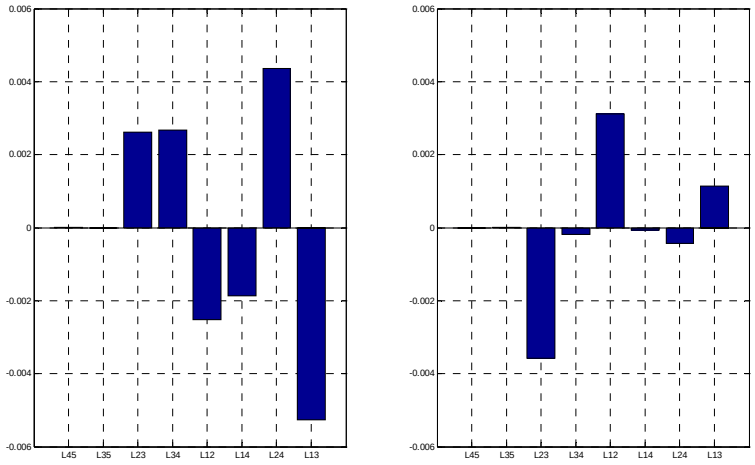

Figure 5.3. Change in distance observation redundancy numbers based on a 1-meter change in the *x* and *y* coordinates of P3 (left) and P4 (right).

It is important at this point to take note of the sizes of the matrices required to compute these differential changes in **R**. The Hessian matrix, **H**, of the observation equations is of order 80 x 10 while the Jacobian matrix, $J(\mathbf{R})$, is of order 64 x 80. While these particular matrices are relatively small, we must consider that we are working with only 8 observations to estimate 7 of the 10 parameters – a very small network. In even modestly sized networks, both **H** and $J(\mathbf{R})$ will quickly become difficult to manage, unless their special pattern can be exploited. In geodetic and photogrammetric networks, the Hessian matrix, **H**, like the design matrix, **A**, is often sparse (Figure 5.3) and modern matrix algebra systems based on LAPACK provide sparse matrix operations that increase speed and reduce memory requirements (Golub and Van Loan, 1996). However, $J(\mathbf{R})$ will rarely, if ever be sparse, since it is formed by the fully-populated, cofactor matrices of both the parameter estimates and the residuals.

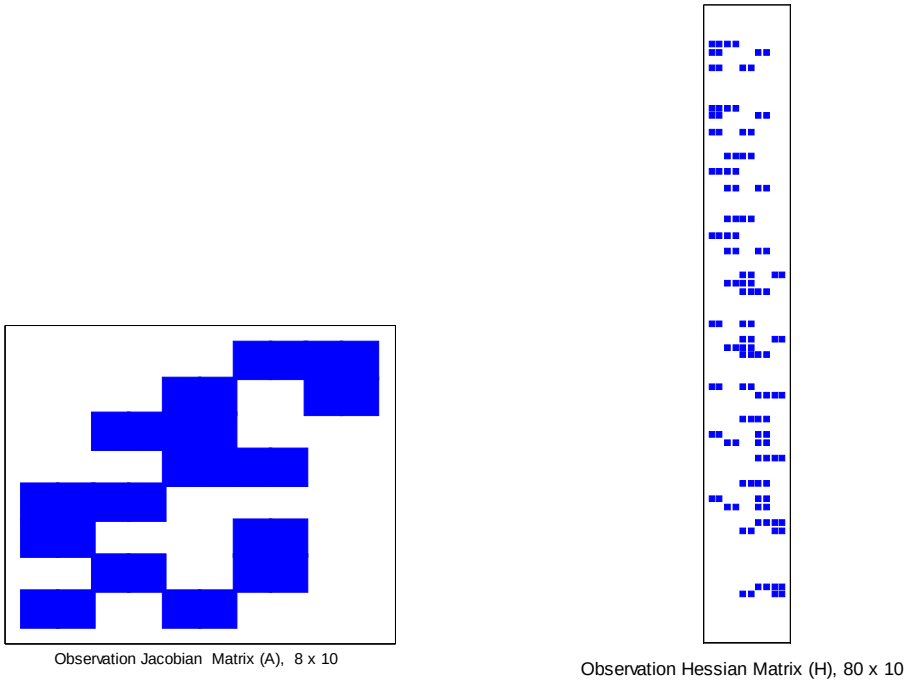

Figure 5.3. Sparseness of the observation equations Jacobian matrix (left) and Hessian matrix (right). Non-zero elements are shown in blue.

CHAPTER 6

RELIABILITY IN PHOTOGRAMMETRIC NETWORK DESIGN

To demonstrate how the results from the preceding chapters may be used in practice, we will apply the derived formulas to two interesting aspects of modern photogrammetric mapping. Aerial surveying is one of the most cost-effective methods available to update existing maps or Geographic Information Systems. It is still quite expensive, though, with most of the cost related to

i. the time and equipment required to collect ground control-points using ground-based methods such as total station or GPS surveys,
ii. the time required by a human operator to measure enough conjugate, or tie-, points on the images comprising the block, to orient the block with aerial triangulation procedures, and finally,
iii. the time required to manually measure features, contours, and elevation grids on the overlapping stereo-pairs that comprise the block.

Extensive research into supplementing aerial surveys (including ground control surveys) with GPS/INS-based systems used to directly observe the exterior orientation of each image in the block has been conducted with some success (cf. Grejner-Brzezinska, 1999 and 2001). In fact, *direct* orientation systems similar to those described in the references now see common commercial use. Likewise, research into automating tie-point selection and matching across overlapping images has resulted in so-called automatic aerial triangulation, or AAT, algorithms finding there way into not only research-oriented, but commercial, photogrammetry software (Heipke and Eder, 1999, Schenk, 1999). Matching errors occur relatively frequently in these systems, especially in large-scale, high-relief aerial surveys. However, the autonomous selection and matching processes result in a relatively large total number of matches. AAT relies on this large number (usually more than a hundred per stereo pair) of possibly low quality (low with respect to what can be attained by a trained human operator) tie-points to precisely estimate the exterior orientation parameters of the block, relying on the principle of repeated measurements for precise parameter estimation. Precise exterior orientation parameter estimates are thus possible even when many of the tie-point measurements themselves are poor (Heipke and Eder, 1999, Schenk, 1999). Despite this success, AAT results are still somewhat suspect and in practice require human quality control and continual intervention. The last cost factor, feature extraction, will not be addressed here.

It is possible that constraints, inferred from existing scene knowledge or developed from ground-based observations, on the object-space coordinates of the tie-points might improve the reliability of the exterior orientation estimates. This would enable properly designed networks to detect and eliminate outliers in these observations and thus further reduce the need for more extensive ground surveys. In indirect orientation, in which no direct EO observations exist, a check of reliability would necessarily involve outer reliability – determining the degree to which undetected outliers in the tie-point matches perturb the parameters. However, because of the increasing use of GPS- and GPS/INS-oriented camera systems, we will consider the case in which all blocks are directly oriented with varying degrees of accuracy. We will examine the effect of several geometric constraints (described in Appendix A) on the reliability of exterior orientation observations – using the theory developed in Chapters 2-4 – in two circumstances that may be applied to modern orientation systems:

i. the reliability of the exterior orientation observations in directly oriented blocks when no ground control is available, and
ii. the reliability of the exterior orientation observations when tie-points are measured autonomously.

6.1 Description of experimental data

Because reliability is a network design characteristic we will make extensive use of a synthetic data set, simulating two block networks based on a simple 1:6,000 scale, *3* x *2* image block, with 60% overlap and 39% sidelap. The camera is assumed to have a focal length of 150 mm with a 200 mm x 200 mm format size digitized with a resolution of 15 microns. The base-to-height ratio is approximately 0.5:1, resulting in relatively strong networks.

Parameters	Covariance Matrix
GPS Ground Control Point Observations $Cov\left\{\begin{bmatrix} X_{gcp} & Y_{gcp} & Z_{gcp} \end{bmatrix}^T\right\}$	$\begin{bmatrix} 0.0004 & - & - \\ 0.0000 & 0.0004 & - \\ 0.0000 & 0.0000 & 0.0004 \end{bmatrix} meters^2$
GPS Exterior Orientation Direct Observations $Cov\left\{\begin{bmatrix} X_o & Y_o & Z_o \end{bmatrix}^T\right\}$	$\begin{bmatrix} 0.004 & - & - \\ 0.000 & 0.004 & - \\ 0.0000 & 0.000 & 0.004 \end{bmatrix} meters^2$
INS Exterior Orientation Direct Observations $Cov\left\{\begin{bmatrix} \omega & \varphi & \kappa \end{bmatrix}^T\right\}$	$\begin{bmatrix} 0.0001 & - & - \\ 0.0000 & 0.0001 & - \\ 0.0000 & 0.0000 & 0.0001 \end{bmatrix} degrees^2$
Horizontal Collinear-Point Constrained Tie Point $Cov\left\{\begin{bmatrix} X_{tie} & Y_{tie} \end{bmatrix}^T\right\}$	$\begin{bmatrix} 9.0 & - \\ 0.0 & 9.0 \end{bmatrix} meters^2$
Manually measured image point $Cov\left\{\begin{bmatrix} u & v \end{bmatrix}^T\right\}$	$\begin{bmatrix} 20.25 & 0 \\ 0 & 20.25 \end{bmatrix} microns^2$
Automatically measured image point $Cov\left\{\begin{bmatrix} u & v \end{bmatrix}^T\right\}$	$\begin{bmatrix} 2025.0 & 0 \\ 0 & 2025.0 \end{bmatrix} microns^2$

Table 6.1. Various observation covariance matrices used in the synthetic data sets.

The first network, which we designate network N9, or simply N9, is a six-image block with nine tie-points per image, arranged in a pattern that reflects traditional, manual tie-point measurements (Figure 6.1). This network takes full advantage of the image overlap so that tie-points are measured in all images in which they appear. Throughout the remainder of this chapter, we will use the term *n*-fold to describe a tie-point that is measured in *n* images, for $n \geq 2$. So, for example, point 13 in network N9 is a six-fold tie-point while point 7 is not a 2-fold tie-point. (2+)-fold tie-points are important to the overall geometric stability and accuracy of the aerial triangulation (Heipke and Eder, 1999, Schenk, 1999).

point\photo	101	102	103	201	202	203
2	x	x				
4		x	x			
22				x	x	
24					x	x
3	x	x	x			
7	x	x				
8	x	x	x			
9		x	x			
11	x			x		
12	x	x		x	x	
13	x	x	x	x	x	x
14		x	x		x	x
15			x			x
17				x	x	
18				x	x	x
19					x	x
23				x	x	x

Table 6.2. Tie point observations from network N9.

Table 6.2 shows the available tie-points and the images in which they are measured. We assume that tie-points in N9 are measured with a relatively high precision of 0.3 pixels, or 4.5 microns. The resulting covariance matrix shown in Table 6.1 assumes no correlation between the *u* and *v* coordinates.

The second network, N25, is formed with the same *3* x *2* image arrangement but with 25 tie-points per image and is meant to reflect either a more intensive manual aerial triangulation effort or an automatic aerial triangulation effort in which a relatively large number of tie-points is automatically selected and matched in multiple images (Figure 6.2). This network also contains several *n*-fold tie-points. We distinguish two forms of N25 based on the precision with which tie points are measured,

i. N25a, representing the manually measured network, with a tie-point precision of 4.5 microns and
ii. N25b, representing the automatically measured network, with a relatively poor tie-point precision of 3.0 pixels.

The exterior orientation parameters of the images in both networks are directly observed, say with an integrated and calibrated GPS/INS system. We assume that calibration includes estimation of the biases of the GPS phase center and INS origin relative to the perspective center of the camera. Ground control points are available at the corners of the networks as shown in Figures 6.1 and 6.2, but in keeping with the goal of this experiment the points will most often be treated simply as tie-points. For the sake of simplicity, GPS derived coordinates are considered here to be uncorrelated. However, we should note that GPS coordinates, in general, exhibit significant correlations depending upon the estimation method. Orientation angle estimates derived from an on-board INS are also assumed to be uncorrelated with a standard deviation of approximately ± 30 arc seconds. Table 6.2 summarizes the assumed quality of additional observations as well as the precision of the image tie-point observations in each network.

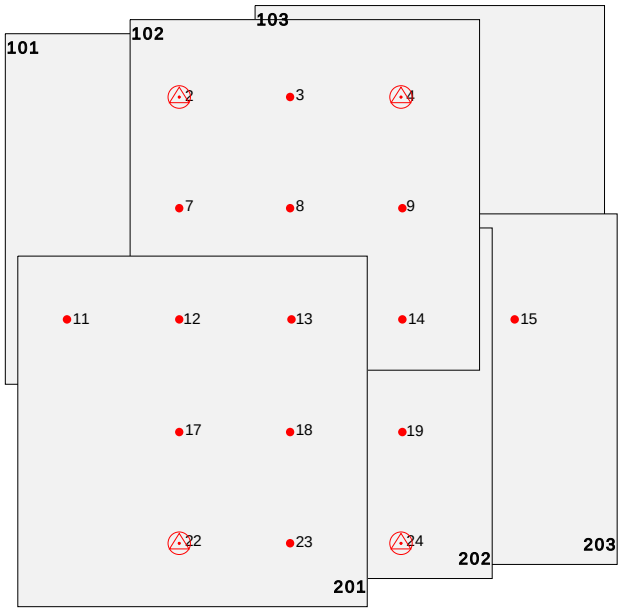

Figure 6.1. Network N9 tie-point configuration showing points 2, 4, 22, and 24 as ground control points.

Since N9 and N25 represent design data the measured image coordinates of tie-points are not required, and we may form the matrices required by (3.1) from the data uncorrupted by random error. We may compute the network's reliability directly from these matrices without performing a bundle adjustment since they contain all the information required to evaluate a particular network design.

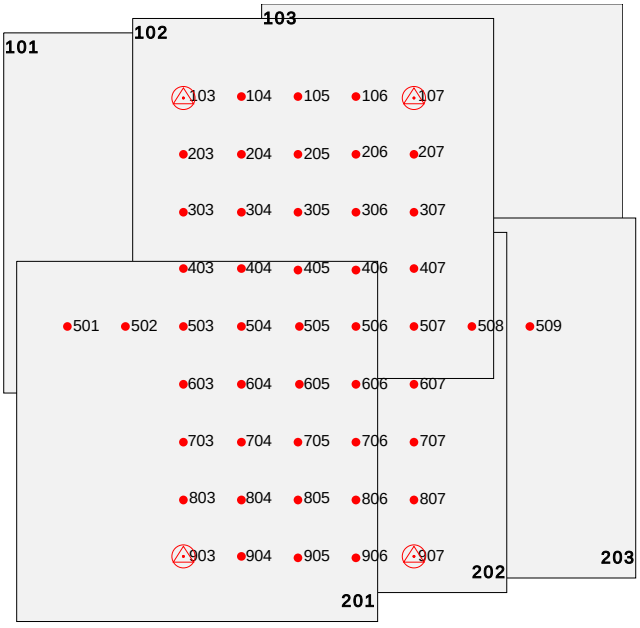

Figure 6.2. Network N25a-b tie-point configuration showing points 103, 107, 903, and 907 as ground control points.

In addition to the simulated, or design, networks N9 and N25, we will also examine, albeit in less detail, an actual 1:20,000 scale network consisting of a *3* x *2* block with 60% overlap and 20% sidelap. The RC30 aerial camera used in the survey was calibrated to a focal length 152.3 mm and flown at 3,000 meters above mean terrain flying height, resulting in a in a base-to-height ratio of approximately 0.5:1. The block, taken over a sparsely settled portion of the Mayflower quadrangle northwest of Little Rock, Arkansas, was flown by the Arkansas Highway and Transportation Department in April, 2003. The 9" x 9" color aerial film was scanned on a Zeiss PS2 scanner with a pixel size of 14 microns yielding approximately 0.33 meter ground sample distance. Airborne GPS perspective center points were available for each image although covariance information was unavailable. We will use the precision provided by the manufacturer: $\sigma_{X_o} = \sigma_{Y_o} = \pm 1.0 \text{ meter}$ and $\sigma_{Z_o} = \pm 3.0 \text{ meters}$. INS observations were not available. However, we will assume they are observed with poor precision $\left(\sigma_\omega = \sigma_\varphi = \sigma_\kappa = \pm 5.0 \text{ degrees}\right)$ so that we may include them as pseudo-observations in the adjustment. Tie-points were measured manually with a precision of $\pm$ 14 microns. The configuration of network R9, as we shall refer to it from this point on, is shown in Figure 6.3.

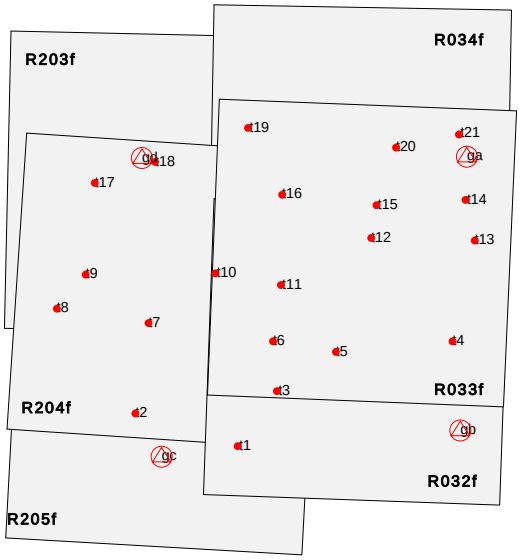

Figure 6.3. Network R9 tie-point configuration showing points ga, gb, gc, and gd as ground control points.

The four ground control points in R9 were derived from existing GIS vector information and are of relatively poor quality with assumed precision $\sigma_{X_o} = \sigma_{Y_o} = \pm 5 \text{ meters}$ and $\sigma_{Z_o} = \pm 7.0 \text{ meters}$. R9 represents a different network from the design networks N9 and N25 with significant differences in photo-scale, tie-point distribution, and availability of quality of direct orientation.

6.2 Increasing the reliability of directly-oriented blocks with geometric constraints

Direct observation of exterior orientation (EO) with integrated GPS/INS systems, or *direct* orientation, is becoming more common in photogrammetric systems because, under optimal circumstances, it can reduce or eliminate the need for expensive ground control. However, with current GPS/INS technology, direct EO observations are subject to errors due to GPS cycle slips, INS drift, and other causes (Grejner-Brzezinska, 1999 and 2001). Errors in position and orientation caused by cycle-slips and INS drift, for example, can deform a block and, in the absence of redundancy, these deformations may go undetected by current outlier detection schemes. Even with steady improvement in the reliability of GPS/INS systems, it is still true that errors arise in EO estimation often enough that photogrammetric mapping firms measure tie-points and ground control point observations to verify the accuracy of direct orientation systems (correspondence with representatives of EarthData, Inc). With this in mind, we address the question of whether geometric

constraints on a selected number of tie-points would improve the ability of the adjustment to detect direct orientation observation outliers, especially in the absence of ground control points. Geometric constraints are generally plentiful, at least in urban areas, but we will focus on one that commonly appears in both rural and urban areas – "roadway" linearity constraints. It is often possible to measure tie points along a road surface which may be constrained to lie along a horizontal (i.e. 2D in the *xy* mapping plane) or slant (i.e. 3D in *xyz* space) line. Note that this geometric constraint, containing shape information, does not provide datum information so we are relying on it to strengthen the relative orientation of the block. In particular, we expect the redundancy of the exterior orientation parameters of images, in which the constrained tie-points appear, to increase.

A natural extension to this "collinearity" constraint is to use a straight tie-*feature* extracted, say, from the edge of the road. Edge features can be reliably extracted from digital images and feature-based matching routines exist to find conjugate edge features in overlapping images (Schenk, 2004). However, Schenk also points out that unless the extracted edges lie in the epipolar plane of the stereo pair, a straight line tie feature provides no orientation information unless it is measured and matched in more than two images. So while it is certainly appropriate to pursue an investigation into the reliability provided by "tie-lines", we will only address the presumably stronger "collinear-point" constraint among tie-points.

In order to test the effect of collinear-point constraints on the reliability of directly observed exterior orientation parameters, we will examine network designs N9, N25a, N25b (remember that we consider reliability a design issue so that simulated data are acceptable and, at this point, preferred). After computing the reliability of the three unconstrained networks we will insert into each of them one or more horizontal, collinear-point constraints (see Appendix A.3.1 for the mathematical formulation) in varying orientations relative to the block.

1. Along-strip (Figure 6.4) - a single constraint passing along the center of the strip crossing strip and stereo-pairs. This simulates a block flown so that the two strips are parallel and overlap a road straight segment.
2. Two-along-strip (Figure 6.5) - two constraints passing along the edges of the strips.
3. Across-strip (Figure 6.6) - two constraints perpendicular to the direction of flight and crossing stereo-pairs but not strips.
4. X-pattern (Figure 6.7) - four constraints in a double "X" pattern crossing both strips and stereo-pairs.

In each of the four orientations, every image contains a measured, constrained tie-point. Each set of collinear-point constraints is treated as a stochastic constraint, with a covariance matrix computed from the assumed covariance of each point along the constraining line listed in Table 7. We use model (2.1) and include direct EO observations as "base" observations so that base normal equations have full-rank and the formulas in Section 3.1 (Case 1) apply.

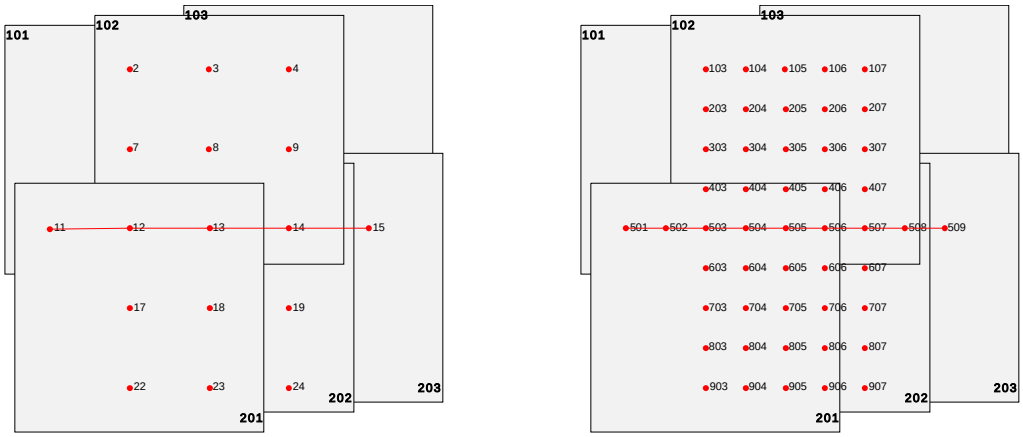

Figure 6.4. Networks N9 (left) and N25a-b (right). Position of "along-strip" horizontal collinear-point constraints. No ground control points are included.

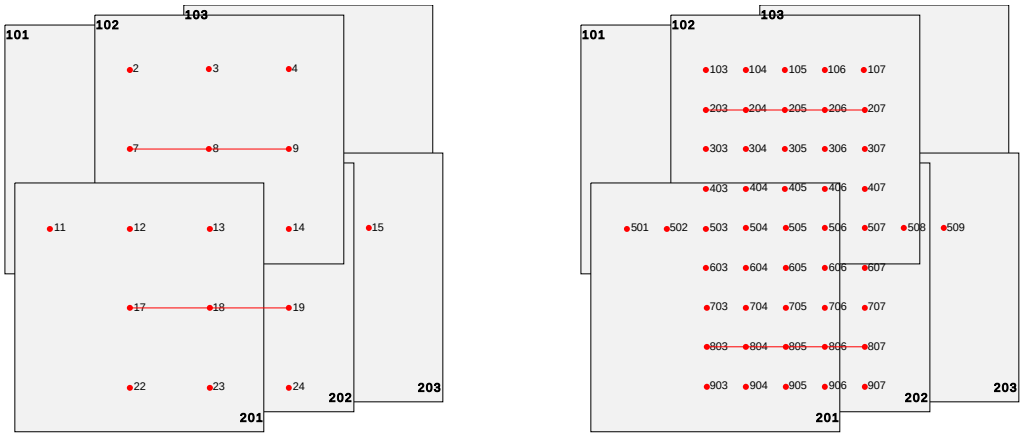

Figure 6.5. Networks N9 (left) and N25 (right). Position of multiple "along-strip" horizontal collinear-point constraints. No ground control points are included.

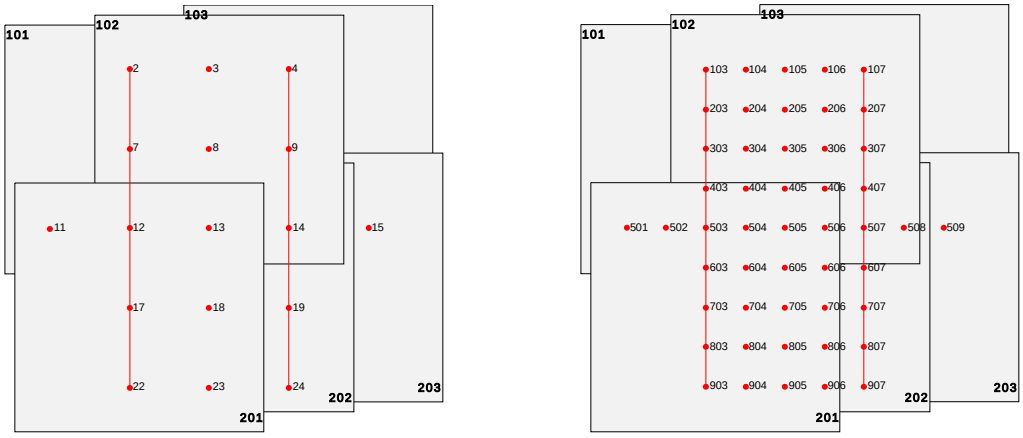

Figure 6.6. Networks N9 (left) and N25a-b (right). Position of two "across-strip" horizontal collinear-point constraints. No ground control points are included.

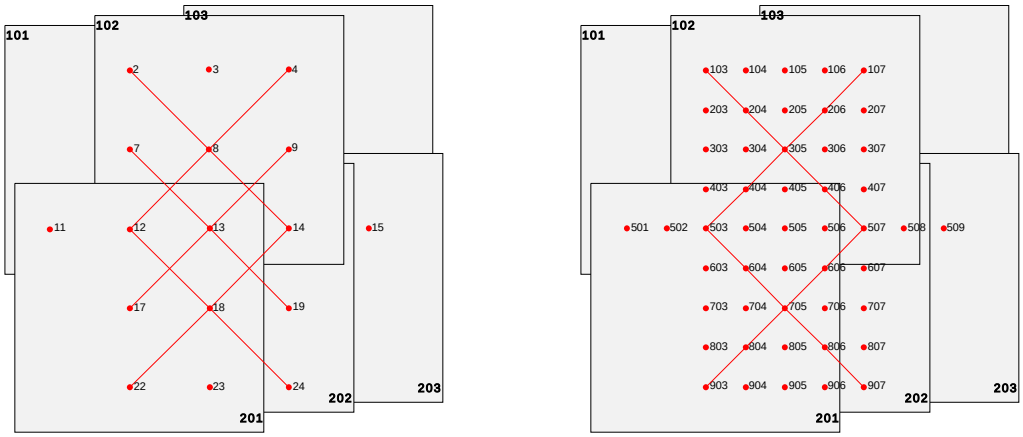

Figure 6.7. Networks N9 (left) and N25 (right). Position of "x-pattern" horizontal collinear-point constraints. No ground control points are included.

For the unconstrained networks, the contribution of each set of direct EO observations to the overall redundancy of the block may be computed by extracting the appropriate diagonal elements from the Gauss-Markov model reliability matrix defined in (1.5). These redundancy numbers are graphed in Figure 6.8 by parameter and by image.

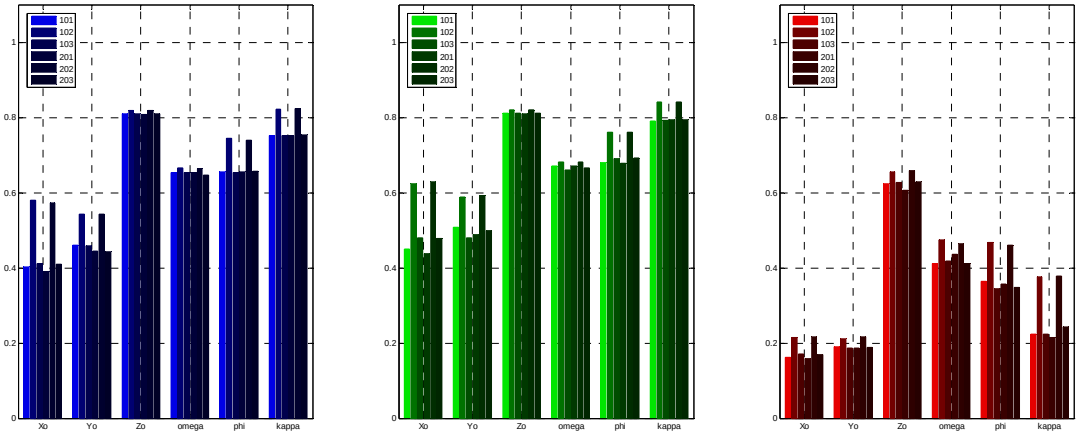

Figure 6.8. Networks N9 (left), N25a (middle) and N25b (right). Redundancy numbers in the unconstrained blocks (Direct EO observations provide only datum information).

We may make several remarks about the redundancy numbers.

1. In the networks with high-precision tie-points, N9 and N25a, the EO parameters show fair reliability in the sense that about 40% to 80% of any error in these observations is mapped into the corresponding residual. In the poor-precision network, N25b, only Z_o shows good reliability. Only about 20% of errors in X_o and Y_o are mapped to the corresponding residual.
2. X_o and Y_o add the least redundancy to the system. This is likely due to the fact that, in the absence of control points, these parameters, along with Z_o , define the network datum. Z_o also contributes to the datum but adds a great deal more redundancy to the system than the horizontal parameters. This seeming inconsistency is related to the fact that Z_o has a larger variance than the horizontal components and thus contributes less to its own estimation. If the EO observations are treated as constraints, this result is predicted by (4.2).

3. The orientation angles of the images have little or no affect on the datum determination (that is, they can be estimated by the tie-point measurements alone) so they tend to add more redundancy to the network.
4. The redundancy numbers change little between networks N9 and N25a. However, the redundancy numbers in N25b are significantly lower. Essentially, what we see in N25a is the larger role played by the exterior orientation observations in their own estimates due to the lower precision of the tie-point observations.
5. All EO parameters in images 102 and 202 exhibit relatively strong reliability. We also expect this since these images are in the middle of the block and thus contain more *n*-fold tie-points.

We may now compute the incremental increase in the redundancy numbers from the introduction of the horizontal collinear-point constraints using (3.2). The redundancy increase resulting from the addition of collinear-point constraints are shown in Figures 6.9, 6.10, 6.11 and 6.12 corresponding to the four configurations in Figures 6.4, 6.5, 6.6 and 6.7, respectively.

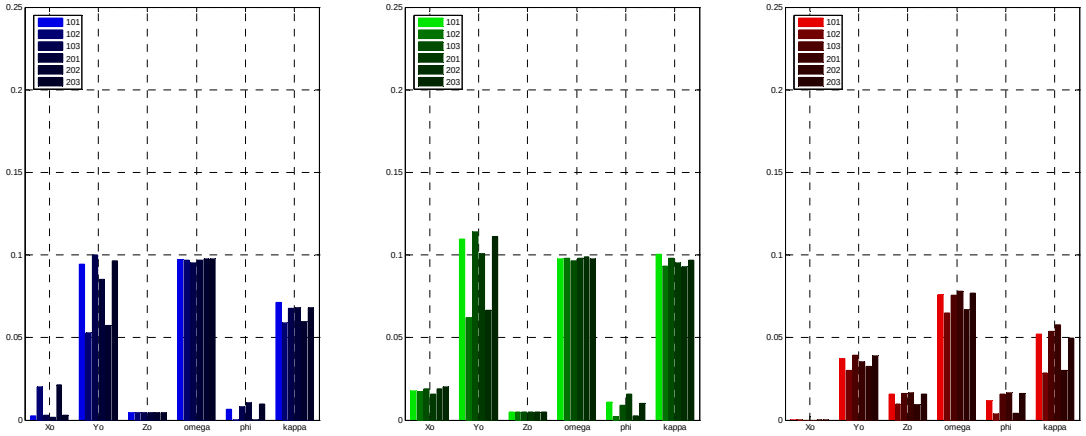

Figure 6.9. Networks N9 (left), N25a (middle) and N25b (right). Redundancy increase due to single along-strip constraint (configuration in Figure 6.4).

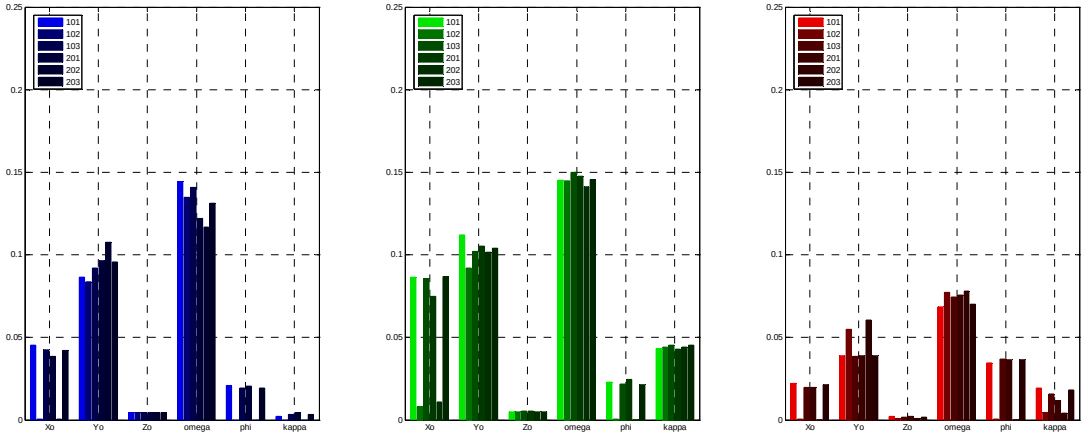

Figure 6.10. Networks N9 (left), N25a (middle) and N25b (right). Redundancy increase due to two along-strip constraints (configuration in Figure 6.5).

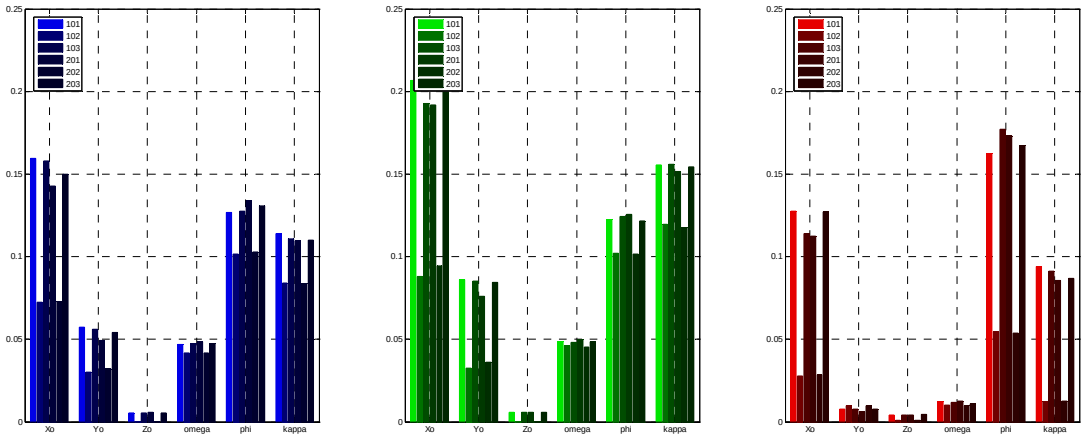

Figure 6.11. Networks N9 (left), N25a (middle) and N25b (right). Redundancy increase due to across-strip constraints (configuration in Figure 6.6).

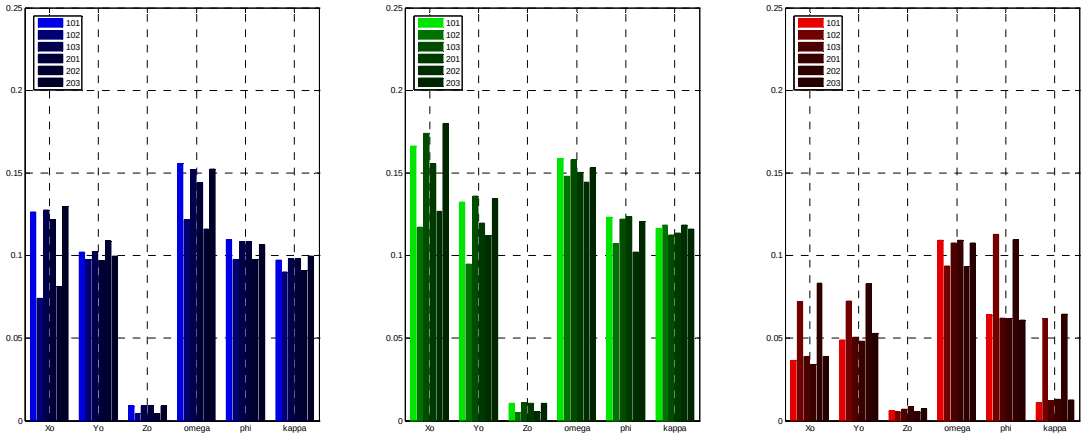

Figure 6.12. Networks N9 (left), N25a (middle) and N25b (right). Redundancy increase due to X-pattern constraint (configuration in Figure 6.7).

We may draw several conclusions from the incremental increases in redundancy.

1. The additional constraints significantly increased the redundancy of at least some of the exterior orientation parameters.
2. The across-strip constraints generally had a larger effect on the outer four images of the block (101, 103, 201, 203).
3. Across-strip constraints aided in the estimation of X_o and φ subsequently making outliers in the direct observations of these parameters more detectible.
4. In every case, the constraints added less redundancy to the orientation parameters of N25b.
5. Along-strip constraints had a larger effect on Y_o and ω subsequently making outliers in the direct observations of these parameters more detectible.
6. Multiple along-strip constraints improved the reliability of Y_o and ω observations over a single along-strip constraint but added relatively less redundancy to κ observation. This is likely due to the fact that the single along-strip constraint connected the strips (i.e. constrained tie-points appearing in every image to a single line) while the multiple constraints did not connect tie-points across the strip.

7. X-pattern constraints have a consistent effect on redundancy (except for Z_o) since they are essentially a combination of both across- and along-strip constraints. Furthermore, they constrain a relatively large number of tie-points.

We turn now to network R9 and graph the redundancy numbers of the exterior orientation parameters in Figure 6.13a. The results with respect to the GPS observed exposure center generally agree with our design networks except for the orientation angle results which show almost full redundancy (the values are 0.9999 to four significant figures). Evidently, the quality of these observations (which we added only so that they would be included in the bundle adjustment to perhaps stabilize the block) is such that they contribute virtually nothing to their own estimation and are thus completely redundant. Another notable result is that the redundancy of the exposure center observations are rather poor except for images R033 and R204 in the middle of the block.

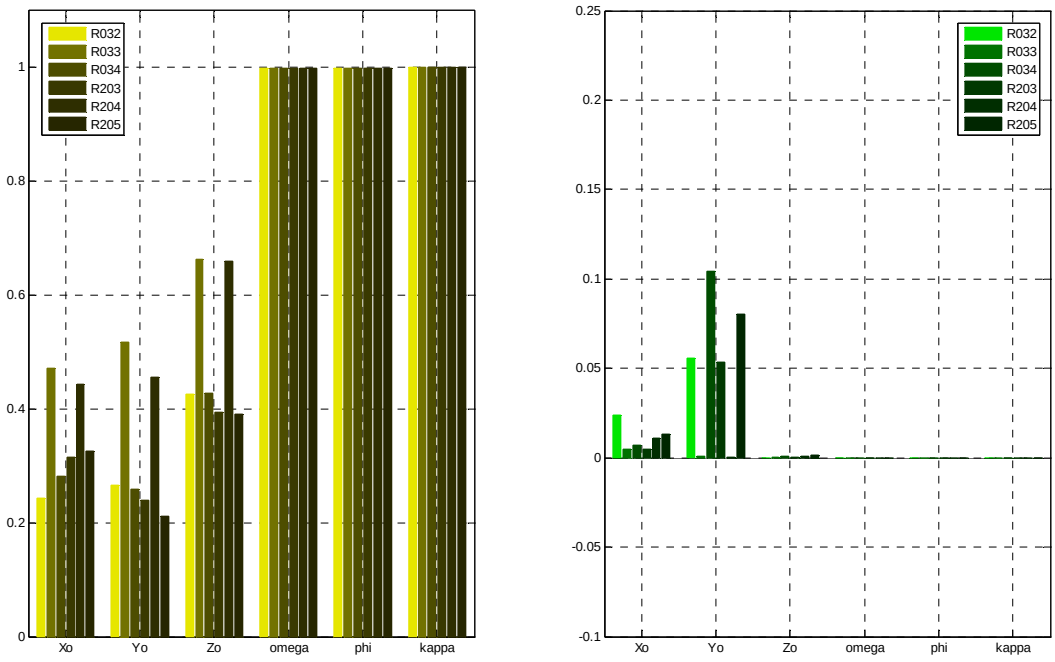

Figure 6.13. (a) Network R9, exterior orientation redundancy numbers. (b) Change in redundancy numbers due to the addition of two 3D distance constraints.

Next we use (3.2) to model the effects of absolute distance constraints (Appendix A.3.3). These constraints, unlike the collinear-point constraints, require actual measurements corrupted by random error, rather than geometric inferences. In addition, the absolute distance constraints contribute to the determination of the datum scale. Points t11 and t1 are constrained to a distance of 2,693.9 meters with a variance of 0.0002 meters^2 while points t4 and t7 are constrained to a distance of 4,923.8 meters with the same variance (Figure 14).

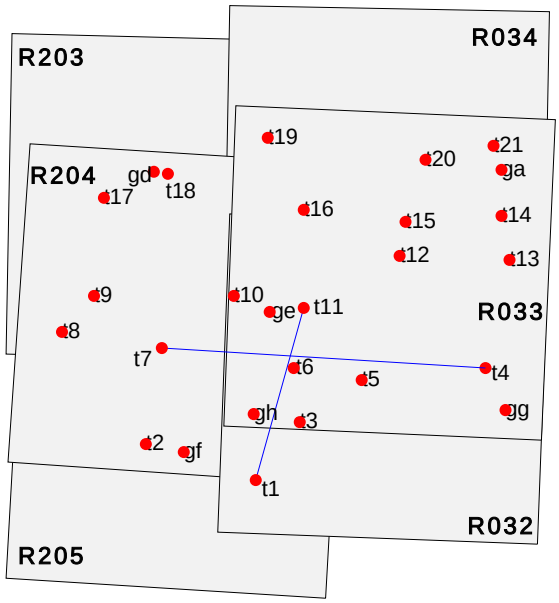

Figure 6.14. Absolute distance constraints in network R9.

The effect of these two constraints are shown in Figure 6.13b. Apparently these constraints have a significant, positive effect on the redundancy numbers of X_o and Y_o, but only for the images on the outer block border.

6.3 Reliability of aerial triangulation with 2-fold tie-points only

A persisting problem with automatic aerial triangulation (AAT) is that it is still difficult to autonomously measure and match a tie-point in more than two images. This is perhaps a critical short-coming because we know that tie-points measured in more than two images provide geometric strength to the block (Kraus, 1997, Mikhail et al., 2001, Förstner, 1985). AAT algorithms tend to address this problem by selecting and matching a large number of two-fold tie points across the block and rely on this large quantity of observations to achieve reliable and precise estimates of exterior orientation. So, in place of a single *n*-fold tie-point (for example, point 13 in Figure 6.1 and Table 6.2), we substitute multiple two-fold tie-points. The redundancy added by an *n*-fold point is $2n-3$, so that the six measurements of point 13 contribute 9 to the total redundancy of the network. A two-fold point contributes only 1 to the total redundancy, so that in general, we need $2n-3$ two-fold tie-points to "make up" the redundancy contributed by an *n*-fold point. Two aspects of this practice need to be addressed: 1) Are the EO parameter estimates as precise as those estimated with *n*-fold points?, and 2) Are we still able to detect outliers in direct observations of the exterior orientation parameters? We will attempt to address the second question with some of the tools developed in this paper, particularly the differential relations from Chapter 5. We recall that these relations determine how changes in parameter seed values – and hence the network design – affect the reliability matrix of the observations. It may be that some redundancy numbers are sensitive to changes to the locations of a particular set of tie-points, ground control points, or image exposure stations. This sensitivity in the neighborhood around a design parameter may be expressed through the Jacobian matrix (5.13). If small changes in one or more of the coordinates of a tie-point affect the reliability on the exterior orientation parameters, proper care should be taken when relying on AAT algorithms to match points in this region. This would provide information about how poor tie-point matches - which cause movement in the design or seed values of the tie-point object space coordinates - might affect the reliability of exterior orientation observations.

To gain a better understanding of these circumstances we will address the following questions:

(i). In the case of direct EO observations, do multiple two-fold tie-points or a single *n*-fold tie-point contribute more to the redundancy numbers of the EO observations?

(ii). How does the redundancy number of an *n*-fold tie-point change with respect to changes in its XYZ ground coordinates, and what is the outer reliability of the exterior orientation parameters relative to this point?

(iii). How do the redundancy numbers of the exterior orientation observations change with respect to changes in a particular tie-point's XYZ ground coordinates?

(iv). Will a reasonable geometric constraint, such as coplanarity in object space, on two-fold tie points contribute to the redundancy of their observations?

Again, we are dealing with a network design problem, so we will begin with networks N9 and from it derive network N9c, in which every *n*-fold tie-point has been decomposed into at least $2n-3$ two-fold points. For example, tie-point 13 in N9 is replaced by points 13a, 13b, 13c, 13d, 13e, 13f, 13g, 13h, and 13i in N9c. Table 6.3 shows how the decomposed point measurements are spread across the block. We follow the same procedure to derive network N25c form N25a. Note that the tie-point precision remains fixed throughout this section.

point/photo	101	102	103	201	202	203
3a	x	x				
3b	x		x			
3c		x	x			
8a	x	x				
8b	x		x			
8c		x	x			
12a	x	x				
12b				x	x	
12c	x			x		
12d		x			x	
12e	x				x	
13a	x	x				
13b	x		x			
13c		x	x			
13d				x	x	
13e				x		x
13f					x	x
13g	x			x		
13h		x			x	
13i			x			x
14a		x	x			
14b					x	x
14c		x			x	
14d			x			x
14e		x				x
18a				x	x	
18b				x		x
18c					x	x
23a				x	x	
23b				x		x
23c					x	x

Table 6.3. Network N9c. Distribution of decomposed *n*-fold two-fold tie-points.

To answer question (*i*), we may use the reliability matrix defined in (1.5) to compare, for example, the reliability numbers of image observations of points 13 and 23 in network N9 to image observations of points 13a – 13i, and 23a – 23c in network N9c. Each of these points consists of two observations, but as we discussed in Chapter 2, they may practically be treated as a single 2D-observation. Therefore, we will not simply consider the redundancy of each coordinate of the point measurement, but rather its *2* x *2* block, $\mathbf{R}_{u_i v_i}$, in the reliability matrix. For a scalar measure, we will use the sum of the redundancy numbers in the block, defined by $\overline{r}_i = \tau^T \mathbf{R}_{u_i v_i} \tau$ for tie-point observation *i*. Such redundancy numbers may now exceed 1 even though the observation weight matrix is diagonal.

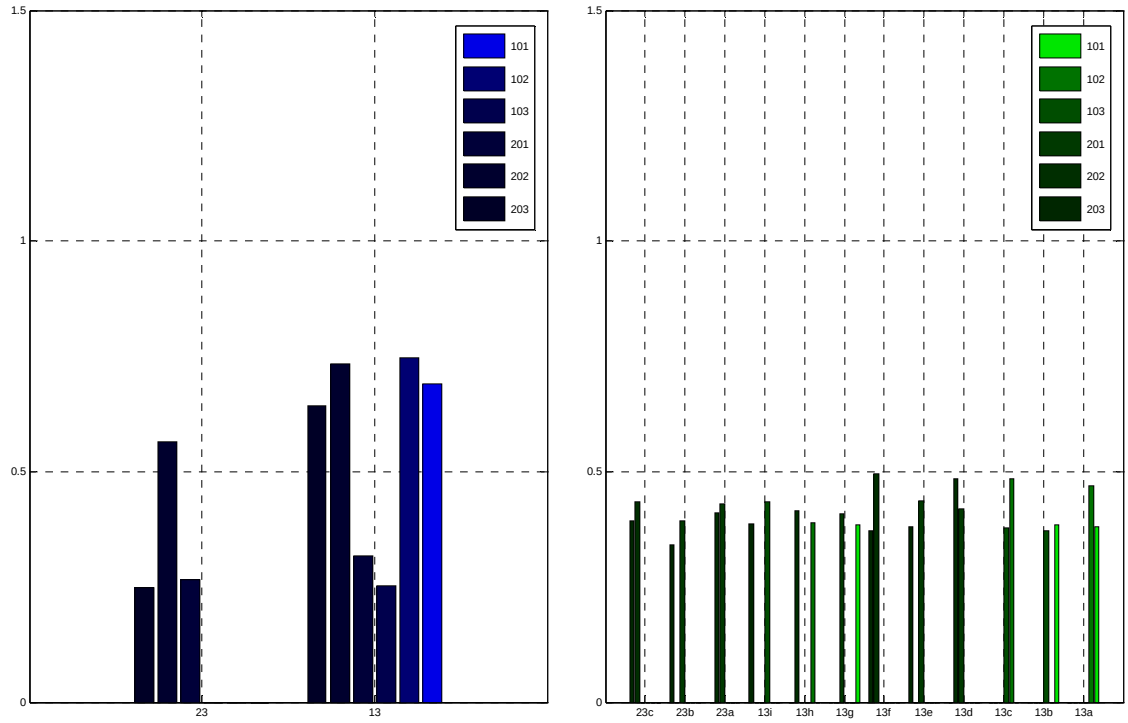

Figure 6.15. Comparison of redundancy numbers of *n*-fold points versus two-fold points.

The graphs in Figure 6.15 confirm our intuition that the *n*-fold points 13 and 23 have very high redundancies, while the decomposed, two-fold points add somewhat less redundancy individually. However, since a major purpose of aerial triangulation is to determine exterior orientation parameters for subsequent operations, tie-point object coordinate accuracy is not typically required. In addition, outer reliability of the EO parameters may be estimated through (2.18). Förstner (1985) reported extensively on outer reliability in block bundle adjustments, but we will not pursue an outer reliability measure in network N9c here. Instead, we will take the approach of determining the reliability of direct observations of the EO parameters.

We address question (*ii*) by graphing the difference between the exterior orientation redundancy numbers when *n*-fold tie-points are measured and when they are decomposed into many two-fold tie-points. Figure 6.16 graphs the changes from N9 to N9c and from N25a to N25c. In the network with few tie-points (left graph), there is a small but significant advantage in using *n*-fold tie-points. However, as the number of tie points increases (right graph), the advantage of *n*-fold tie-points in this context seems less clear. It seems that the κ rotation angle is slightly more reliable when *n*-fold points are measured but the

changes in the reliability of all other exterior orientation parameters are insignificant.

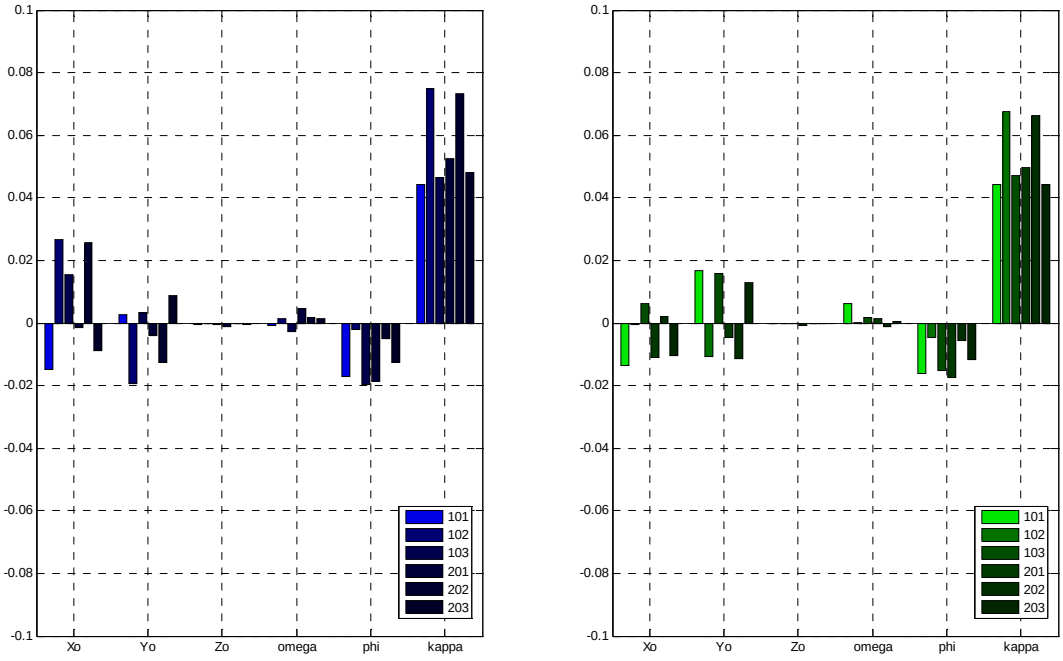

Figure 6.16. Change in redundancy due to the transition from N9 – N9c (left) and N25a – N25c (right).

We should note that in both cases, the effect of a few *n*-fold points measured instead of many two-fold points is not usually negative in terms of reliability and may even be slightly advantageous. For example, the increase in redundancy of κ in image 102 due to the inclusion of *n*-fold points – one of the larger increases – represents an approximately 10% redundancy improvement.

Decomposing *n*-fold tie-points as we have done results in several closely spaced two-fold points in object-space. In many circumstances, it might be reasonable to assume that these points are coplanar. For example, several two-fold points might occur on the roof of a building or on the painted surface of a parking lot. In any case, we address question (*iv*) and explore whether constraining the decomposed points in this way improves the reliability of the exterior orientation using the same formula as in the preceding section. For network N9c, we constrain decomposed points to be coplanar with a single plane of unknown orientation using the constraint model for coplanar points in Appendix A. For example, points 13a-i are constrained to a plane, points 12a-12d to another plane, and so on, for all the decomposed points listed in Table 6.3). The resulting change (from N9c to the constrained N9c) in exterior orientation redundancy numbers are graphed in Figure 6.17.

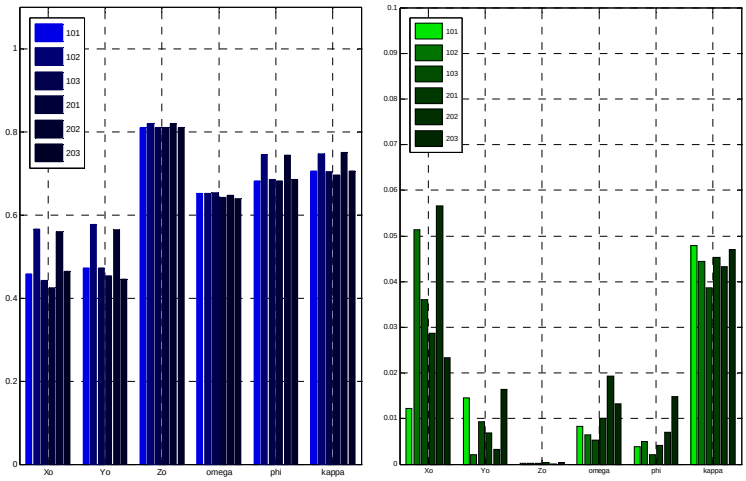

Figure 6.17. Exterior orientation redundancy numbers in N9c (left) and the change caused by applying coplanarity constraints on the decomposed points (right).

From these results we see that while the coplanarity constraints add some information to the exterior orientation estimates – they increased the redundancy of the direct observations of these parameters – the effect on exterior orientation redundancy is small compared to the collinear-point constraint considered earlier. Part of the reason for this must be related to the degree of proximity of the points relative to the covariance of the coplanarity constraints. The results in Figure 6.17 assumed a point covariance matrix as described in Table 6.1. We may strengthen the constraint by assuming a much smaller covariance matrix, say $Cov\left\{\begin{bmatrix} X_{tie} & Y_{tie} & Z_{tie} \end{bmatrix}^T\right\} = \begin{bmatrix} 0.004 & - & - \\ 0.000 & 0.004 & - \\ 0.0000 & 0.000 & 0.004 \end{bmatrix} \text{meters}^2$, equivalent to a ground control point in the data set. Even with the increased precision, the constraints have a similarly small effect on the exterior orientation redundancy (Figure 6.18).

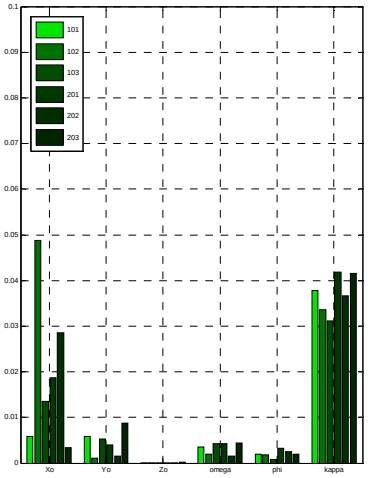

Figure 6.18. Change of exterior orientation redundancy in Network N9c after applying tight coplanarity constraints.

6.4 Differential reliability in photogrammetric networks

We may also compare the stability of the observation redundancy numbers in *n*-fold and two-fold networks in the presence of small changes in tie-point position using the differential relations developed in Chapter 5, specifically (5.12), (5.13), (5.16), and (5.17). In particular, we are interested in answering the question whether the redundancy of the exterior orientation observations are more or less sensitive to small changes in the position of an *n*-fold tie-point and its decomposed two-fold constituents.

Before detailing the experiment, we should mention the size of the matrices involved in the differential forms. In Section 5.3 we stated that the matrices required for this analysis, in particular **H** and $J(\mathbf{R})$, grow large as the number of observations and parameters increase. Our design network N9 consists of 87 parameters and 128 observations leading to a 11,136 x 87 **H** matrix and a 16,384 x 11,136 $J(\mathbf{R})$ matrix. Network N25 consists of 159 parameters (the increase over N9 is due to the multiple decomposed tie-point coordinates) and 200 observations leading to a 31,800 x 159 **H** matrix and a 40,000 x 31,800 $J(\mathbf{R})$ matrix. In both networks **H** is relatively sparse, but $J(\mathbf{R})$ is full which can create memory problems even in relatively small networks. However, we may exploit the sparseness of **H** by computing the second Kronecker product in (5.13) one observation, *i*, at a time to build the (somewhat) sparse *nm* x *n* matrices $\left[\left(\mathbf{A}\mathbf{N}^{-1}\right)_i \otimes \mathbf{Q}_{\hat{\mathbf{e}}}\mathbf{P}\right]\mathbf{H}$. The resulting matrices may be stacked and exploited as required, thus avoiding the need to form and store in memory the full matrix inside the brackets.

We will first look exclusively at network N9 to see how small positional changes (1 meter in *x*, *y* and *z*) of points 13 (a six-fold point) and 22 (a two-fold point observed on images 201 and 202) affect the redundancy numbers of the exterior orientation observations.

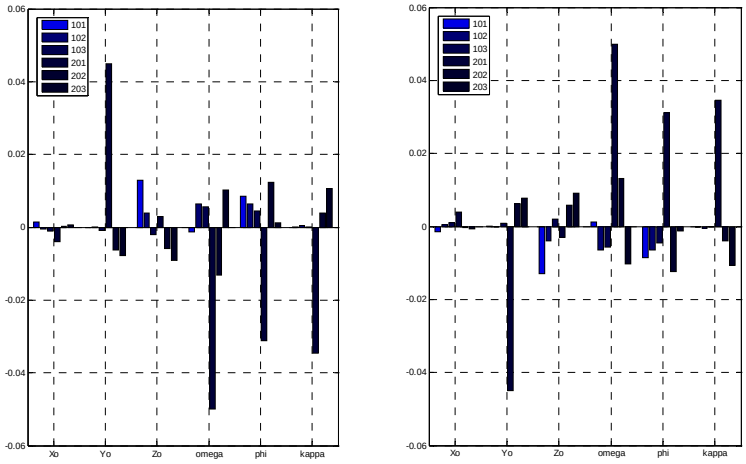

Figure 6.19. Differential changes in exterior orientation observation redundancy due to a 1-meter change of the coordinates of point 13 (left) and point 22 (right).

The resulting changes are graphed in Figure 6.19 which shows relative changes in orientation observations of photos 201, 202, and 203 compared to the first strip. This is to be expected perhaps in the case of point 22, but is unusual – and unexplained so far – in the case of point 13 which presumably would affect all images equally, considering its location and the symmetry of the block. We are dealing with changes in a small neighborhood (small by necessity since (5.12) is a first-order approximation of the non-linear mapping from *vec***A** to *vec***R**) around the "seed" values and, because of this, the size of the changes in Figure 6.19 are less important than the relative changes among images and parameters.

Next, we compare changes to the exterior orientation redundancy numbers in networks N9 and N25a, and try to answer whether the stability of the exterior orientation redundancy numbers in response to changes in the network geometry is larger in network N9 or in N25. Whereas in the previous sections of this chapter we were looking for an increase in exterior orientation redundancy, here we are most interested in stability and thus small changes in response to movements in tie-point coordinates. Stability of the

exterior orientation redundancy in response to changes in tie-point locations could give the network designer confidence that small departures from the design, whether due to AAT algorithms automatically selecting points or due to unavailable natural tie-points, will not adversely affect the orientation redundancy.

We recall that point 13 in N9 was decomposed into nine two-fold tie-points 13a-i. We will use this point to measure the stability of the networks N9 and N25. A 1-meter shift of tie-point 13 within N9 should be equivalent to a 1-meter shift of the tie-points 13a-I within N25. The results of these changes are graphed in Figure 6.19. Apparently these supposedly equivalent shifts affect the exterior orientation redundancy in N9 more than that in N25, thus indicating that N25 is perhaps more stable in the presence of small changes in the location of the tie-points. However, this does not necessarily mean that the overall redundancy is better in N25 (although in the discussion concerning Figure 6.8 we have shown that it is indeed marginally better), only that small changes in points 13 and 13a-i from the design values seem to have little effect on exterior orientation redundancy. These results may be repeated in turn for all points in the network and provide an important additional measure of reliability in any network.

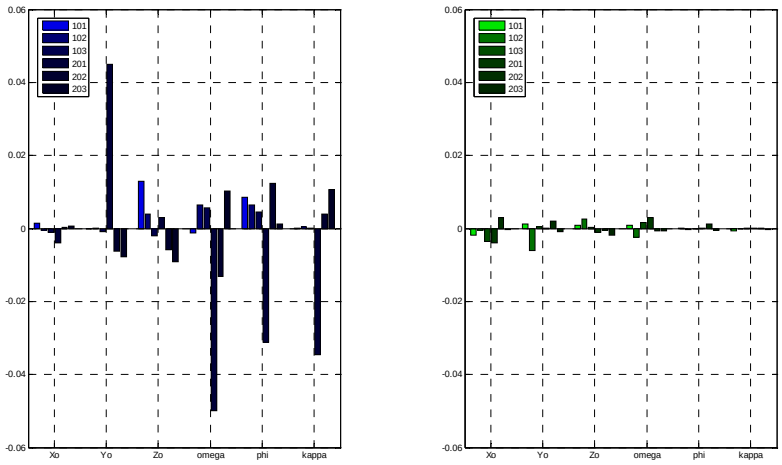

Figure 6.20. Differential redundancy changes in network N9 (left) and in network N25 (right) resulting from a 1-meter shift in the points 13 and 13a-i, respectively.

CHAPTER 7

CONCLUSIONS

Reliability analysis explains the contribution of each observation to the total redundancy of an estimation model, taking into account the geometry of the network as well as the precision of the observations themselves. It is principally used to design networks that are resistant to outliers in the observations by making them more detectible when using standard statistical tests. This approach has been studied extensively, and principally, in (linearized) Gauss-Markov models. Here it has been shown how the same analysis may be extended to various rank-deficient and constrained (linearized) Gauss-Markov models, beside preliminary work for its use in unconstrained Gauss-Helmert models. In particular, the prominent "reliability matrix" of the constrained model has been analyzed in order to separate the contribution of the constraints to the redundancy of the observations from the contribution of the observations themselves.

In addition, extensive use of matrix differential calculus has been made to find the Jacobian of the reliability matrix with respect to the parameters that define the network, through both the original design matrix and the constraint matrix. The resulting Jacobian matrix reveals the sensitivity of elements of the observation reliability matrix (and the redundancy numbers along its diagonal) to particular design parameters and allows the model to identify weak areas in the network where changes in observations may result in unreliable observations.

We have applied this analytical framework to photogrammetric networks in which the exterior orientation parameters of images comprising a block are directly observed by calibrated GPS/INS systems. Such directly oriented blocks offer the potential of significantly reduced ground control survey cost, but suffer from lack of redundancy. Tie-point observations provide some redundancy (for relative orientation only), and even a few collinear tie-point and tie-point distance constraints improve the reliability of these direct observations by as much as 33%. Using the same theory we have compared networks in which tie-points are observed on multiple photos (*n*-fold points) and tie-points are observed in photo pairs only (two-fold points). Apparently, the use of *n*-fold tie-points does not significantly degrade the reliability of the direct exterior orientation observations. Coplanarity constraints added to the common two-fold points do not improve significantly the reliability of the direct exterior orientation observations.

The differential calculus results may be used to provide a new measure of redundancy number stability in networks. We have shown that a typical photogrammetric network with *n*-fold tie-points is not as stable with respect to at least some tie-point movement as an equivalent network with *n*-fold tie-points decomposed into many two-fold tie-points.

However, we have left several questions unanswered which require future work.

1. Although we have provided some insight into extending the theory to the Gauss-Helmert model, real work remains as the necessary formulae to fully analyze the reliability matrix still need to be developed.
2. In Chapter 4 we focused on the reliability of the original observations in the analysis of the reliability matrix and consequently did not fully explore the effects on the constraint observations themselves.
3. The differential analysis of Chapter 5 also did not explore the reliability matrix of the constraints and focused solely on the original observations. While we were able to put this theory to some practical use, more analysis and experimentation remains necessary for the incorporation of any constraints.
4. The practical application of this theory to photogrammetric networks only explored the most obvious questions. It is, for example, not clear if other network configurations behave similarly to the addition of constraints and the decomposition of *n*-fold points.
5. We only touched the surface of *n*-fold decomposition using differential analysis. Network stability in terms of reliability is promising and more research needs to be done, for example, as to how much the addition of constraints on the decomposed points (as was examined with the analytical results) would affect the stability of the network.
6. Can other constraints be applied in practice that have similar positive effects on the direct observation redundancy? For example, do epipolar line constraints add more or less redundancy to these observations?

7. Finally, much more work with real data that harbor known outliers would be recommended to test the assumptions on which the theory is based and to further refine its practical application.

LIST OF REFERENCES

Baarda, W. (1967). Statistical Concepts in Geodesy, Publications on Geodesy, Netherlands Geodetic Commissions Geodetic Commission, Vol. 1(2), Delft, The Netherlands.

Baarda, W. (1968). A Testing Procedure for Use in Geodetic Networks, Publications on Geodesy, Netherlands Geodetic Commission, Vol. 2(5), Delft, The Netherlands.

Baltsavias, E. (1999). A Comparison Between Photogrammetry and Laser Scanning. ISPRS Journal of Photogrammetry and Remote Sensing, Vol. 54 (2-3), 83-94.

Beach, R. (1991). An Introduction to the Curves and Surfaces of Computer-Aided Design. Van Nostrand Reinhold. New York, New York. pp. 37-47.

Filin, S. Csathó, B. (2002). A Novel Approach for Calibrating Satellite Altimeter Systems. Presented at the 3rd Annual Workshop on Mapping Geo-Surficial Processes Using Laser Altimetry. Columbus, OH, October, 2002.

Flood, M. (1999). Commercial Development of Airborne Laser Altimetry – A Review of the Commercial Instrument Market and its Projected Growth. International Archives of Photogrammetry and Remote Sensing, Vol. 32., Part 3-W14, pp. 13-21.

Förstner, W. (1985). Reliability of Block Triangulation. Photogrammetric Engineering and Remote Sensing, Vol. 51, No 6, pp. 1137-1149.

Förstner, W. (1987). Reliability Analysis of Parameter Estimation in Linear Models with Applications to Mensuration Problems in Computer Vision. Computer Vision, Graphics, and Image Processing. Vol. 40, pp. 273-310.

Förstner, W. (1994). Diagnostics and Performance Evaluation in Computer Vision. Proc. Performance vs. Methodology in Computer Vision, NSF/ARPA Workshop, Seattle, pp. 11-25.

Golub, G., Van Loan, C. (1996). Matrix Computations, Third Edition. Johns Hopkins University Press, Baltimore, MD. pp. 256-264.

Grejner-Brzezinska, D. A. (1999). Direct Exterior Orientation of Airborne Imagery with GPS/INS System: Performance Analysis. Navigation. Vol. 46, No. 4, pp. 261-270.

Grejner-Brzezinska, D. A. (2001). Direct Sensor Orientation in Airborne and Land-based Mapping Applications. Department of Civil and Environmental Engineering and Geodetic Science, Ohio State University, Department Report no. 461.

Grün, A. (1978). Accuracy, Reliability, and Statistics in Close Range Photogrammetry. Inter-Congress Symposium of ISP Commission V. Unbound paper No. 9. Stockholm, 1978.

Grün. A. (1980). Precision and Reliability Aspects in Close Range Photogrammetry. International Archives of Photogrammetry, Vol. 11(23B). pp. 378-391.

Heipke, C., Eder K. (1999). Performance of tie point extraction in automatic aerial triangulation. OEEPE Official Publications No. 36, pp. 125-185.

Jaw, J.J. (1999). Control Surface in Aerial Triangulation. Ph.D. dissertation, Dept. of Civil and Environmental Engineering and Geodetic Science, The Ohio State University, Columbus, Ohio.

Koch, K.R. (1999). Parameter Estimation and Hypothesis Testing in Linear Models. Springer Verlag. Berlin/Heidelberg/New York. pp. 134-136, 263-269, 302-307.

Kraus, K. (1997). Photogrammetry Volume 2, Advanced Methods and Applications (English version). Ferd. Dümmler Verlag. Bonn. pp. 208-235.

Lanczos, C. (1956). Applied Analysis. Prentice-Hall, Englewood Cliffs, New Jersey. pp. 321-324.

Leick, A. (1995). GPS Satellite Surveying, 2nd Edition. John Wiley and Sons, New York. pp. 93-174.

Magnus J.R., Neudecker, H. (1999). Matrix Differential Calculus with Applications in Statistics and Econometrics, 2nd Edition. John Wiley & Sons. New York. pp. 99-115.

Mikhail, E., Bethel, J., McGlone, C. (2001). Introduction to Modern Photogrammetry. John Wiley and Sons. New York. pp. 107-112.

Pope, A. J. (1972). Some Pitfalls to be Avoided in the Iterative Adjustment of Nonlinear Problems. Proceedings of the 38th Annual Meeting American Society of Photogrammetry. Washington D.C. pp. 449-473.

Pope, A. J. (1976). The Statistics of Residuals and the Detection of Outliers. NOAA Technical Report NOS 65 NGS 1, National Technical Information Center, NOAA, Rockville, MD.

Schaffrin, B. (1997). Reliability Measures for Correlated Observations. Journal of Surveying Engineering, Vol. 123, No 3, pp. 126-133.

Schaffrin, B. (2000). On the Reliability of Data Obtained by Kriging. International Archives of Photogrammetry and Remote Sensing, 33, Part B4/3, pp. 893-900.

Schenk, T. (1999). Digital Photogrammetry, Volume 1. TerraScience., Columbus, OH. pp. 355-360.

Schenk, T. (2002). Photogrammetry and Laser Altimetry. Presented at the 3rd Annual Workshop on Mapping Geo-Surficial Processes Using Laser Altimetry. Columbus, OH. October, 2002.

Schenk, T., Seo., S., Csathó, B. (2002). Accuracy Study of Airborne Scanning Data with Photogrammetry. Presented at the 3rd Annual Workshop on Mapping Geo-Surficial Processes Using Laser Altimetry. Columbus, OH, October.

Schenk, T., Csathó, B. (2002). Fusion of LIDAR Data and Aerial Imagery for a More Complete Surface Description. Proceedings of the ISPRS Technical Commission III Symposium, "Photogrammetric Computer Vision", PCV'02. Graz, Austria, September. pp. 310-317.

Schenk, T., (2004). Digital Photogrammetry, Volume 2. TerraScience., Columbus, OH.

Searle, S., Casella, G., McCullough, C. (1992). Variance Components. John Wiley & Sons, Inc. New York, pp. 466-467.

Snow, K., Schaffrin, B. (2003). Three-dimensional outlier detection for GPS networks and their densification via the BLIMPBE approach. GPS Solutions, Vol. 7. pp. 130-139.

Tamim, N., Schaffrin, B. (1995). A Methodology to Create a Digital Cadastral Overlay Through Upgrading Digitized Cadastral Data. Surveying and Land Information Systems. Vol. 55. pp. 3-12.

Triggs B., McLauchlan P., Hartley R., Fitzgibbon A. (2000). Bundle Adjustment - A Modern Synthesis. Vision Algorithms: Theory and Practice. Springer, Lectures Notes in Computer Science. Berlin/Heidelberg/New York. pp. 298-375.

Wang, J., Chen, Y. (1994). On the Reliability Measure of Observations, Acta Geodaet. et Cartograph. Sinica, English Edition, pp. 42-51.

APPENDIX A

BUNDLE ADJUSTMENT AND SELECTED CONSTRAINT EQUATIONS

A.1 Collinearity model

The collinearity equations form the foundation for photogrammetric bundle adjustments. They are based on the central perspective principle and describe the straight line path of the principle optic ray from point *i* on the ground through the camera optic system to the image plane:

$$\begin{aligned} u_i - u_o &= -f\left(\frac{U_i}{W_i}\right) + \left(\delta r_u + \delta t_u + \delta c_u\right) u_i + \left(\delta r_v + \delta t_v + \delta c_v\right) v_i \\ v_i - v_o &= -f\left(\frac{V_i}{W_i}\right) + \left(\delta r_u + \delta t_u + \delta c_u\right) u_i + \left(\delta r_v + \delta t_v + \delta c_v\right) v_i \end{aligned} \tag{A.1}$$

where u, v are the observed image coordinates of point i, here, assumed to be noise-free, and u_o, v_o are the coordinates of the principle point; f is the focal length of the optical system. The equations

$$\begin{bmatrix} U_i \\ V_i \\ W_i \end{bmatrix} = R(\omega, \varphi, \kappa) \begin{bmatrix} X_i - X_o \\ Y_i - Y_o \\ Z_i - Z_o \end{bmatrix}, \tag{A.2}$$

describe the path of the principle ray from the ground point (X_i, Y_i, Z_i) to the exposure center (X_o, Y_o, Z_o), rotated into image space through the Cardan angles $(\omega, \varphi, \kappa)$. The additional parameters $\delta r_{u,v}, \delta t_{u,v}, \delta c_{u,v}$ describe deviations from the straight line path caused by radial lens distortions, tangential lens distortions, and atmospheric refraction, respectively. They may be included as estimable parameters in so-called self-calibrating bundle adjustments to calibrate, or refine the calibration of, metric and non-metric cameras; alternatively, estimates from a previous calibration may be introduced. Note that, in the absence of these additional parameters, the linearized collinearity equations are linear in the image coordinate observations and may be modeled using the Gauss-Markov model. A self-calibrating adjustment requires the Gauss-Helmert model. The linearization of the collinearity equations using the linear terms of the Taylor series expansion has been thoroughly presented and will not be covered here (Kraus, 1997, Schenk, 1999).

A.2 Handling rank-deficiency in the collinearity model

Many photogrammetric operations make use of observation equations derived from the photogrammetric collinearity equations that are inherently rank-deficient in that they do not establish a datum for the block of photographs. This datum deficiency may be covered in several ways. One method is to separate the photogrammetric triangulation process into two steps: 1) relative orientation, in which seven exterior orientation parameters are fixed and stereo models are formed based on the datum so defined, followed by 2) absolute orientation, in which the stereo models (model points) undergo a Helmert transformation to align them with fixed or stochastic ground control (Schenk, 1999). Another method, often preferred in analytical and digital photogrammetry, is to augment the linearized collinearity equations with direct observations of control point coordinates and their associated covariance matrices in the form of stochastic constraints and solve both relative and absolute orientation in a single adjustment step (Kraus, 1997, Schenk, 1999). However, minimum constraints often play a role in bundle adjustment theory and are used in situations where datum-invariant quantities such as relative distances, are under consideration. For that reason we will consider the following datum definitions. Considering model (2.1), we may apply the minimum constraints

$$\underset{7xm}{\mathbf{K}}\,\xi = \mathbf{0} \qquad rk(\mathbf{K}) = m - q = 7 \qquad rk\left(\begin{bmatrix}\mathbf{A}^T & \mathbf{K}^T\end{bmatrix}\right) = m \tag{A.3}$$

and define **K** in one of potentially many ways. First, to implement direct relative orientation (DRO) of a stereo-pair, we may fix one photograph's exterior orientation parameters $(X_{o1}, Y_{o1}, Z_{o1}, \omega_1, \varphi_1, \kappa_1)$ to zero or some other constants, and fix the baseline (often in stereo-pairs X_{o2}) to a known or assumed distance. In the linearized model, this amounts to linearizing around the fixed parameters and not allowing the parameters to change, or equivalently, to applying the minimum constraints

$$\begin{bmatrix} \mathbf{I}_7 & \mathbf{0} \end{bmatrix} \begin{bmatrix} \xi_{dro} \\ \xi \end{bmatrix} = \mathbf{0} \tag{A.4}$$

where the parameter vector is partitioned to isolate the appropriate elements. Indirect relative orientation (IRO) may be implemented by fixing the length and orientation of the baseline vector $(X_{o1}, Y_{o1}, Z_{o1}) - (X_{o2}, Y_{o2}, Z_{o2})$ between the images and the rotation of one of the images about the baseline (usually accomplished by setting $X_{o1} = Y_{01} = Z_{01} = 0$, $Y_{02} = Z_{02} = 0$, $X_{02} = D$ and $\kappa_2 = 0$. The constraint equations are identical to (A.4) except for the repartitioning of the parameter vector. We may also apply the free net constraints (Kraus, 1997, Koch, 1999), in which the datum is defined by fixing the seven Helmert parameters that relate the coordinate system of the ground points' initial approximations (and possibly the camera station's initial approximations as well) to the coordinate system of the estimated ground points. This is achieved by defining

$$\mathbf{K} = \begin{bmatrix} 1 & 0 & 0 & 1 & 0 & 0 & \cdots & 0 & 0 & 0 \\ 0 & 1 & 0 & 0 & 1 & 0 & \cdots & 0 & 0 & 0 \\ 0 & 0 & 1 & 0 & 0 & 1 & \cdots & 0 & 0 & 0 \\ 0 & -Z_i & Y_i & 0 & -Z_j & Y_j & \cdots & 0 & 0 & 0 \\ Z_i & 0 & -X_i & Z_j & 0 & -X_j & \cdots & 0 & 0 & 0 \\ -Y_i & X_i & 0 & -Y_j & X_j & 0 & \cdots & 0 & 0 & 0 \\ X_i & Y_i & Z_i & X_j & Y_j & Z_j & \cdots & 0 & 0 & 0 \end{bmatrix} \tag{A.5}$$

where the columns are placed so that they correspond to the like ground points and/or perspective centers in the design matrix and parameter vector. It can be shown that these constraints on a bundle adjustment based on the collinearity equations result in a parameter dispersion matrix with minimum partial trace where only the diagonal elements corresponding to ground points are considered (Koch, 1999). These minimum constraints, if so defined, also constitute a partial MInimum NOrm LEast Squares Solution (partial MINOLESS) to the bundle adjustment. If points only are treated as parameters to be estimated as is the case with most total station-based triangulation or trilateration networks, then there are no zero columns in **K** and **K** = **E**. This result, indeed is the MINOLESS and (3.55) may be computed as $\hat{\xi} = \mathbf{N}^{+}\mathbf{c}$ with $\mathbf{N}^{+}$ as the "pseudo-inverse" of **N**.

Any one of these three definitions of **K** provide a means of overcoming the datum deficiency associated with the collinearity equations and **K** can thus be substituted into the expressions in Table 3.6. When constraints are added to the Gauss-Markov model in addition to these minimal constraints, care must be taken that the added constraints are consistent with the minimal constraints. For example, if absolute distance constraints between two ground points are applied along with free-net constraints, the last row of **K** as defined in (A.5) (which fixes the scale of the resulting ground point system to the scale of the initial approximations) supplies redundant information possibly inconsistent with the datum information in the distance constraints. Finally, since the inclusion of these minimal constraints perturb neither the residuals nor their dispersion, they will likewise not affect their reliability.

A.3 Constraints on object points

We detail here two "geometric" constraints, in which we model alternative geometric conditions that must be met by multiple points, or an observational constraint between points. All three options have proven useful for photogrammetric networks (Mikhail, 2001).

A.3.1 Collinear points.

Because straight lines often occur across the rural and urban landscapes where aerial surveys are usually conducted, constraining three or more points to be collinear might prove to be useful in two forms. First, we may constrain only the *x* and *y* coordinates to be collinear. This horizontal (in the *xy*-map plane) only constraint is useful for road surfaces which are straight but not necessarily flat. The relation $\frac{(x_j - x_i)}{(x_k - x_j)} = \frac{(y_j - y_i)}{(y_k - y_j)}$ among any three points *i*, *j*, and *k*, forces equality of the slope of the line between points *i* and *j* and the slope of the line between points *j* and *k*. The relation may be rearranged to form the constraint equation

$$g_{ijk} = (x_j - x_i)(y_k - y_j) - (x_k - x_j)(y_j - y_i) = 0\,. \tag{A.6}$$

The collinearity of more than three points may be enforced by forming additional constraints. For example, points *i*, *j*, and *k* would lead to g_{ijk} while points *j*, *k*, and *l* would lead to g_{jkl}. If the constraint is considered to be stochastic, we replace "0" in (A.6) by an error term with zero expectation and variance that reflects the presumed relative accuracy of the constrained points. If the combined coordinates of *n* constrained points are allowed a covariance of Σ_{xy} (of order 2*n* x 2*n*) then the we may compute $\sigma_g = \mathbf{J}\Sigma_{xy}\mathbf{J}^T$ where **J** is the (*n*-2) *x* 2*n* Jacobian matrix of *g* with respect to the coordinates.

Collinearity of three points along an unknown three-dimensional line provides two relations representing horizontal collinearity (as before) and vertical collinearity. The second constraint equation may be written using the *z* coordinates,

$$h_{ijk} = (x_j - x_i)(z_k - z_j) - (x_k - x_j)(z_j - z_i) = 0 \tag{A.7a}$$

or

$$h_{ijk} = (y_j - y_i)(z_k - z_j) - (y_k - y_j)(z_j - z_i) = 0\,, \tag{A.7b}$$

either (but not both since one of the three constraints is dependent on the other two) of which may be chosen. The uncertainty of h_{ijk} may be computed as before with the (*n*-1) x 3*n* Jacobian matrix.

A.3.2 Coplanar points

We may enforce the coplanarity of four three-dimensional points by applying the scalar triple product

$$g_{ijkl} = \mathbf{p}_{il} \cdot (\mathbf{p}_{ij} \times \mathbf{p}_{ik}) = 0 \tag{A.8}$$

where $\mathbf{p}_{ij} = \begin{bmatrix} x_{ij} \\ y_{ij} \\ z_{ij} \end{bmatrix} = \begin{bmatrix} x_i - x_j \\ y_i - y_j \\ z_i - z_j \end{bmatrix}$, $\mathbf{p}_{ik} = \begin{bmatrix} x_{ik} \\ y_{ik} \\ z_{ik} \end{bmatrix} = \begin{bmatrix} x_i - x_k \\ y_i - y_k \\ z_i - z_k \end{bmatrix}$, and $\mathbf{p}_{il} = \begin{bmatrix} x_{il} \\ y_{il} \\ z_{il} \end{bmatrix} = \begin{bmatrix} x_i - x_l \\ y_i - y_l \\ z_i - z_l \end{bmatrix}$ for points *i*, *j*, *k*, and *l*.

No three of the four points may be collinear. More than four points may be constrained to lie on the same plane by forming an additional constraint from each set of four points. For example, points *i*, *j*, *k*, and *l* form one constraint, while *j*, *k*, *l* and *m* form a second constraint. In general, *n* – 3 constraints are formed from *n* points. If the constraint is allowed to have random error, its variance (and the covariance among multiple constraints formed from a group of points) may be computed from the (*n*-3) x 3*n* Jacobian matrix of the constraint equations and the assumed covariance matrices of the constrained points.

The total differential of the scalar triple product,

$$
\begin{aligned}
dg_{ijkl} &= d\mathbf{p}_{il} \cdot \left(\mathbf{p}_{ij} \times \mathbf{p}_{ik}\right) + \mathbf{p}_{il} \cdot d\left(\mathbf{p}_{ij} \times \mathbf{p}_{ik}\right) \\
&= d\mathbf{p}_{il} \cdot \left(\mathbf{p}_{ij} \times \mathbf{p}_{ik}\right) + \mathbf{p}_{il} \cdot \left[\left(d\mathbf{p}_{ij} \times \mathbf{p}_{ik}\right) + \left(\mathbf{p}_{ij} \times d\mathbf{p}_{ik}\right)\right] \qquad \text{(A.9)} \\
&= \begin{bmatrix} x_{ij} & y_{ij} & z_{ij} \end{bmatrix} \mathbf{S}_{ik} \begin{bmatrix} dx_{il} \\ dy_{il} \\ dz_{il} \end{bmatrix} + \begin{bmatrix} x_{il} & y_{il} & z_{il} \end{bmatrix} \left(\mathbf{S}_{ik} \begin{bmatrix} dx_{ij} \\ dy_{ij} \\ dz_{ij} \end{bmatrix} - \mathbf{S}_{ij} \begin{bmatrix} dx_{ik} \\ dy_{ik} \\ dz_{ik} \end{bmatrix} \right) = 0
\end{aligned}
$$

with, for example, $\mathbf{S}_{ij} = \begin{bmatrix} 0 & z_{ij} & -y_{ij} \\ -z_{ij} & 0 & x_{ij} \\ y_{ij} & -x_{ij} & 0 \end{bmatrix}$, may be used to generate the Jacobian matrix required for linearization and error propagation.

A.3.3 Distance between points

The observed distance between two three-dimensional points, *i* and *j*, may be modeled as $\rho_{ij}^2 = \left(x_i - x_j\right)^2 + \left(y_i - y_j\right)^2 + \left(z_i - z_j\right)^2$. The variance of this constraint should be based on the observation method and instrument. An example of this constraint and its total derivative is given in Section 2.2.

APPENDIX B

MATRIX OPERATIONS

B.1 Kronecker product and *vec* operator

Let **A** be an *n* x *m* matrix and **B** a *p* x *q* matrix. The *nm* x *pq* matrix

$$\mathbf{A} \otimes \mathbf{B} = \begin{bmatrix} a_{11}\mathbf{B} & a_{12}\mathbf{B} & \dots & a_{1m}\mathbf{B} \\ a_{21}\mathbf{B} & a_{22}\mathbf{B} & \dots & a_{2m}\mathbf{B} \\ \vdots & \vdots & \ddots & \vdots \\ a_{m1}\mathbf{B} & a_{m2}\mathbf{B} & \dots & a_{nm}\mathbf{B} \end{bmatrix} \tag{B.1}$$

is called the Kronecker product of A and B.

The *vec* operator creates a column vector from a matrix $\mathbf{A}$ by stacking the column vectors of $\mathbf{A} = \begin{bmatrix} \mathbf{a}^1 & \mathbf{a}^2 & \dots & \mathbf{a}^m \end{bmatrix}$ below one another

$$vec(\mathbf{A}) = \begin{bmatrix} \mathbf{a}^1 \\ \mathbf{a}^2 \\ \vdots \\ \mathbf{a}^m \end{bmatrix}. \tag{B.2}$$

These two operators together yield the useful property

$$vec(\mathbf{AXB}) = \left(\mathbf{B}^T \otimes \mathbf{A}\right) vec(\mathbf{X}). \tag{B.3}$$

More details may be found in Magnus and Neudecker (1999) and Koch (1999).

B.2 Commutation Matrices

For any *n* x *m* matrix **A** we define $\mathbf{K}_{nm}$ as the *nm* x *nm* commutation matrix satisfying

$$vec\mathbf{A} = \mathbf{K}_{nm} vec\left(\mathbf{A}^T\right). \tag{B.4}$$

The commutation matrix derives its name from the relation $K_{pn}(\mathbf{A} \otimes \mathbf{B}) = (\mathbf{B} \otimes \mathbf{A}) K_{qm}$ that holds for any *p* x *q* matrix **B**.

B.3 Matrix Derivatives

For any *n* x *m* matrix **A** whose elements are differentiable functions of the *q* elements, **x**, the *nmq* derivatives may be written in the *nm* x *q* matrix

$$\frac{\partial(vec\mathbf{A})}{(\partial\mathbf{x})^T} = \begin{bmatrix} \frac{\partial(vec\mathbf{A})}{\partial\mathbf{x}_1} & \frac{\partial(vec\mathbf{A})}{\partial\mathbf{x}_2} & \dots & \frac{\partial(vec\mathbf{A})}{\partial\mathbf{x}_q} \end{bmatrix}. \tag{B.5}$$

This form is convenient for expressing the total differential, *d***A**,

$$d(vec\mathbf{A}) = \begin{bmatrix} \frac{\partial(vec\mathbf{A})}{\partial x_1} & \frac{\partial(vec\mathbf{A})}{\partial x_2} & \dots & \frac{\partial(vec\mathbf{A})}{\partial x_q} \end{bmatrix} \begin{bmatrix} dx_1 \\ dx_2 \\ \vdots \\ dxq \end{bmatrix} = \frac{\partial(vec\mathbf{A})}{(\partial\mathbf{x})^T} d\mathbf{x}. \tag{B.6}$$